Higher Order Lattice Boltzmann for Thermo-Hydrodynamics

A Thesis
Submitted for the Degree of
Master of Science (Engineering)

by

Shahajhan H. S.

Engineering Mechanics Unit
Jawaharlal Nehru Centre for Advanced Scientific Research
(A Deemed University)
Bangalore – 560 064

AUGUST 2013

DECLARATION

I hereby declare that the matter embodied in the thesis entitled "**Higher Order Lattice Boltzmann for Thermo-Hydrodynamics** " is the result of investigations carried out by me at the Engineering Mechanics Unit, Jawaharlal Nehru Centre for Advanced Scientific Research, Bangalore, India under the supervision of **Prof. Santosh Ansumali** and that it has not been submitted elsewhere for the award of any degree or diploma.

In keeping with the general practice in reporting scientific observations, due acknowledgment has been made whenever the work described is based on the findings of other investigators.

Shahajhan H. S.

CERTIFICATE

I hereby certify that the matter embodied in this thesis entitled “**Higher Order Lattice Boltzmann for Thermo-Hydrodynamics** ” has been carried out by **Mr. Shahajhan H. S.** at the Engineering Mechanics Unit, Jawaharlal Nehru Centre for Advanced Scientific Research, Bangalore, India under my supervision and that it has not been submitted elsewhere for the award of any degree or diploma.

Prof. Santosh Ansumali
(Research Supervisor)

Acknowledgments

This thesis is the sole outcome of vision and immense effort towards that from my advisor Prof. Santosh Ansumali. Had it not been for his faith on me and enduring patience, this work would have been impossible. I put to record my sincere thanks and heartiest gratitude toward him. This thesis is dedicated to his brilliance and expertise.

I am especially grateful to Mr. Sunil D. Sherlekar, Mr. Anand M. Deshpande and Mr. Aniruddha G. Shet, all from Parallel Computing Intel Labs, Bangalore, India as well as JNCASR and Prof. Santosh Ansumali for giving me an opportunity to work on the high performance computing and optimization project that our research group carried out in collaboration with their team. We express our indebtedness for their generous support and funding. In this regard, its worth mentioning that Siddharth, PhD student from our research group, contributed immensely and single–handedly to the HPC project. I had always received full support from him in the computational work related to my thesis. He is a rare combination of being an experimentalist with a sound knowledge of theory and being a brilliant programmer.

Indeed ! the teachers and researchers here in JNCASR and IISc has left an ever lasting impression on me. I am really grateful to them and feel fortunate to be one of their students, though not the best one. I also wish to thanks a lot of people, friends and well wishers from EMU-JNCASR, IISc, IITs, NITs etc. I don't want to pain them further by explicitly putting their names here as I believe that the present work falls short of to their glory and the high standards they have set through their work. My fellow colleagues have been excellent researchers and I have learn a lot from them.

Thank you all !
Shahajhan

Abstract

In the last two decades, lattice Boltzmann method has emerged as one of the alternatives to do complex isothermal and incompressible CFD simulations. It is based on kinetic theory which is a molecular description of the transport phenomenon in liquids and gases. In lattice Boltzmann method, similar to discrete velocity methods, one solves simplified Boltzmann equation over a grid/lattice. Thus, lattice Boltzmann method involves discrete velocity space and time. The present thesis is an attempt to examine such a discrete description from theoretical and computational point of view for its utility in modelling Navier-Stokes-Fourier thermo-hydrodynamics.

The present thesis deals with the construction and implementation of an "higher order lattice Boltzmann model" for thermal flows. The objective here is that the model so constructed should not only be accurate but also be computationally efficient to simulate Navier-Stokes-Fourier thermo-hydrodynamics. In this thesis, it is shown that this can be done by adding just 6 more velocities to the discrete velocity set of D3Q27 model. A "multi-speed on lattice thermal lattice Boltzmann model" with 33 velocities in 3D with a consistent H-theorem is obtained. The numerical studies have been performed for a variety of isothermal and thermal flows like uni-directional flows, lid driven cavity set up, Rayleigh-Bénard instability, velocity and temperature slip in micro flows. It is shown that the procedure outlined in this thesis for higher order model construction can then be utilized to construct more better and accurate models.

The second part of the present thesis deals with optimal implementation of lattice Boltzmann method algorithm. The objective here is that such an optimized lattice Boltzmann method code must allow for full memory bandwidth usage and it should also be compute friendly. It is shown in this thesis that based on symmetry and isotropy consideration of underlying lattice, it is possible to have a unified data layout that is both advection and collision friendly.

List of Figures

List of Tables

Contents

Appendices

Chapter 1

Introduction

Mesoscale method such as the lattice Boltzmann (hereafter LB) method are an efficient alternative to conventional computational fluid dynamics tools for simulating isothermal hydrodynamics [1, 2, 3, 4]. A few important and attractive features of LB method are: efficient parallelization, the ease in handling of complex boundaries, and the possibility to guarantee non-linear numerical stability via entropic formulation [1, 4, 5, 6, 7]. LB method has been applied to a variety of hydrodynamic applications including porous media [8, 9], suspension dynamics[10, 11], hemodynamics[12] and turbulence [13]. However, this success in modeling isothermal hydrodynamics has not been replicated in modeling of thermo–hydrodynamics [7, 14]. It was pointed in Ref. [14] that a minimum of 26 discrete velocities in 3-D are needed to recover Navier-Stokes-Fourier dynamics via LB method and numerical stability is of serious concern in such thermo-hydrodynamic modeling. It was proposed by various groups that additional particle velocities must be selected to achieve numerical stability as well as better accuracy [15, 16].

In the present thesis, the construction of lattice Boltzmann model based on the entropic quadrature method is revisited. The goal is to find the minimum number of discrete velocities that can be used to derive thermal lattice Boltzmann model for an on-lattice case. In lattice Boltzmann model, grid spacing, Δx, is very often chosen in such a way that the particles in one time step during streaming reaches the next lattice site. Hereafter, those lattice Boltzmann models where this condition is fulfilled are termed as an "on-lattice" LB model. This formulation is used to restrict the choice of lattices under consideration to a set which has well defined H-function and symmetries. For such class of lattices, a general expression for the equilibrium is derived in such a fashion that the discrete H-function gets minimized under the constraints for conservation of mass, momentum and energy . These general expression are then used for finding conditions on discrete velocity models which can lead to Navier-Stokes-Fourier (hereafter NSF) equations in an appropriate limits. These condition are then evaluated in the form of system of equations to derive a 33 velocity lattice model (hereafter D3Q33) for thermo-hydrodynamics.

Furthermore, an optimal data storage and data access scheme for the general LB models is presented. An algorithmic feature of LB method is that one updates array elements according to some predefined pattern and data is exchanged only between neighbouring sites. This enables a high degree of parallelism, suitable for massively parallel computing [1, 17, 18, 19]. However, an aspect not often discussed is that these algorithms are "memory bound" rather than "CPU bound" [20, 21]. Memory bound algorithms are likely to suffer due to the existing wide gap between computing and data access speeds which are expected to widen over the foreseeable future. Also, LB method involves two basic algorithms "collision" and "advection" that has conflicting data structure requirement [20]. This implies that the choice of data structure for LB method is not obvious beforehand [20, 22]. The conflicting data structure requirements for collision and advection results in a sharp performance drop (as compared to the peak computer performance) for LB methods with large stencils where bandwidth limitations are important.

One may ask then what is the natural choice for the data structure for the LB method ? In this thesis it is shown that, for the Lattice Boltzmann (LB) model, the existing paradigm available in computer science for the choice of data structure is suboptimal. The requirements of physical symmetry as discussed in the context of entropic quadrature are used to propose a hybrid data layout. This new hybrid data structure, which is termed as the "Structure of Array of Structures (SOAOS)" is shown to be optimal for LB method. The possible advantages of this new idea for establishing a connection between group-theoretic symmetry requirements with the construction of the data structure is discussed in this thesis in the broader context of grid-based methods. The thesis is organized as follows

- **Chapter 2 : Lattice Boltzmann for thermo-hydrodynamics** In this chapter the entropic quadrature is revisited in the light of present discussion on higher order model. It starts with a general LB model and introduces lattice dependent parameters that need to be fixed in order to obtain Navier-Stokes-Fourier dynamics.

  The details about D3Q33 model construction is discussed in this chapter as well as the various numerical tests made with the D3Q33 model are highlighted in this chapter, namely the thermal simulation.

- **Chapter 3 : Data structures in LB method** In this chapter the array of structures (AOS) and the structure of array (SOA) type of data structure for implementing LB method are discussed along with their shortcomings. Then, the proposed data structure SOAOS, a hybrid of the two is compared with AOS and SOA. In this chapter it is shown that there is a systematic way of grouping the velocities together based on the ansatzes for symmetry closures (reflection and inversion).

- **Chapter 4 : Outlook** Finally, the outlook chapter provides a brief discussion on what has been achieved and the prospective applications of the theoretical and the numerical framework developed in this thesis.

- **Appendices**: The appendix A provides details of discrete equilibrium calculation as well as it's moments. While the details of advection implementation and the pseudo codes are provided in B

Chapter 2

Lattice Boltzmann for thermo-hydrodynamics

Lattice Boltzmann method is a reduced kinetic description of Boltzmann equation in a discrete velocity space with Bhatnagar-Groos-Krook (BGK) type collision model [23, 24, 25]. It is a refinement over "discrete velocity method" (DVM) introduced by J. E. Broadwell [26, 27] and lattice gas cellular automaton (LGCA) by Hardy, de Pazzis and Pomeau [28, 29, 30, 31]. Historically, Frisch, Hasslacher and Pomeau introduced the first LGCA that recovered Navier-Stokes dynamics [32]. However, their model had serious issue of statistical noise due to the integer valued nature of the particle number density. McNamara and Zanetti [33] resolved this issue by using the real valued discrete single particle distribution function f_i which is an "ensemble average" of the particle number density. Later, it was realized that the evolution equation for particle number density in LGCA mimics the evolution equation for single particle distribution in the discretized Boltzmann equation of DVM [33]. It was also found out that much of the details of collision could be omitted and a simplified collision model could be used [24, 25, 34]. This fusion of LGCA and the discretized Boltzmann equation of DVM gave birth to lattice Boltzmann method (LBM).

Thus, lattice Boltzmann method can be viewed as a discrete method (space, time and velocity) to solve Boltzmann equation. It has been successfully employed to simulate incompressible isothermal flows, multi-species and multiphase flows, to as diverse as magneto-hydrodynamics, acoustics, turbulence etc. (see Ref. [1, 2, 3, 4]). However, extension of lattice Boltzmann method to model thermal flows and flows in high Kn regime has been a non trivial task [14, 35]. Accuracy of velocity space discretization has been shown to be important for modeling thermal flows and micro flows. While stability of the numerical scheme is an extra worry for simulating thermal flows as well as flows at high Reynold numbers [14, 35, 36]. Accuracy in velocity space discretization is usually obtained by including larger number of velocities as compared to the lower order models [37, 38]. Such discrete velocity models with larger number of discrete velocities are termed as higher order lattice Boltzmann models (frequently referred as HOLB model).

One may consider, LB model formulation as finding the best possible discretization in velocity space for the discrete Boltzmann equation in the low Mach number limit. Starting with this point of view, it has been shown that discrete velocity sets used in lower order LB models are roots of Gauss-Hermite quadrature [39, 40]. In case of higher order models this usual approach leads to a large velocity set [6, 38, 36]. For numerically efficient hydrodynamic simulations, one would like to work with small discrete velocity set and a regular space filling on-lattice model . In this regard, it was shown that an efficient alternate to the Gauss-Hermite quadrature is the rational number approximation for constructing a convenient on-lattice models [13, 16, 41, 42].

For example, in one-dimension a rational number approximation with 5 discrete velocities with well defined H-function and third order accurate hydrodynamic models were obtained [41]. This result was consistent with the observation that Gauss-Hermite quadrature is the best choice in terms of number of discrete velocities in 1-D, while rational number approximation are numerically more attractive as “implementation simplicity” compensates for the increase in the number of discrete velocities. However, in Refs. [13, 16, 41, 42, 43], it was pointed that in the multidimensional case tensor-product based Gauss-Hermite quadrature is suboptimal and it is possible to construct discrete velocity models (both on-lattice and off-lattice) with number of discrete velocities which are a lot less than the number of discrete velocities used in Gauss-Hermite quadrature. Ref. [43] gave an alternate framework to create discrete velocity set based on a thermodynamic interpretation to quadrature construction and showed that it is possible to find a minimal entropic lattice Boltzmann of given accuracy. As an example of such a minimal “entropic quadrature procedure”, they created an isothermal Galilean-invariant lattice Boltzmann model for micro flows with 27 discrete velocities, however, it being an off-lattice model [43].

This chapter, revisits the construction procedure for higher order lattice Boltzmann model and develops a lattice Boltzmann formulation for simulating thermo-hydrodynamics. In this chapter, a minimal lattice Boltzmann framework that requires a small number of discrete velocities in 3-D for modeling thermo-hydrodynamic is proposed. Numerical simulations have been performed and have shown to be in good agreement with the analytical results and benchmarks. The work is organized as follows: In Section 2.1, the basic set-up of discrete kinetic theory and the corresponding moment system relevant for Navier-Stokes dynamics is recalled. Then the entropic quadrature method is introduced in the Section 2.3. The entropic quadrature method is then used to derive a general form of equilibrium distribution function in terms of lattice dependent parameters in Section 2.4. The ansatzes introduced in entropic quadrature method is then used to construct the discrete velocity set in Section 2.5. The space time discretization for the present numerical scheme is discussed in Section 2.6 while the discretization of the diffusive boundary condition is presented in Section 2.6.1. Numerical results for the case of isothermal and thermal flows is covered in Section 2.7 and Section 2.8 respectively. A few important thermal simulations, like natural convection and Rayleigh Bénard convection, are studied in Section 2.8.1 and 2.8.2 respectively. Finally, in Section 2.9 we conclude the merits of the present model and summarize what has been achieved in the present work.

2.1 Discrete Kinetic Theory

In this section, the construction principles of discrete velocity models are briefly discussed in terms of an arbitrary discrete velocity model in spatial D dimension. Discrete velocity models consider fictitious particles whose permissible velocities are restricted in a discrete velocity set $\mathcal{C}$ with N_d members such that $N_d > D + 2$. In such a description, at every spatial location $\mathbf{x}$ and time t, one defines a set of discrete populations $\mathbf{f}$ of fictitious particles with the i^{th} component as $f_i(\mathbf{x}, t)$, where $i = 1, \cdots N_d$ labels discrete velocities in a set $\{\mathbf{c}_i\}$ such that each member $\mathbf{c}_i$ belongs to $\mathcal{C}$ i.e. $\mathbf{c}_i \in \mathcal{C}$. For further analysis, it is convenient to define the Euclidean inner product for two N_d dimensional vectors $\mathbf{V}_1$ and $\mathbf{V}_2$ as

$$\langle \mathbf{V}_1 | \mathbf{V}_2 \rangle = \sum_{i=1}^{N_d} V_{1i} V_{2i}. \tag{2.1}$$

An important example of such a inner product is average operator $\langle \boldsymbol{\phi}(\mathbf{c}) \rangle$ defined for any function $\boldsymbol{\phi}(\mathbf{c})$ of discrete velocities as

$$\langle \boldsymbol{\phi}(\mathbf{c}) \rangle \equiv \langle \boldsymbol{\phi}(\mathbf{c}) | \mathbf{f} \rangle = \sum_{i=1}^{N_d} \phi_i f_i, \tag{2.2}$$

where $\mathbf{c}_\alpha$ with $\alpha = x, y, z$ denotes N_d dimension vector $\{c_{1\alpha}, c_{2\alpha}, \cdots\}$.

Analogous to continuous kinetic theory, in discrete case, one defines hydrodynamic quantities viz; mass density ρ, the momentum density $\mathbf{j}$ (with velocity $u_\alpha = j_\alpha/\rho$) and the energy density E as

$$\rho = \langle \mathbf{1} \rangle, \quad \mathbf{j} = \langle \mathbf{c} \rangle, \quad E = \left\langle \frac{\mathbf{c}^2}{2} \right\rangle. \tag{2.3}$$

We restrict our discussion to the case of ideal gas where $E \equiv (\rho u^2 + D\, p)/2$ and pressure is defined via equation of state as $p = \rho\, \theta$, where the reduced temperature is $\theta = k_{\mathrm{B}} T/m$ in the unit of Boltzmann constant k_{B} and mass of the particle m. In such a description the evolution equation for the distribution function is

$$\partial_t f_i + c_{i\alpha} \partial_\alpha f_i = \Omega_i, \tag{2.4}$$

where the collision term $\boldsymbol{\Omega}$ is chosen in a way that desired conservation laws

$$\langle \boldsymbol{\Omega} \,|\, \mathbf{1} \rangle = 0, \quad \langle \boldsymbol{\Omega} \,|\, \mathbf{c} \rangle = 0, \quad \left\langle \boldsymbol{\Omega} \,|\, \mathbf{c}^2 \right\rangle = 0 \tag{2.5}$$

are recovered. In the present work, collision model which conserves mass, momentum and energy is considered and would be collectively referred as an energy conserving discrete velocity model. Here we remind that in a typical isothermal lattice Boltzmann model the energy conservation is not considered [44]. For energy conserving discrete velocity models, irrespective of details of collision model and discrete velocity set, the conservation laws are in the expected form [45]

$$\begin{aligned}
\partial_t \rho + \partial_\alpha j_\alpha &= 0, \\
\partial_t j_\alpha + \partial_\beta \left(\rho u_\alpha u_\beta + p\, \delta_{\alpha\beta} \right) + \partial_\beta \sigma_{\alpha\beta} &= 0, \\
\partial_t \left(\frac{\rho u^2}{2} + \frac{D}{2}\, p \right) + \partial_\alpha \left(\frac{\rho u_\alpha u^2}{2} + \frac{D+2}{2} p u_\alpha + \sigma_{\alpha\gamma} u_\gamma \right) + \partial_\alpha q_\alpha &= 0,
\end{aligned} \tag{2.6}$$

where $u^2 = \sum_{\alpha=1}^{D} u_\alpha^2$ is square of velocity magnitude. Here for all discrete velocity models under considerations the stress tensor $\sigma_{\alpha\beta}$, the heat flux q_α and traceless part of third order moment $Q_{\alpha\beta\gamma}$ are defined in terms of peculiar velocity $\boldsymbol{\xi}_\alpha = \mathbf{c}_\alpha - \mathbf{u}_\alpha$ as

$$\sigma_{\alpha\beta} = \left\langle \overline{\boldsymbol{\xi}_\alpha \boldsymbol{\xi}_\beta} \right\rangle, \quad q_\alpha = \left\langle \frac{\boldsymbol{\xi}^2}{2} \boldsymbol{\xi}_\alpha \right\rangle, \qquad Q_{\alpha\beta\gamma} = \left\langle \overline{\boldsymbol{\xi}_\alpha \boldsymbol{\xi}_\beta \boldsymbol{\xi}_\gamma} \right\rangle, \tag{2.7}$$

where for any symmetric second order tensor $A_{\alpha\beta}$, and symmetric third order tensor $B_{\alpha\beta\gamma}$

corresponding traceless counterparts are defined, respectively as

$$\overline{A_{\alpha\beta}} = \frac{1}{2}\left(A_{\alpha\beta} + A_{\beta\alpha}\right) - \frac{1}{D} A_{\gamma\gamma}\delta_{\alpha\beta}, \quad \overline{B_{\alpha\beta\gamma}} = B_{\alpha\beta\gamma} - \frac{B_{\alpha\kappa\kappa}\delta_{\beta\gamma} + B_{\beta\kappa\kappa}\delta_{\alpha\gamma} + B_{\gamma\kappa\kappa}\delta_{\alpha\beta}}{D+2}. \tag{2.8}$$

Assuming that discrete velocity model under consideration has enough symmetry that stress tensor and heat flux are independent variable, the evolution equation for the stress tensor $\sigma_{\alpha\beta}$ and the heat flux q_α, obtained by taking appropriate moments of Eq.(2.4), reads

$$\begin{aligned}
&\partial_t \sigma_{\alpha\beta} + \partial_\gamma\left(\sigma_{\alpha\beta} u_\gamma\right) + 2\, p\, \overline{\partial_\alpha u_\beta} + 2\, \overline{\sigma_{\alpha\gamma}\partial_\gamma u_\beta} + \partial_\gamma Q_{\alpha\beta\gamma} + \frac{4}{D+2}\overline{\partial_\alpha q_\beta} = \left\langle \boldsymbol{\Omega} \,|\, \overline{\boldsymbol{\xi}_\alpha \boldsymbol{\xi}_\beta} \right\rangle \\
&\partial_t q_\alpha + \partial_\beta \left(q_\alpha u_\beta + \frac{1}{2} R_{\alpha\beta} + \frac{R}{2\,D}\delta_{\alpha\beta} \right) + \frac{(D+2)}{2} p \partial_\alpha \frac{p}{\rho} + \frac{2}{D+2}\left(q_\gamma \partial_\alpha u_\gamma + q_\alpha \partial_\beta u_\beta\right) \\
&\qquad - \frac{\sigma_{\alpha\beta}}{\rho}\partial_\beta p + \frac{D+4}{D+2}\, q_\beta \partial_\beta u_\alpha + Q_{\alpha\beta\gamma}\partial_\beta u_\gamma - \frac{D+2}{2}\frac{p}{\rho}\partial_\beta \sigma_{\alpha\beta} - \frac{\sigma_{\alpha\kappa}}{\rho}\partial_\beta \sigma_{\kappa\beta} = \left\langle \boldsymbol{\Omega} \,\middle|\, \boldsymbol{\xi}_\alpha \frac{\boldsymbol{\xi}^2}{2} \right\rangle,
\end{aligned} \tag{2.9}$$

where relevant fourth order moments are

$$R_{\alpha\beta} = \left\langle \xi^2 \overline{\xi_\alpha \xi_\beta} \right\rangle, \quad R = \left\langle \xi^4 \right\rangle - (D+2) D \frac{p^2}{\rho}. \tag{2.10}$$

Similar to the moment chain encountered in classical kinetic theories, one sees that the evolution equations are in general not closed at the level of stress tensor and heat flux [45]. Thus, the hydrodynamic description is obtained via Chapman-Enskog analysis of the specific kinetic model [4].

The discrete kinetic equation (Eq.(2.4)) is useful for hydrodynamic modeling only if in the limit of low Knudsen number (defined as ratio of mean free time τ also called as relaxation time to characteristic time-scale L/c_{s} with L as characteristic length scale i.e. $\mathrm{Kn} = \tau\, c_s/L$) Navier-Stokes-Fourier dynamics is recovered. Thus, the dynamics of the stress tensor $\sigma_{\alpha\beta}$ and that of the heat flux q_α should be such that the following constitutive relations are obtained

$$\sigma_{\alpha\beta} = -\left(2\mu \overline{\partial_\alpha u_\beta} + \lambda \partial_\kappa u_\kappa \delta_{\alpha\beta} \right), \quad q_\alpha = -\left(k_T\, \partial_\alpha T\right), \tag{2.11}$$

in hydrodynamic limit where, μ is the coefficient of dynamic viscosity, λ is the coefficient of bulk viscosity and k_T is the thermal conductivity. In the subsequent sections, we analyze the conditions on the discrete velocity model which leads to these desired asymptotic form for the heat flux and stress tensor at least in the low Mach number limit.

2.2 Hydrodynamic Limit via Chapman-Enskog Analysis

In this section, the hydrodynamic limit of the discrete velocity models is studied via Chapman-Enskog analysis [44, 46]. In this procedure, for any arbitrary kinetic model, as a first step one expands a higher order moment say M^{Fast} in power of smallness parameter Kn as

$$M^{\mathrm{Fast}} = M^{\mathrm{eq}}\left(\rho, \mathbf{j}, p\right) + \mathrm{Kn}\, M^{(1)} + \cdots, \tag{2.12}$$

which is basically an expansion around the equilibrium value of the corresponding moment M at zero velocity and reference temperature θ_0. In the present context M^{Fast} is

$$M^{\text{Fast}} = \{\sigma_{\alpha\beta}, Q_{\alpha\beta\gamma}, q_\alpha, R_{\alpha\beta}, R, \cdots\}\,, \tag{2.13}$$

with $\cdots$ representing other higher order moments. Furthermore, time derivative of any quantity ϕ is also expanded in powers of Knudsen number as

$$\partial_t \phi = \partial_t^{(0)}\phi + \text{Kn}\,\partial_t^{(1)}\phi + \cdots \tag{2.14}$$

where for computing derivative of order n for hydrodynamic variables, conservation laws (Eq.(2.6)) is used. For example, the $\mathcal{O}(1)$ hydrodynamics defines zeroth order time derivative as

$$\begin{aligned} \partial_t^{(0)}\rho + \partial_\alpha j_\alpha &= 0, \\ \partial_t^{(0)} j_\alpha + \partial_\beta\left(\rho u_\alpha u_\beta + p\,\delta_{\alpha\beta}\right) &= -\partial_\beta \tilde{\sigma}_{\alpha\beta}, \\ \partial_t^{(0)}\left(\frac{\rho u^2}{2} + \frac{D}{2}p\right) + \partial_\alpha\left(\frac{\rho u_\alpha u^2}{2} + \frac{D+2}{2}p u_\alpha\right) &= -\partial_\alpha\left(\tilde{\sigma}_{\alpha\gamma}u_\gamma + \tilde{q}_\alpha\right), \end{aligned} \tag{2.15}$$

where for any quantity ϕ, $\tilde{\phi} = \phi^{\text{eq}} - \phi^{\text{MB}}$ denotes the departure of discrete equilibrium value from Maxwell-Boltzmann value. Eq. (2.15) is equivalent to Euler description up to $\mathcal{O}(\text{Ma}^2)$ provided that the departure of equilibrium values obtained from discrete velocity model for the stress tensor and heat flux, has an expansion in Mach number of the form

$$\tilde{\sigma}_{\alpha\gamma} = \text{Ma}^3\,\tilde{\sigma}^{(3)}_{\alpha\gamma} + \cdots\,, \qquad \tilde{q}_\alpha = \text{Ma}^3\,\tilde{q}^{(3)}_\alpha + \cdots\,, \tag{2.16}$$

where the superscript, say for e.g. (l), denotes the corresponding l^{th} order expansion coefficient in power of Mach number.

In order to analyze closure for the stress tensor and heat flux at Navier-Stokes-Fourier level, we need to analyze the first correction from Euler value. For convenience without loss of generality, we will restrict out attention to the BGK collision form [23]

$$\mathbf{\Omega}_i = -\frac{1}{\tau}\left(f_i - f_i^{eq}(\rho, \mathbf{j}, p)\right), \tag{2.17}$$

where the element f_i^{eq} of vector $\mathbf{f}^{\text{eq}}$ is chosen such that

$$\langle \mathbf{1}\,|\,\mathbf{f}^{\text{eq}}\rangle = \rho, \quad \langle \mathbf{c}_\alpha\,|\,\mathbf{f}^{\text{eq}}\rangle = j_\alpha, \quad \left\langle \frac{\mathbf{c}^2}{2}\,|\,\mathbf{f}^{\text{eq}}\right\rangle = E. \tag{2.18}$$

With this choice of the collision model, the stress tensor and heat flux at first order using

Eq. (2.9) are in Navier-Stokes form

$$\begin{aligned}
&2\,\mu\overline{\partial_\alpha u_\beta} + \tau\,\left(\partial_t^{(0)}\tilde{\sigma}_{\alpha\beta} + \partial_\gamma\left(\tilde{\sigma}_{\alpha\beta}u_\gamma\right) + 2\,\overline{\tilde{\sigma}_{\alpha\gamma}\partial_\gamma u_\beta} + \partial_\gamma\tilde{Q}_{\alpha\beta\gamma} + \frac{4}{D+2}\overline{\partial_\alpha\tilde{q}_\beta}\right) = -\mathrm{Kn}\,\tilde{\sigma}^{(1)}_{\alpha\beta},\\
&\kappa\partial_\alpha\frac{p}{\rho} + \tau\,\left(\partial_t^{(0)}\tilde{q}_\alpha + \partial_\beta\left(\tilde{q}_\alpha u_\beta + \frac{1}{2}\tilde{R}_{\alpha\beta}\right) + \frac{2}{D+2}\left(\tilde{q}_\gamma\partial_\alpha u_\gamma + \tilde{q}_\alpha\partial_\beta u_\beta\right)\right)\\
&+\tau\,\left(\partial_\alpha\left(\frac{\tilde{R}}{2\,D}\right) - \frac{\tilde{\sigma}_{\alpha\beta}}{\rho}\partial_\beta p + \frac{D+4}{D+2}\,\tilde{q}_\beta\partial_\beta u_\alpha + \tilde{Q}_{\alpha\beta\gamma}\partial_\beta u_\gamma - \frac{D+2}{2}\frac{p}{\rho}\partial_\beta\tilde{\sigma}_{\alpha\beta} - \frac{\tilde{\sigma}_{\alpha\kappa}}{\rho}\partial_\beta\tilde{\sigma}_{\kappa\beta}\right) = -\mathrm{Kn}\,\tilde{q}^{(1)}_\alpha,
\end{aligned}\tag{2.19}$$

with dynamic viscosity as $\mu = p\,\tau$, thermal conductivity as $\kappa = \mu(D+2)/2$ and similar to continuous kinetic theory, time derivative of higher order moment at any order is evaluated via chain rule using dependence on hydrodynamic variables. Thus, for an energy conserving model, Eq. (2.16) could be revised to take into account order of temperature perturbation $\Delta\theta = \theta/\theta_0 - 1$ which is the deviation from reference temperature θ_0 as

$$\begin{aligned}
\tilde{\sigma}_{\alpha\gamma} &= \mathrm{Ma}^3\,\tilde{\sigma}^{(3)}_{\alpha\gamma} + \left(\mathrm{Ma}^3, \Delta^2\theta\right)\,\tilde{\sigma}^{(3)}_{\alpha\gamma} + \left(\mathrm{Ma}^3, \Delta^3\theta\right)\,\tilde{\sigma}^{(3)}_{\alpha\gamma} + \cdots\,,\\
\tilde{q}_\alpha &= \mathrm{Ma}\,\tilde{q}^{(1)}_\alpha + \left(\mathrm{Ma}, \Delta^2\theta\right)\,\tilde{q}^{(1)}_\alpha + \left(\mathrm{Ma}^2, \Delta^2\theta\right)\,\tilde{q}^{(2)}_\alpha + \cdots\,,
\end{aligned}\tag{2.20}$$

These expressions (Eq. (2.19) and (2.20)) shows that Navier-Stokes-Fourier dynamics is recovered provided

$$\begin{aligned}
\tilde{\sigma}_{\alpha\gamma} =& \mathrm{Ma}^3\,\tilde{\sigma}^{(3)}_{\alpha\gamma},\\
\tilde{Q}_{\alpha\beta\gamma} =& \left(\mathrm{Ma}, \Delta^2\theta\right)\,\tilde{Q}^{(1)}_{\alpha\beta\gamma} + \cdots\,,\\
\tilde{q}_\alpha =& \left(\mathrm{Ma}, \Delta^3\theta\right)\,\tilde{q}^{(1)}_\alpha + \cdots\,,\\
\tilde{R}^{\mathrm{eq}}_{\alpha\gamma} =& \Delta^3\theta\,\tilde{R}^{(3)}_{\alpha\gamma} + \cdots\,,\\
\tilde{R} =& \Delta^3\theta\,\tilde{R}^{(3)} + \cdots
\end{aligned}\tag{2.21}$$

Thus, one sees that Eq. (2.21) defines minimum requirements on the discrete velocity model for mimicking Navier-Stokes-Fourier dynamics. In subsequent sections, it will be shown that indeed one can find a discrete velocity model with desirable properties of Eq. (2.21) (see Eq. (2.46))

An important conclusion from the current analysis is that to get correct temperature dynamics and thus get a correct energy equation it is sufficient that third order moment be accurate up to $\mathcal{O}(\mathrm{Ma}^2)$ rather than $\mathcal{O}(\mathrm{Ma}^2)$ (see for example Ref. [15, 47, 48, 43], where $Q_{\alpha\beta\gamma}$ were obtain correct up to $\mathcal{O}(\mathrm{Ma}^3)$). However, for getting correct temperature dynamics one needs to get terms of $\mathcal{O}\left(\mathrm{Ma}^2, \Delta^2\theta\right)$ correct . Here, it should be noted that going by the existing approach in the literature if one tries to obtain $R_{\alpha\beta}$ and R to a high order accuracy, then one requires a large velocity set with enough isotropy and symmetry so as to to recover simultaneously all the second, third, fourth order moments correctly. Present analysis has shown that such a higher order isotropy is not needed to get a $\mathcal{O}(\mathrm{Ma}^2)$ correct hydrodynamics.

2.3 Entropic Quadrature Method

In this section, we briefly review the recently proposed entropic quadrature method [43] for the construction of discrete velocity models with desirable properties of accuracy and stability. In this formulation, the following ansatzes are taken as the starting point for the model construction

1. **Discrete H-function:** There exists a discrete H-function of the Kullback form [49]

$$H = \sum_{i=1}^{N_d} f_i \left(\ln \left(\frac{f_i}{w_i} \right) - 1 \right) \qquad w_i > 0, \tag{2.22}$$

   where the weights w_i are unknown positive numbers such that

$$\sum_{i=1}^{N_d} w_i = 1, \quad \sum_{i=1}^{N_d} w_i \, y_i = D, \tag{2.23}$$

   and $y_i = c_i^2/\theta_0$ with θ_0 as some reference temperature. Eq. (2.23) provides normalization for the weights w_i and ensures that they physically corresponds to discrete equilibrium at reference state (see Eq. (2.27)). In this formulation, similar to the continuous kinetic theory f_i^{eq} is defined as the minimum of discrete H-function under the constraints of conservation of mass, momentum and energy. This implies

$$f_i^{\mathrm{eq}} = w_i \rho A B_{ix}^{c_{ix}/\sqrt{\theta_0}} \, B_{iy}^{c_{iy}/\sqrt{\theta_0}} \, B_{iz}^{c_{iz}/\sqrt{\theta_0}} \, \Gamma^{c_i^2/\theta_0}, \tag{2.24}$$

   with

$$A = \frac{1}{\rho} \exp{(\alpha)}, \quad B_{i\kappa} = \exp{\left(\beta_{i\kappa} \sqrt{\theta_0}\right)}, \quad \Gamma = \exp{(\gamma \theta_0)} \tag{2.25}$$

   where α, β_κ and γ are the Lagrange multipliers associated with the mass, momentum and energy conservation, respectively.

2. **Energy dependent Weights:** Similar to all existing LB models, it is assumed that discrete weights are function of c_i^2 only. This condition is motivated from Maxwell-Boltzmann expression at zero velocity and reference temperature.

3. **Closure under Inversion:** If a discrete velocity, $\mathbf{c}_i \equiv (c_{ix}, c_{iy}, c_{iz})$ is an element of the set i.e. $\mathbf{c}_i \in \mathcal{C}$, then inverse of it is also in the set $-\mathbf{c}_i \in \mathcal{C}$. This implies for any natural numbers m, n and p

$$\sum_{i=1}^{N_d} w_i c_{ix}^{2n+1} c_{iy}^{2m+1} c_{iz}^{2p+1} = 0. \tag{2.26}$$

   This symmetry along with Eq.(2.23) ensures that weights are zero velocity equilibrium at some non–zero reference temperature θ_0 as

$$f_i^{\mathrm{eq}}(\mathbf{u} = 0, \theta = \theta_0) = w_i \rho. \tag{2.27}$$

   At this point, we enforce the desired conditions on moments (Eq.(2.16) and (2.21)) which requires at reference temperature $\theta = \theta_0$ and velocity $\mathbf{u} = 0$

$$\sum_{i=1}^{N_d} w_i \, y_i (y_i - 1) = D(D+1). \tag{2.28}$$

This condition is obtained from the consideration for contracted fourth order moment R at zero velocity and some non–zero reference temeprature for a discrete model i.e. $\sum_{i=1}^{N_d} w_i \, y_i^2 = D(D+2)$ needed for correct Navier-Stokes-Fourier dynamics (see Eq. (2.21)).

4. **Closure under Reflection:** If a discrete velocity, $\mathbf{c}_i \equiv (c_{ix}, c_{iy}, c_{iz})$ is an element of the set i.e. $\mathbf{c}_i \in \mathcal{C}$, then all possible reflection of it are also a member of the set (i.e. $(\bar{c}_{ij}, \bar{c}_{ik}, \bar{c}_{il}) \in \mathcal{C}$), where $\bar{c}_i$ is such that jth component of it i.e. $\bar{c}_{ij}$ is chosen via possible permutation of the original velocity vector. This implies for any natural numbers m and n

$$\begin{gathered}\sum_{i=1}^{N_d} w_i c_{ix}^{2n} = \sum_{i=1}^{N_d} w_i c_{iy}^{2n} = \sum_{i=1}^{N_d} w_i c_{iz}^{2n}, \\ \sum_{i=1}^{N_d} w_i c_{ix}^{2n} c_{iy}^{2m} = \sum_{i=1}^{N_d} w_i c_{ix}^{2n} c_{iz}^{2m} = \sum_{i=1}^{N_d} w_i c_{iy}^{2n} c_{iz}^{2m}.\end{gathered} \tag{2.29}$$

This condition of isotropy ensures that there is no preference on any specific i^{th} direction. An important consequence of Eq. (2.29) along with Eq.(2.23) is that

$$\sum_{i=1}^{N_d} w_i y_i^n c_{i\alpha} c_{i\beta} = \frac{1}{D} \delta_{\alpha\beta} \, \theta_0 \sum_{i=1}^{N_d} w_i y_i^{n+1} \quad \text{for} \quad n = 0, 1, 2, 3, ... \tag{2.30}$$

These ansatzes reduce the available degrees of freedom for the construction of discrete velocity models [43]. Before deriving discrete velocities required for thermal hydrodynamics, we derive equilibrium distribution for discrete velocity models satisfying these ansatzes.

2.4 Evaluation of Discrete Equilibrium Distribution

The inversion of Lagrange multipliers in Eq. (2.25) is a difficult task and explicit expressions are in general not possible. However, for numerical computation often it is possible to build a series expression around some reference solution. In this section, such a procedure for the current model is followed to develop equilibrium distribution for an arbitrary discrete velocity model.

- The Lagrange multipliers can be found perturbatively as a solution of following set of equations

$$\sum_i^{N_d} f_i^{\text{eq}} = \rho, \quad \sum_i^{N_d} f_i^{\text{eq}} c_{i\kappa} = \epsilon \, \rho u_\kappa, \quad \sum_i^{N_d} f_i^{\text{eq}} \frac{c_i^2}{2} = \epsilon^2 \rho \, u^2 + D \, \rho \, \theta, \tag{2.31}$$

  where smallness parameter ϵ physically corresponds to Mach number.

- Similar to isothermal hydrodynamics, it is straightforward to see that the Lagrange multiplier associated with the momentum conservation is $B_{i\kappa} = 1$ i.e $\beta_\kappa = 0$ at the reference state [5, 6] (see Eq.(A.1) in appendix A). However, unlike isothermal hydrodynamics, this information is not sufficient to build perturbation expansion of Lagrange multipliers. Thus, for further analysis, we rewrite zero velocity equilibrium (hereafter referred as $\bar{f}_i^{\mathrm{eq}}$) as

$$\bar{f}_i^{\mathrm{eq}} \equiv f_i^{\mathrm{eq}}(\rho, \mathbf{u} = 0, \theta) = w_i \rho A_0 \, z_i, \tag{2.32}$$

where $z_i = \Gamma_0^{y_i}$ and subscript zero for Lagrange multipliers is introduced to indicate that the Lagrange multipliers correspond to $\mathbf{u} = 0$.

- The zero velocity equilibrium (Eq.(2.32)) is found pertubatively by noticing that we do know the solution at the reference temperature θ_0 (Eq.(2.27)). In order to build a pertubative solution, Eq.(2.31) is rewritten for zero velocity case as

$$\sum_{i=1}^{N_d} w_i \, z_i = {A_0}^{-1}, \qquad \sum_{i=1}^{N_d} w_i \, z_i \, y_i = D\,(1 + \Delta\theta) \sum_{i=1}^{N_d} w_i \, z_i, \tag{2.33}$$

which can be solved pertubatively in powers of $\Delta\theta$.

- The zero velocity equilibrium obtained via solving Eq. (2.33) reads (for details see appendix A)

$$\begin{aligned}
\bar{f}_i^{\mathrm{eq}} = w_i \rho \Bigg[& 1 + \frac{\Delta\theta}{2}(y_i - 3) + \frac{\Delta^2\theta}{8}\left(15 - 10y_i + y_i^2\right) + \frac{\Delta^3\theta}{48}\left(-105 + 105y_i - 21y_i^2 + y_i^3\right) + \\
& \frac{\Delta^4\theta}{384}\left(945 - 1260y_i + 378y_i^2 - 36y_i^3 + y_i^4\right) + \\
& (y_i - 3)\underline{\left(-h_3\frac{\Delta^2\theta}{48} + \frac{\Delta^3\theta}{48}\left(\frac{h_3^2}{12} - \frac{h_4}{6}\right) - h_3^3\frac{\Delta^4\theta}{5529.6} - h_5\frac{\Delta^4\theta}{2304} + h_3\,h_4\frac{\Delta^4\theta}{1382.4}\right)} \\
& + \frac{\Delta^3\theta}{48}\left(\underline{\frac{h_3}{2}\left(-35 + 16y_i - y_i^2\right)}\right) + \frac{\Delta^4\theta}{384}\left(\underline{\frac{h_3^2}{12}\left(267 - 110y_i + 5y_i^2\right)}\right) + \\
& \frac{\Delta^4\theta}{384}\left(\underline{\frac{h_3}{18}\left(8163 - 4881y_i + 594y_i^2 - 18y_i^3\right)}\right) + \frac{\Delta^4\theta}{384}\left(\underline{\frac{h_4}{6}\left(-153 + 69y_i - 4y_i^2\right)}\right) + \dots \Bigg]
\end{aligned} \tag{2.34}$$

where, $\Delta^n\theta$ should be read as an n^{th} power of $\Delta\theta$ i.e. $(\Delta\theta)^n$. The underlined part represents the residues or deviations from the expected discrete projections of f^{MB} i.e. f_i^{MB} in terms of lattice dependent parameter h_n's defined as

$$h_n = \sum_{i=1}^{N_d} w_i \prod_{k=1}^{n}(y_i - k + 1) - \int e^{-y_i} \prod_{k=1}^{n}(y_i - k + 1)\, d\mathbf{c} \tag{2.35}$$

- Finally, the equilibrium distribution at finite velocity can be obtained via solving Eq.(2.31) pertubatively with Eq.(2.34) as reference point solution. In explicit form the equilibrium is (see appendix A for details)

$$f_i^{\mathrm{eq}} = \bar{f}_i^{\mathrm{eq}} \left[1 + \frac{u_\alpha c_{i\alpha}}{\theta} - \frac{u^2}{2\theta}\left(1 - \hat{h}_4\right) + \frac{1}{2}\left(\frac{u_\kappa c_{i\kappa}}{\theta}\right)^2 + \dots \right]. \tag{2.36}$$

where, $\hat{h}_4$ is a non dimensional lattice dependent constant defined as

$$\hat{h}_4 = \frac{\bar{h}_4 \left(\frac{\theta_0}{\theta}\right)^2}{\frac{\bar{h}_4}{3}\left(\frac{\theta_0}{\theta}\right)^2 + 2} \tag{2.37}$$

and $\bar{h}_4$ is

$$\begin{aligned}\bar{h}_4 = \Bigg[& h_3 \frac{\Delta\theta}{6} + \frac{\Delta^2\theta}{144}\left(-84h_3 - h_3^2 + 6h_4\right) + \frac{\Delta^3\theta}{1728}\left(1308h_3 + 120h_3^2 + h_3^3 - 252h_4 - 8h_3h_4 + 12h_5\right) \\ & + \frac{\Delta^4\theta}{384 \times 216}\left(-49104h_3 - 23988h_3^2 - 780h_3^3 - 5h_3^4 + 20016h_4 + 3396h_3h_4\right) + \\ & \frac{\Delta^4\theta}{384 \times 216}\left(50h_3^2h_4 - 48h_4^2 - 2232h_5 - 84h_3h_5 + 72h_6\right)\Bigg],\end{aligned} \tag{2.38}$$

see appendix A for details. From the knowledge of the equilibrium distribution, we can represent Eq.(2.16) and Eq.(2.21) in terms of lattice dependent parameters as

$$\begin{aligned}\tilde{\sigma}_{\alpha\beta} = & -\hat{h}_4 \frac{\rho u^2}{3}\delta_{\alpha\beta} + \left(k_1 + \frac{\Delta\theta}{2}k_2\right)\frac{\rho\, u_\kappa u_\gamma}{2(\theta/\theta_0)^2}\left(\Delta_{\alpha\beta\kappa\gamma} - 5\delta_{\alpha\beta\kappa\gamma}\right), \\ \tilde{Q}_{\alpha\beta\gamma} = & \left(k_1 + \frac{\Delta\theta}{2}k_2 + \frac{\Delta^2\theta}{8}\left(k_3 - \frac{h_3}{6}k_2\right)\right)\frac{\rho\, u_\kappa}{\theta}\left(\Delta_{\alpha\beta\kappa\gamma} - 5\delta_{\alpha\beta\kappa\gamma}\right)\theta_0^2 + \\ & \bar{h}_4\left(\frac{\rho\, u_\kappa}{\theta}\right)\delta_{\alpha\beta\gamma\kappa}\,\theta_0^2, \\ \tilde{q}_\alpha = & \frac{1}{2}\left(\frac{\rho\, u_\alpha}{\theta}\right)\theta_0^2\,\bar{h}_4, \quad \tilde{R}_{\alpha\beta} = \rho\,\theta_0^2\,\delta_{\alpha\beta}\,\bar{h}_4, \quad \tilde{R} = \rho\,\theta_0^2\,3\,\bar{h}_4,\end{aligned} \tag{2.39}$$

where $\delta_{\alpha\beta\gamma\kappa}$ denotes fourth order Kronecker delta and the non-dimensional numbers k_1, k_2 and k_3 are defined as

$$\begin{aligned} k_1 &= \left\langle w_i, \frac{c_{ix}^2 c_{iy}^2}{\theta_0^2} - 1\right\rangle, \\ k_2 &= \left\langle w_i, \frac{c_{ix}^2 c_{iy}^2}{\theta_0^2}\left(y_i - 3\right) - 4\right\rangle, \\ k_3 &= \left\langle w_i, \frac{c_{ix}^2 c_{iy}^2}{\theta_0^2}\left(15 - 10\,y_i + y_i^2\right) - 8\right\rangle \end{aligned} \tag{2.40}$$

Thus, it is possible to get correct hydrodynamics till $\mathcal{O}(\mathrm{Ma}^2)$ and correct temperature dynamics till $\mathcal{O}(\Delta^2\theta)$ if

$$\{k_1, k_2, h_1, h_2, h_3, h_4\} \to 0 \tag{2.41}$$

These expressions define the requirements on the discrete velocity model for mimicking Navier-Stokes-Fourier (NSF) dynamics in terms of the leading order errors in the kinetic moments. Due to the symmetry of lattices under consideration, Eq. (2.41) reduces to

$$\begin{aligned}\sum_i^{N_d} w_i = 1, \quad \sum_i^{N_d} w_i c_{ix}^2 = \theta_0, \quad \sum_i^{N_d} w_i c_{ix}^2 c_{iy}^2 = \theta_0^2, \quad \sum_i^{N_d} w_i c_{ix}^4 = 3\,\theta_0^2,\\ \sum_i^{N_d} w_i c_i^4 (c_{ix}^2) = 35\,\theta_0^3, \quad \sum_i^{N_d} w_i c_i^8 = 945\,\theta_0^4\end{aligned} \tag{2.42}$$

Thus, the constraints stated in Eq. (2.42) represents a system of 6 scalar equations to solve for the present case to construct a 3-D thermal higher order LB model. Here, it needs to be noted that while procedure described in literature will reduce to a system of 23 simultaneous non-linear equations. Thus, current formulation leads to a substantial reduction on degree of freedom required for a discrete velocity model to represent thermo-hydrodynamics in a meaningful fashion. In the next section, Eq. (2.42) will be solved simultaneously to obtainNavier-Stokes a discrete velocity set.

2.5 $D3Q33$ Model for Thermo-hydrodynamics

In the present section, we follow Ref.[43], to construct discrete velocity model which satisfies the ansatzes of entropic quadrature method. In this procedure, one starts with elementary shells of type simple cubic (SC), body centred cubic (BCC) and face centred cubic (FCC), to construct discrete model. However, unlike Ref.[43], to obtain an on-lattice model and satisfy Eq.(2.42) we add an extra elementary shell. Thus, we start with 5 elementary shells (see Fig.2.1)

- Zero velocity shell with weight w_0,
- a BCC shell with weight w_d and spacing d,
- a FCC shell with weight w_b and spacing $b = \bar{m}\, d$, where $\bar{m}$ is the ratio of unit cell spacing between FCC and BCC.
- Two SC shells with weights w_{a_1}, w_{a_2} and spacing $a_1 = \bar{m}_1\, d$, $a_2 = \bar{m}_2\, d$ respectively, where $\bar{m}_1$ and $\bar{m}_2$ represents the ratio of unit cell spacings of SC and BCC.

We have to solve a system of six non-linear equations (Eq (2.42)) with 9 unknowns. Thus, we can chose 3 variables in an arbitrary fashion. We have chosen $\bar{m} = 2$, $\bar{m}_1 = 3$ and $\bar{m}_2 = 1$, which leads to a system of 6 non-linear equations in six variables.

$$\begin{aligned} w_0 + 6w_{a_1} + 6w_{a_2} + 12w_b + 8w_d &= 1,\\ 2{a_1}^2 w_{a_1} + 2{a_2}^2 w_{a_2} + 8b^2 w_b + 8d^2 w_d &= \theta_0,\\ 2{a_1}^4 w_{a_1} + 2{a_2}^4 w_{a_2} + 8b^4 w_b + 8d^4 w_d &= 3\,\theta_0^2,\\ 4b^4 w_b + 8d^4 w_d &= \theta_0^2,\\ 2{a_1}^6 w_{a_1} + 2{a_2}^6 w_{a_2} + 32b^6 w_b + 72d^6 w_d &= 35\,\theta_0^3,\\ 6{a_1}^8 w_{a_1} + 6{a_2}^8 w_{a_2} + 192b^8 w_b + 648d^8 w_d &= 945\,\theta_0^4,\end{aligned} \tag{2.43}$$

with the condition that $w_i > 0$. Thus, one is solving here a set of non–linear simultaneous equations which may have infinitely many solutions. These solutions could be real and imaginary. As, magnitudes of velocities and weights are real, the the complex roots are discarded and even among the real roots only those are selected that meet the criteria of $w_i > 0$. Thus, the solution set is narrowed down to fewer roots (for e.g. in Ref. [43] there were two sets of possible solution). In the present case, the set of equations in (2.43) were found to have unique solution with the value of reference velocity found out to be $d = 1.1257022876352714$ with each $w_i > 0$. The weights and the magnitudes of discrete velocities are given in Table 2.1.

Shells	Stride	Weight
$SC-3$	$3d$	0.00671160426630702
$SC-1$	d	0.04156302642478303
$FCC-2$	$2d$	0.00117298924397337
$BCC-1$	d	0.06845841452356295

Table 2.1: Energy shells in the velocity ratio $(3:1:2:1)\,d$ and their corresponding weights

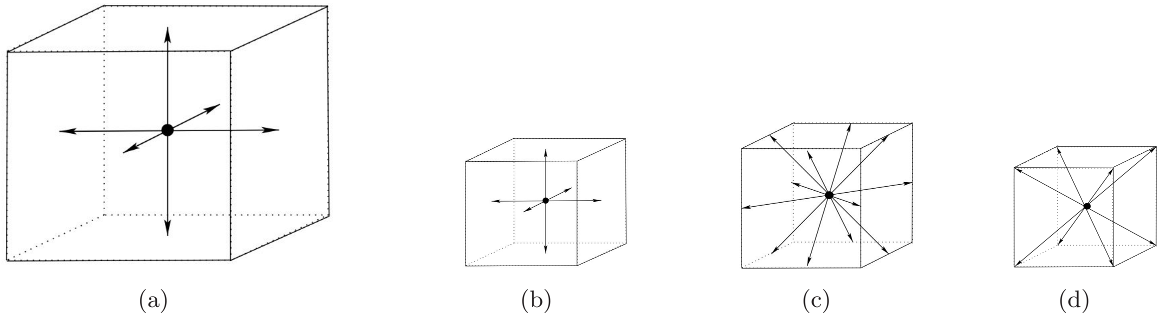

Figure 2.1: (a) SC-3 (b) SC-1 (c) FCC-2 and (d) BCC as building blocks of LB

Note that, we have decided to measure unit cell of BCC as the the reference velocity in terms of which the magnitudes of velocities for other shells is characterized. This choice is motivated by idea that even in multi-speed lattice inter-node communication can be kept to a minimum provided grid connectivity is as compact as possible. Here, we remind that BCC require interaction between nearest as well as next nearest and next to next nearest neighbor too. Thus, multi-speed with BCC will have much larger communication cost and should be avoided.

Finally, substituting lattice dependent parameters in Eq (2.34) and (2.36) to obtain the following equilibrium expressions for the current model as

$$f_i^{\mathrm{eq}} = \bar{f}_i^{\mathrm{eq}}\left[1 + \frac{u_\alpha c_{i\alpha}}{\theta} - \frac{u^2}{2\theta} + \frac{1}{2}\left(\frac{u_\kappa c_{i\kappa}}{\theta}\right)^2\right] \tag{2.44}$$

where the zero velocity equilibrium $\bar{f}_i^{\mathrm{eq}}$ is

$$\begin{aligned}\bar{f}_i^{\mathrm{eq}} =& w_i\rho\Bigg[1 + \frac{\Delta\theta}{2}\left(y_i-3\right) + \frac{\Delta^2\theta}{8}\left(15-10y_i+y_i^2\right) + \frac{\Delta^3\theta}{48}\left(-105+105y_i-21y_i^2+y_i^3\right) + \\ & \frac{\Delta^4\theta}{384}\left(945-1260y_i+378y_i^2-36y_i^3+y_i^4\right) - \frac{\Delta^4\theta}{384}\left(\frac{h_5}{6}\left(y_i-3\right)\right)\Bigg],\end{aligned} \tag{2.45}$$

with this expression for equilibrium, residual moments for the present model are

$$\begin{aligned}\tilde{\sigma}_{\alpha\beta} = 0, \quad \tilde{q}_\alpha &= \left(\frac{\Delta^3\theta}{48}h_5\right)\frac{\rho\,u_\alpha}{\theta}\theta_0^2,\\ \tilde{Q}_{\alpha\beta\gamma} &= \left(k_3\frac{\Delta^2\theta}{8}\right)\frac{\rho\,u_\kappa}{\theta}\left(\Delta_{\alpha\beta\kappa\gamma} - 5\delta_{\alpha\beta\kappa\gamma}\right)\theta_0^2 + \left(h_5\frac{\Delta^3\theta}{24}\right)\frac{\rho\,u_\kappa}{\theta}\delta_{\alpha\beta\gamma\kappa}\,\theta_0^2,\\ \tilde{R}_{\alpha\beta} &= \left[\frac{\Delta^3\theta}{48}\left(2h_5\right) + \frac{\Delta^4\theta}{384\times 216}\left(-2232h_5+72h_6\right)\right]\rho\,\theta_0^2\,\delta_{\alpha\beta},\\ \tilde{R} &= 3\left[\frac{\Delta^3\theta}{48}\left(2h_5\right) + \frac{\Delta^4\theta}{384\times 216}\left(-2232h_5+72h_6\right)\right]\rho\,\theta_0^2.\end{aligned} \tag{2.46}$$

Indeed, one can see that the leading order terms that we get in the residues above are the lattice dependent parameters k_3, h_5, h_6 that we haven't been able to fix. However, these moments still gives correct temperature dynamics till $\mathcal{O}(\Delta^2\theta)$ as the leading order term in $\tilde{q}_\alpha$ starts at $\mathcal{O}(\Delta^3\theta)$. From the equilibrium distribution functions Eq (2.44) it can also be seen that the H-theorem is obeyed till $\mathcal{O}(\mathrm{Ma}^3)$ and $\mathcal{O}(\Delta^4\theta)$.

2.6 Space-time Discretization

In the present section, the discretization of evolution equation for the distribution function f_i and the boundary condition for a multi-speed discrete velocity model is discussed. In LB method, the discrete kinetic equation with a body force term is modeled as

$$\partial_t f_i + c_{i\alpha}\partial_\alpha f_i = -\frac{1}{\tau}\left(f_i - f_i^{eq}(\rho,\mathbf{u},\theta)\right) + \rho\,w_i\frac{g_\alpha\,c_{i\alpha}}{\theta_0}. \tag{2.47}$$

where, g_α is the discrete body force per unit mass [50, 51, 52, 53, 54] and $\tau = \mu/p$ based on Chapmann-Enskog expansion. The diffusive wall boundary condition in discrete form [55] is represented as

$$f_i\left(\mathbf{x},t\right)\big|_{\mathbf{c}\cdot\mathbf{n}>0} = \frac{\tilde{\mathrm{F}}_{\mathrm{out}}\left(\mathbf{x},t\right)}{\tilde{\mathrm{F}}^{\mathrm{eq}}_{\mathrm{in}}\left(\mathbf{x},t\right)}f_i^{eq}(1,\mathbf{U}_{\mathrm{wall}},\theta_{\mathrm{wall}}), \tag{2.48}$$

where $\mathbf{n}\left(\mathbf{x},t\right)$ is the normal at the wall directed into the fluid domain, $\mathbf{U}_{wall}$ is the wall velocity and θ_{wall} is the wall temperature (see Fig. 2.2). While $\tilde{\mathrm{F}}_{\mathrm{out}}\left(\mathbf{x},t\right)$ is the net flux going out of the domain and $\tilde{\mathrm{F}}^{\mathrm{eq}}_{\mathrm{in}}\left(\mathbf{x},t\right)$ is the net incoming flux calculated at the wall velocity and temperature.

These fluxes are defined as

$$\begin{aligned}\tilde{\mathrm{F}}_{\mathrm{out}}\left(x,y,z,t\right) &= \sum\nolimits_{\mathbf{c}_j\cdot\mathbf{n}<0}|(\mathbf{c}_j\cdot\mathbf{n})|f_j,\\ \tilde{\mathrm{F}}^{\mathrm{eq}}_{\mathrm{in}}\left(x,y,z,t\right) &= \sum\nolimits_{\mathbf{c}_j\cdot\mathbf{n}<0}|(\mathbf{c}_j\cdot\mathbf{n})|f^{eq}_j\left(1,\mathbf{U}_{\mathrm{wall}},\theta_{\mathrm{wall}}\right).\end{aligned} \tag{2.49}$$

In order to implement equation (2.47), we integrate it along the characteristic using trapezoidal rule, to obtain the evolution equation as (see Ref. [56] for proof)

$$\tilde{f}_i\left(\mathbf{x}+\mathbf{c}_i\,\Delta t,t+\Delta t\right)=\tilde{f}_i\left(\mathbf{x},t\right)+2\,\beta\,\left(\tilde{f}^{\mathrm{eq}}_i(\rho,\tilde{\mathbf{u}},\theta)-\tilde{f}_i\right)+2\,\beta\,\left(\rho\,w_i\frac{g_\alpha\,c_{i\alpha}}{\theta_0}\right), \tag{2.50}$$

where $\beta=\Delta t/(2\tau+\Delta t)$ and the transformation $\tilde{f}_i$ is an auxiliary population defined at location $(\mathbf{x})$ and time t as

$$\tilde{f}_i=f_i-\frac{\Delta t}{2\tau}\left(f^{\mathrm{eq}}_i-f_i\right)-\frac{\Delta t}{2}\left(\rho\,w_i\frac{g_\alpha\,c_{i\alpha}}{\theta_0}\right) \tag{2.51}$$

and the modified velocity $\tilde{\mathbf{u}}$ defined as

$$\tilde{u}_\alpha=u_\alpha\left(\tilde{f}_i\right)+\frac{\Delta t}{2}g_\alpha \tag{2.52}$$

Eq. (2.50) is then written as being made of collision with post-collision distribution functions $(\tilde{f}^{\star}_i)$ written as

$$\tilde{f}^{\star}_i\left(\mathbf{x},t\right)=\tilde{f}_i\left(\mathbf{x},t\right)+2\,\beta\,\left(\tilde{f}^{\mathrm{eq}}_i\left(\rho,\tilde{\mathbf{u}},\theta\right)-\tilde{f}_i\left(\mathbf{x},t\right)\right)+2\,\beta\,\left(\rho\,w_i\frac{g_\alpha\,c_{i\alpha}}{\theta_0}\right) \tag{2.53}$$

and in advection the computed $\tilde{f}^{\star}_i$'s are streamed as

$$\tilde{f}_i\left(\mathbf{x},t+\Delta t\right)=\tilde{f}^{\star}_i\left(\mathbf{x}-\mathbf{c}_i\,\Delta t,t\right), \tag{2.54}$$

where for the present case we choose $\Delta\mathrm{x}=\Delta\mathrm{y}=\Delta\mathrm{z}=d\Delta\mathrm{t}$. Thus, one can see that due to on-lattice model the space discretization is exact and the time stepping is second order accurate. The next step is to model the boundary condition for the present multi-speed model which is discussed in the next sub-section.

2.6.1 Discretized Diffusive Boundary Condition

In this section, discretization of the diffusive boundary condition and its relevance to the present multi-speed model is presented. The diffusive wall boundary condition requires that the particles reaching the wall are redistributed in a way consistent with the mass-balance and normal-flux condition. For the present model with unit cell spacings $c=1,2\,\mathrm{and}\,3$, let the flux contribution from corresponding unit cells be $\mathrm{F}_1\left(\mathbf{x},t\right),\mathrm{F}_2\left(\mathbf{x},t\right)\,\mathrm{and}\,\mathrm{F}_3\left(\mathbf{x},t\right)$ respectively and $\mathrm{F}^{\mathrm{eq}}_1\left(\mathbf{x},t\right),\mathrm{F}^{\mathrm{eq}}_2\left(\mathbf{x},t\right)$ and $\mathrm{F}^{\mathrm{eq}}_3\left(\mathbf{x},t\right)$ be the corresponding equilibrium flux at wall velocity and temperature. For a particular example of the top wall (see Fig. 2.2) the explicit expressions for outgoing fluxes are

$$\begin{aligned}
\mathrm{F}_1(\mathbf{x},t) =& d \times \left(f_{(0,1,0)} + \sum f_{(\pm1,1,\pm1)}\right), \\
\mathrm{F}_2(\mathbf{x},t) =& 2d \times \left(\sum f_{(\pm2,2,0)} + \sum f_{(0,2,\pm2)}\right), \\
\mathrm{F}_3(\mathbf{x},t) =& 3d \times \left(f_{(0,3,0)}\right).
\end{aligned} \tag{2.55}$$

Similarly, the outgoing equilibrium flux could be obtained.

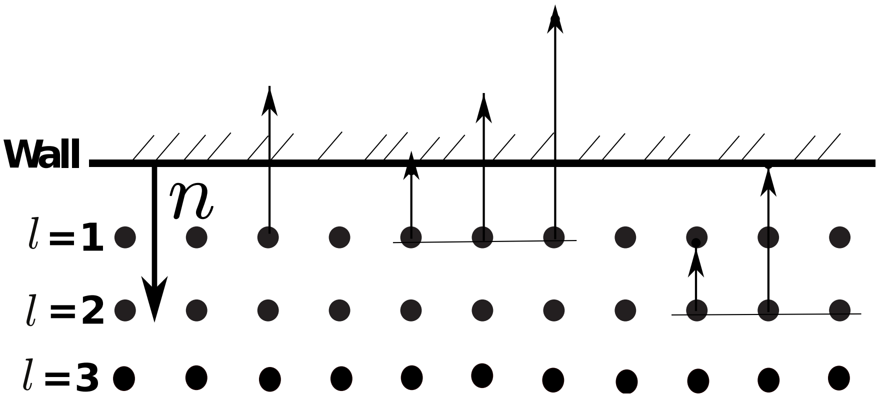

Figure 2.2: Streaming for a multi-speed model, adapted from [57]

The contribution of the different discrete populations at the layers near and at the wall are described below

- At the 'wall', the out going flux is

$$\mathrm{F}_{\text{out}}(x, y_{\text{wall}}, z, t) = \mathrm{F}_1(x, y_{\text{wall}}, z, t) + \mathrm{F}_2(x, y_{\text{wall}}, z, t) + \mathrm{F}_3(x, y_{\text{wall}}, z, t) \tag{2.56}$$

- At the layer $l = 1$, the part of outgoing flux which will reach the wall in time interval Δt is $\mathrm{F}_2(x, y_{\text{wall}} - \Delta y, z, t) + \mathrm{F}_3(x, y_{\text{wall}} - \Delta y, z, t)$.
- Similarly, at the layer $l = 2$, the populations with $c = 1$ and 2 are streamed during advection and hence only flux $\mathrm{F}_3(x, y_{\text{wall}} - 2\Delta y, z, t)$ contributes.

Therefore, the boundary condition i.e. Eq. (2.48) at the layers near and at the wall becomes

- At the 'wall'

$$\tilde{\mathrm{F}}_{\text{out}}(x, y_{\text{wall}}, z, t) = \mathrm{F}_{\text{out}}(x, y_{\text{wall}}, z, t) + \mathrm{F}_2(x, y_{\text{wall}} - \Delta y, z, t) + \mathrm{F}_3(x, y_{\text{wall}} - 2\Delta y, z, t), \tag{2.57}$$

similarly the $\tilde{\mathrm{F}}^{\text{eq}}(x, y_{\text{wall}}, z, t)$ can be calculated. Therefore,

$$f_i(x, y_{\text{wall}}, z, t)\big|_{\mathbf{c}\cdot\mathbf{n}>0} = \frac{\tilde{\mathrm{F}}_{\text{out}}(x, y_{\text{wall}}, z, t)}{\tilde{\mathrm{F}}^{\text{eq}}_{\text{in}}(x, y_{\text{wall}}, z, t)} f_i^{eq}(1, \mathbf{U}_{\text{wall}}, \theta_{\text{wall}}) \tag{2.58}$$

- At the layer $l = 1$, Eq. (2.48) becomes

$$f_i \left(x, y_{\text{wall}} - \Delta y, z, t\right)\big|_{\mathbf{c}\cdot\mathbf{n}>0,|c|>1} = \frac{\tilde{\mathrm{F}}_{\text{out}}\left(x, y_{\text{wall}} - \Delta y, z, t\right)}{\tilde{\mathrm{F}}^{\text{eq}}_{\text{in}}\left(x, y_{\text{wall}} - \Delta y, z, t\right)} f_i^{eq}(1, \mathbf{U}_{\text{wall}}, \theta_{\text{wall}}) \tag{2.59}$$

- Similarly, at the layer $l = 2$, Eq. (2.48) becomes

$$f_i \left(x, y_{\text{wall}} - 2\Delta y, z, t\right)\big|_{\mathbf{c}\cdot\mathbf{n}>0,|c|>2} = \frac{\tilde{\mathrm{F}}_{\text{out}}\left(x, y_{\text{wall}} - 2\Delta y, z, t\right)}{\tilde{\mathrm{F}}^{\text{eq}}_{\text{in}}\left(x, y_{\text{wall}} - 2\Delta y, z, t\right)} f_i^{eq}(1, \mathbf{U}_{\text{wall}}, \theta_{\text{wall}}) \tag{2.60}$$

Thus, the proposed way of applying boundary condition allows one to give desired wall velocity and temperature. It also allows the populations at $l = 1$ and $l = 2$ to be function of the flow field near the wall. Thus it is more realistic to calculate scattering probability the way it is mentioned here. It also allows the conservation of mass which requires that the total incoming mass to the ghost nodes must be the same as remitted mass such that the total mass in the domain remains the same.

2.7 Isothermal flows

In this section, we benchmark the numerical results obtained by the present model with the analytical results available for a variety of simplified flow set-up(s) [57, 58, 59]. As a first example, we study the convergence of the present scheme for Taylor-Green vortex simulation. The analytical form for the evolution of velocity and pressure in this case [60] is

$$\begin{aligned}
\mathrm{u_x}\left(\mathrm{x,y,z=0,t}\right) &= -\mathrm{u_0}\cos\left(\frac{2\pi \mathrm{x}}{\mathrm{L}}\right)\sin\left(\frac{2\pi \mathrm{y}}{\mathrm{L}}\right)\exp\left(-2\mathrm{k}^2\nu \mathrm{t}\right),\\
\mathrm{u_y}\left(\mathrm{x,y,z=0,t}\right) &= \mathrm{u_0}\cos\left(\frac{2\pi \mathrm{y}}{\mathrm{L}}\right)\sin\left(\frac{2\pi \mathrm{x}}{\mathrm{L}}\right)\exp\left(-2\mathrm{k}^2\nu \mathrm{t}\right),\\
\mathrm{p}\left(\mathrm{x,y,t}\right) &= -\frac{\mathrm{u_0^2}}{4}\left[\cos\left(\frac{4\pi \mathrm{x}}{\mathrm{L}}\right)+\cos\left(\frac{4\pi \mathrm{y}}{\mathrm{L}}\right)\right]\exp\left(-4\mathrm{k}^2\nu \mathrm{t}\right)+\mathrm{p_0}
\end{aligned} \tag{2.61}$$

where $k = 2\pi/L$ is the wave number, $p_0 = \rho\,\theta_0$ and the initial conditions on density and temperature is taken as

$$\rho(x, y, z = 0, t = 0) = 1, \quad \theta(x, y, z = 0, t = 0) = \theta_0. \tag{2.62}$$

The Reynold number here is taken as $u_0\,L/\nu$ and Kn is chosen for the case of continnum limit as 0.001 so that the Mach no. is Kn × Re. In the present simulations, we vary the grid spacing and report the difference between the numerical and theoretical kinematic viscosity as a convergence criteria. The numerical kinematic viscosity was calculated by monitoring pressure at the center of domain as

$$\nu_{\text{numerical}} = \frac{-1}{4\,\mathrm{t}}\mathrm{Ln}\left|\frac{2\,\mathrm{p(t)}}{\mathrm{u_0^2}}\right|. \tag{2.63}$$

From Fig 2.3, one can see that the order of convergence for the present scheme is of 2^{nd} order. Next we simulate flow problems involving boundaries.

As a second example, we simulate the fluid flow due to a suddenly started flat plate with

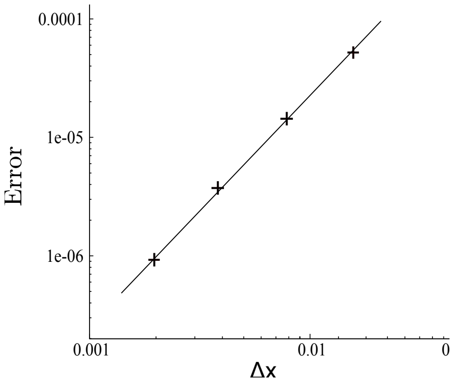

Figure 2.3: Error=$\nu_{\text{numerical}} - \nu_{\text{theoretical}}$, is plotted against grid spacing Δx. The simulation was carried out for square grids of lattice points 64, 128, 256 and 512 at Ma = 0.01, Re = 10 and Kn = 0.001. Plus symbol (+) for simulation and line is the fit with slope 2.

velocity $\mathrm{u_w}$ (see Fig.2.4) for which the initial condition and the boundary conditions on the velocity field u_x are

$$u_x\,(t=0, 0 \le y < \infty) = 0, \quad u_x\,(t>0, y=0) = u_w, \quad u_x\,(t \ge 0, y \to \infty) = 0. \tag{2.64}$$

In Fig.2.5, the dimensionless velocity profile obtained via simulation is contrasted with the analytical solution [59]

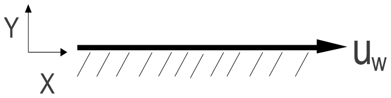

Figure 2.4: Wall is suddenly started at constant velocity u_w in positive x-direction at $t = 0$

$$u^* = \frac{u_x}{u_w} = \mathrm{erfc}\left(\frac{y}{\sqrt{4\nu t}}\right), \tag{2.65}$$

with which agreement is visible.

In order to test the method in bounded domain, as third example the simulation of Couette flow is performed (see Fig.2.6). The initial condition and the boundary conditions on the velocity field u_x are

$$u_x\,(t=0, 0 \le y \le L) = 0, \quad u_x\,(t>0, y=L) = u_w, \quad u_x\,(t \ge 0, y=0) = 0. \tag{2.66}$$

The Reynold number here is taken as $u_w\,L/\nu$ where L is separation between the plates and the Mach no. is u_w/c_s. In Fig. 2.7, the numerical solution is contrasted with the analytical solution [57, 61, 62]

$$u^* = \frac{u_x}{u_w} = \frac{y}{L} - \frac{2}{\pi}\sum_{k=1}^{\infty}\frac{1}{k}\sin(\frac{k\,\pi\,y}{L})\exp\left\{-\frac{k^2\,\pi^2\,\nu t}{L^2}\right\}, \tag{2.67}$$

and the agreement between the two solutions is visible.

As fourth example, the simulation of gravity driven plane-Poiseuille flow in a channel of

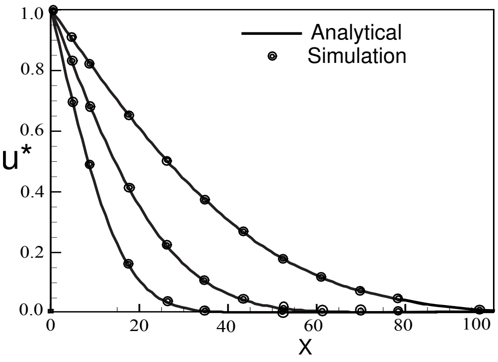

Figure 2.5: Velocity profile development in case of a suddenly started plate.Here, $u^* = \mathrm{u_y}/\mathrm{u_w}$ is normalized velocity plotted against distance in lattice units, with 1000 grid points in X direction. The bottom wall is maintained at velocity $\mathrm{u_w}$ where $\mathrm{Ma} = \mathrm{u_w}/c_s = 0.002$, as such there is no length scale here so Re = 2 is considered appropriate so that Kn= Ma/Re falls in continnum limit whith Kn = 0.001.

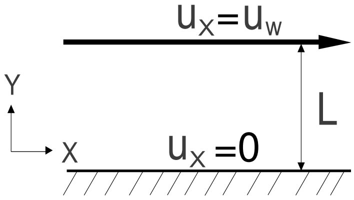

Figure 2.6: Plane Couette flow set-up; top wall is dragged at constant velocity while the bottom plate plate is held stationary for all $t > 0$

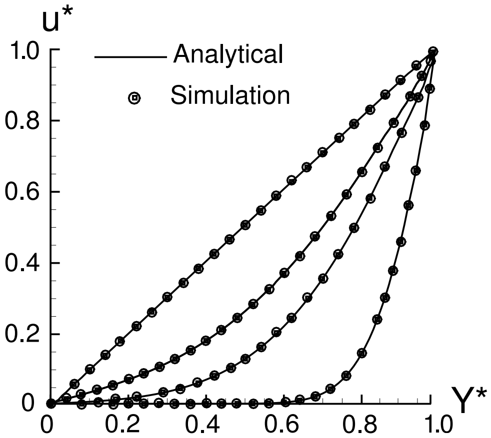

Figure 2.7: Velocity profile development in case of a plane Couette flow. Here, $\mathrm{u}^* = \mathrm{u_x}/\mathrm{u_w}$ is normalized velocity plotted against normalized coordinate, $\mathrm{Y}^* = y/L$. 2-D simulation for grid size 250 × 50 with wall maintained at $\mathrm{u_w}$ for Ma = 0.002, Re = 2 and Kn = 0.001.

height H is performed. The external body force (gravity) acts along the length of the channel in the positive x direction (see Fig. 2.8). The initial and the boundary conditions are

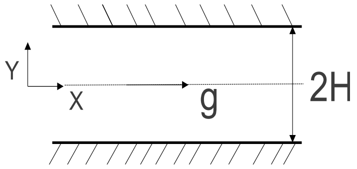

Figure 2.8: Set-up for gravity driven plane-Poiseuille flow; both the walls are held stationary for $t > 0$.

$$u_x\,(t = 0, 0 \le y \le H) = 0, \quad u_x\,(t \ge 0, y = 0) = 0, \quad u_x\,(t \ge 0, y = H) = 0. \tag{2.68}$$

The analytical solution [57] for this set up is

$$u_x(y,t) = -\frac{g\,H^2}{2\,\nu}\left[1 - \left(\frac{y}{H}\right)^2 - \frac{32}{\pi^3}\sum_{k=1}^{\infty}\frac{(-1)^{k+1}}{(2k-1)^3}\cos(\frac{(2k-1)\,\pi\,y}{2H})\exp\left\{-\frac{(2k-1)^2\,\pi^2\,\nu t}{4H^2}\right\}\right]. \tag{2.69}$$

The Reynold number here is taken as $u_{\max}\,(2H)/\nu$ where $u_{\max}$ is the centre–line velocity when $y = 0$ in Eq. (2.69) and the Mach no. is $u_{\max}/c_s$. The analytical solution is compared with the simulation results in Fig. 2.9, which shows the expected hydrodynamic behavior.

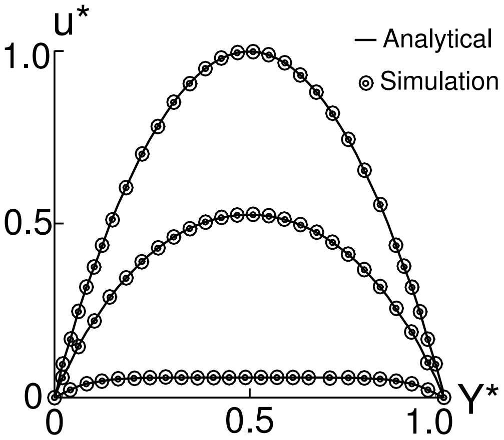

Figure 2.9: Velocity profile development in case of a transient gravity driven plane-Poiseuille flow. $u^* = \mathrm{u_x}/\mathrm{u_{max}}$ is a normalized velocity, where $\mathrm{u_{max}}$ is the centre line velocity; u^* is plotted against normalized coordinate, $\mathrm{Y}^* = \mathrm{y}/(\mathrm{H})$. 2-D simulation with 100 × 50 lattice size was performed with Ma= 0.001, Re = 1 and Kn = 0.001 with periodic inlet and outlet.

The plane-Poiseuille flow at high Knudsen number has been extensively used in the past for assessing usefulness of various LB models and boundary conditions formulation for gaseous micro flows [43, 63]. We compare the results obtained by D3Q33 model with those in Ref. [64, 63, 65]. In literature related to rarefied gas dynamics, often in order to compare the result for slip velocity, the ratio of fluid velocity at the wall u_{slip} to the centreline flow velocity $u_{\text{centreline}}$ is parametrized in terms of Kn number as

$$u^* = \frac{u_{\text{slip}}}{u_{\text{centreline}}} = \frac{A_1\,\mathrm{Kn} + 2A^2\,\mathrm{Kn}^2}{\frac{1}{4} + A_1\,\mathrm{Kn} + 2A_2\,\mathrm{Kn}^2} \tag{2.70}$$

where the Knudsen number defined as$\mathrm{Kn} = \sqrt{3}\,\tau\, c_s/L$ and for the linearized solution of Boltzmann BGK equation $A_1 = 0.8297$ and $A_2 = 0.5108$ [64], while for the D2Q9 slip flow model it is $A_1 = 1$ and $A_2 = \frac{2}{3}$ [63]. From Fig.2.10 it can be seen that the amount of slip measured by the D3Q33 model is in agreement with that of linearized solution by Cercignani and is indeed better than that of result provide by lower D2Q9 model of Ref.[63]. Thus, we can conclude that for unidirectional isothermal flows, $D3Q33$ model preserves good accuracy of the existing lower order LB models for continuum flows and is an attractive alternate to them for high Knudsen flows.

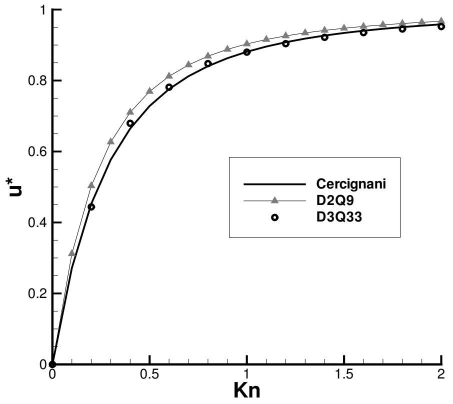

Figure 2.10: Slip velocity versus Knudsen numbers for the Poiseuille flow. Symbols, simulation; line, analytical solution by Cercignani [65]

Finally, simulation results for flow in a 2-D lid driven Cavity, which is considered as a more strict benchmark due to presence of a large primary vortex in the centre of domain and appearance of a number of secondary vortices at high Reynolds number, is presented. In this case, the flow is confined among the walls and the top wall or a lid is constantly drawn at a fixed velocity (see Fig. 2.11) In Fig. 2.12, streamlines are plotted as a function of Reynolds number. Further, values of location of vortices and the corresponding stream function for the present D3Q33 model is compared with existing literature [66, 67, 68, 69, 70, 71, 72, 73, 74, 75]. The comparison among various methods is presented in Table. 2.2, Table. 2.3, Table. 2.4 and Table. 2.5 for a few representative Reynold numbers of 100, 400, 1000 and 5000 respectively.

Further the velocity profiles along the mid section of lid is compared with the data from Ref [66] in Fig. 2.13. A grid independence study was performed at Re=1000 with the location of primary vortex as a benchmark value and the results were compared with those given by Bruneau & Saad [74]. As can be seen in Fig. 2.14, the discretization of the diffusive boundary condition is first order accurate. Note that the finite intercept ($\beta = 0.88$) in the convergence fit in Fig. 2.14 indicates finite Kn number effect.

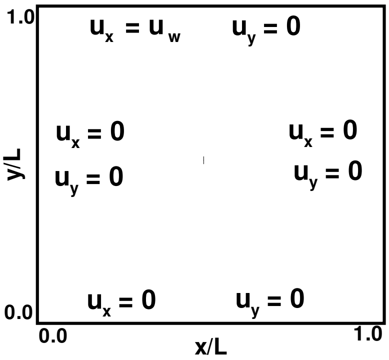

Figure 2.11: 2D Lid Driven Cavity flow geometry

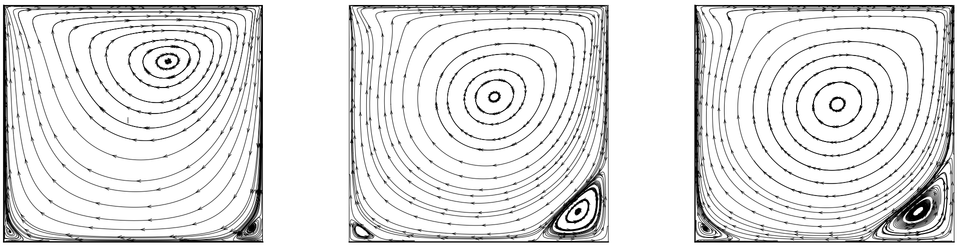

Figure 2.12: Streamlines for a lid driven cavity for the D3Q33 model (a) at Re= 100 (b) at Re= 400 and (d) Re= 1000 from left to right, respectively.

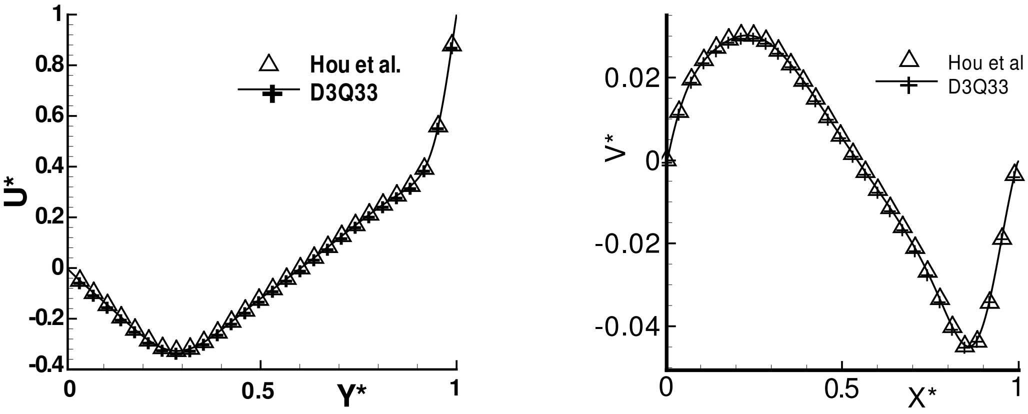

(a) (b)

Figure 2.13: Comparison for the the velocity profile for Re= 1000 (a) horizontal velocity at x*= 0.5 (b) vertical velocity at y*= 0.5 for a grid size of 256 × 256 at Ma=0.1

Table 2.2: Locations of vortex centres in a lid driven cavity flow at Re=100

Works	Primary Vortex	Lower left Vortex	Lower right vortex	Grid Size
	(x, y, ψ_{max})	(x, y, ψ_{min})	(x, y, ψ_{min})	
D3Q33	(0.6176,0.7346,0.1034)	(0.0345,0.0393,-1.82e-6)	(0.9351,0.0676,-1.27e-5)	128×128
	(0.6169,0.7342,0.1032)	(0.0341,0.0395,-1.81e-6)	(0.9355,0.0678,-1.28e-5)	256×256
S Hou[66]	(0.6196,0.7373,0.1030)	(0.0392,0.0353,-1.72e-6)	(0.9451,0.0627,-1.22e-5)	256×256
Ghia[72]	(0.6172,0.7344,0.1034)	(0.0313,0.0391,-1.75e-6)	(0.9453,0.0625,-1.25e-5)	129×129
Vanka [73]	(0.6188,0.7375,0.1034)	(0.0375,0.0313,-1.94e-6)	(0.9375,0.0563,-1.14e-5)	321×321

Table 2.3: Locations of vortex centres in a lid driven cavity flow at Re=400

Works	Primary Vortex	Lower left Vortex	Lower right vortex	Grid Size
	(x, y, ψ_{max})	(x, y, ψ_{min})	(x, y, ψ_{min})	
D3Q33	(0.5675,0.6071,0.1125)	(0.0540,0.0501,-1.39e-5)	(0.8895,0.1175,-6.42e-4)	128×128
	(0.5645,0.6075,0.1121)	(0.0545,0.0500,-1.36e-5)	(0.8891,0.1155,-6.45e-4)	256×256
S Hou[66]	(0.5608,0.6078,0.1121)	(0.0549,0.0510,-1.30e-5)	(0.8902,0.1255,-6.19e-4)	256×256
Z. Guo[67]	(0.5547,0.6094,0.1126)	(0.0508,0.0469,-1.36e-5)	(0.8867,0.1250,-6.23e-4)	——
Borok[70]	(0.5608,0.6118,0.1125)	(0.0549,0.0510,-1.00e-5)	(0.8883,0.1294,-6.20e-4)	256×256
Ghia[72]	(0.5547,0.6055,0.1139)	(0.0508,0.0469,-1.42e-5)	(0.8906,0.1250,-6.42e-4)	257×257
Vanka[73]	(0.5563,0.6000,0.1136)	(0.0500,0.0500,-1.46e-5)	(0.8875,0.1188,-6.45e-4)	321×321

Table 2.4: Locations of vortex centres in a lid driven cavity flow at Re=1000

Works	Primary Vortex	Lower left Vortex	Lower right vortex	Grid Size
	(x, y, ψ_{max})	(x, y, ψ_{min})	(x, y, ψ_{min})	
D3Q33	(0.5319,0.5671,0.1175)	(0.0901,0.0714,-2.19e-4)	(0.8643,0.1125,-1.67e-3)	256×256
	(0.5313,0.5675,0.1172)	(0.0903,0.0715,-2.15e-4)	(0.8645,0.1121,-1.65e-3)	512×512
S Hou[66]	(0.5333,0.5647,0.1178)	(0.0902,0.0784,-2.22e-4)	(0.8667,0.1137,-1.69e-3)	256×256
Z. Guo[67]	(0.5313,0.5625,0.1170)	(0.0859,0.0781,-2.21e-4)	(0.8672,0.1172,-1.68e-3)	——
Borok[70]	(0.5333,0.5686,0.1172)	(0.0863,0.0823,-2.20e-4)	(0.8667,0.1176,-1.70e-3)	256×256
Ghia[72]	(0.5313,0.5625,0.1170)	(0.0859,0.0781,-2.21e-4)	(0.8672,0.1172,-1.68e-3)	129×129
Vanka[73]	(0.5438,0.5625,0.1173)	(0.0750,0.0813,-2.22e-4)	(0.8625,0.1063,-1.74e-3)	321×321
Saad[74]	(0.5312,0.5625,0.1178)	(——, ——, ——)	(0.8593,0.1093,-1.70e-3)	128×128
Botella[75]	(0.5308,0.5652,0.1189)	(——, ——, ——)	(0.8639,0.1118,-1.72e-3)	$N = 160$

Table 2.5: Locations of vortex centres in a lid driven cavity flow at Re=5000

Works	Primary Vortex (x, y, ψ_{max})	Lower left Vortex (x, y, ψ_{min})	Lower right vortex (x, y, ψ_{min})	Grid Size
D3Q33	(0.5144,0.5346,0.1198)	(0.0784,0.1357,-1.30e-4)	(0.8084,0.0741,-3.05e-3)	256 × 256
	(0.5151,0.5335,0.1195)	(0.0781,0.1352,-1.33e-4)	(0.8080,0.0745,-3.00e-3)	512 × 512
S Hou[66]	(0.5176,0.5373,0.1214)	(0.0784,0.1373,-1.35e-3)	(0.8078,0.0745,-3.03e-3)	256 × 256
Z. Guo[67]	(0.5159,0.5391,0.1120)	(0.0781,0.1328,-1.29e-3)	(0.8086,0.0781,-2.85e-3)	——
Gorban[68]	(0.5152,0.5354, —)	(0.0808,0.1313, ——)	(0.8081,0.0808, ——)	100 × 100
Toshi[69]	(0.5150,0.5400, —)	(0.0780,0.1350, ——)	(0.8050,0.0750, ——)	100 × 100
Borok [70]	(0.5176,0.5412,0.1081)	(0.0784,0.1373,-1.29e-4)	(0.8039,0.0784,-3.13e-3)	256 × 256
Asinari[71]	(0.5155,0.5355, ——)	(——, ——, ——)	(0.8058,0.0740, ——)	256 × 256
Ghia[72]	(0.5117,0.5352,0.1190)	(0.0703,0.1367,-1.36e-3)	(0.8086,0.0742,-3.08e-3)	257 × 257
Vanka[73]	(0.5125,0.5313,0.0921)	(0.0625,0.1563,-1.67e-3)	(0.8500,0.0813,-5.49e-3)	161 × 161
Saad[74]	(0.5156,0.5351,0.1206)	(——, ——, ——)	(0.8085,0.0742,-3.03e-3)	128 × 128

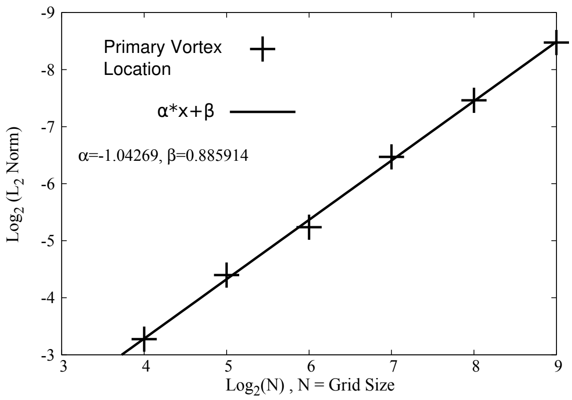

Figure 2.14: Error analysis for primary vortex location. Plot shows Log$_2$(L$_2$ Norm) versus grid size on same log scale

2.8 Thermal Hydrodynamics

In this section, we present thermo-hydrodynamic simulation results using D3Q33 model. As first example, the sound speed for the present energy conserving D3Q33 LB model is measured numerically. Unlike isothermal lattice Boltzmann, the sound speed in an energy conserving models should be isentropic value

$$c_s^2 = \left.\frac{\partial p}{\partial \rho}\right|_{\mathrm{S}} = \gamma\theta. \tag{2.71}$$

The sound speed can be measured numerically by analyzing the decay of initial acoustic perturbations of the form

$$\rho(x, y, z = 0, t = 0) = \rho_0 \left(1 + 0.01 \cos\left(\frac{2\pi}{L}x\right)\right), \tag{2.72}$$

in a quiescent fluid. In the present work we set reference density $\rho_0 = 1$, reference temperature $T_0 = 1$ and domain length $L = 2\,\pi$.

In Fig. 2.15, the density perturbation, defined as $\Delta\rho = \rho - \rho_0$, is plotted at the centre of domain, where one can see that time period of oscillation is approximately 4.84. Thus, sound speed computed from time period is $2\,\pi/4.84 \sim 1.29870$ which matches with the expected value $\sqrt{5/3}$ up to 5 decimal places. Thus, the current model is able to predict the correct sound speed.

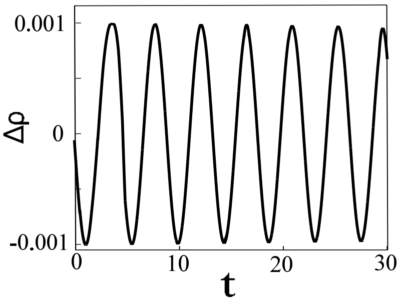

Figure 2.15: Density perturbations ($\Delta\rho$) with time (t) in LB simulation at the centre of domain for Re=10, Ma=0.001 and grid-size $L \times L$.

As second example, 1-D transient thermal conduction is simulated. For this, the fluid is maintained at the constant temperature $\Delta\theta + \theta_0$ ($=\theta_s$) at one end while the other end is kept at fixed temperature θ_0 (see Fig.2.16). The initial condition and boundary conditions on the

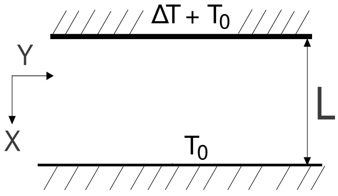

Figure 2.16: Set-up for studying 1-D heat conduction between two parallel plates.

temperature field θ are

$$\theta\,(t=0, \leq y \leq L) = \theta_0, \quad \theta\,(t>0, x=L) = \theta_0, \quad \theta\,(t \geq 0, x=0) = \theta_s. \tag{2.73}$$

The analytical solution with θ^* as the normalized temperature [58] is

$$T^* = \frac{\theta(x,t)-\theta_s}{\theta_0-\theta_s} = \frac{x}{L} + \frac{2}{\pi}\sum_{k=1}^{\infty}\frac{1}{k}\sin(\frac{k\,\pi\,x}{L})\exp\left\{-\frac{k^2\,\pi^2\,\nu t}{L^2}\right\}. \tag{2.74}$$

which compared with the numerical result in Fig. 2.17 shows a good agreement between the two.

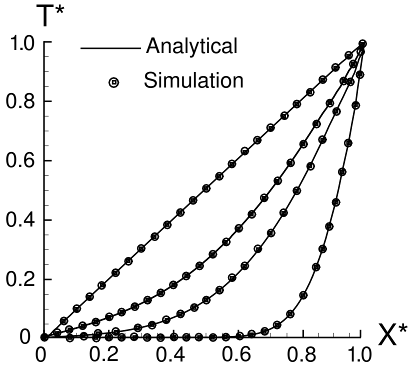

Figure 2.17: Temperature development profile in case of a transient 1-D heat conduction problem. Here, T* $= \theta/\theta_\text{w}$ is a non-dimensional temperature plotted against non dimensional length, X* $= X/L$. 2-D simulation for grid size 250 × 50 with wall maintained at $\theta_\text{w} = 1.01 \times \theta_0$ and Kn $= 0.0001$.

In order to validate the model for steady-state case of both heat and momentum diffusion, numerical simulation of the thermal Couette flow where the fluid is confined between two parallel plates with a linear temperature gradient is considered. In this set up, one of the plate is moved with a fixed velocity u_w and maintained at constant temperature $\theta_0 + \Delta\theta$ while the other wall is at a constant temperature of θ_0 and held stationary for all $t > 0$. The schematic in Fig. 2.18 shows the described set up.

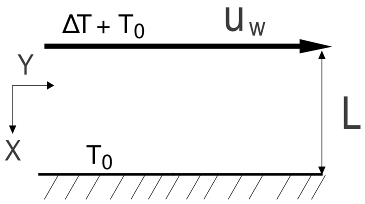

Figure 2.18: Thermal Couette flow set-up; top wall is at a constant velocity u_w and fixed temperature $\theta_0 + \Delta\theta$ with respect to stationary bottom plate at T_0 for all $t > 0$.

The steady state non-dimensional temperature reads

$$T^* = \frac{\theta(X)}{\theta_0} = 1 + \frac{\Delta\theta}{\theta_0}\left[1 - X^* + \frac{\mu u_w^2}{2\,k_T\,c_p\,\Delta\theta} X^*(1 - X^*)\right] \tag{2.75}$$

In Fig. 2.19, simulation results are contrasted with Eq. (2.75). This confirms that the present model is accurate enough for simulating heat conduction problems.

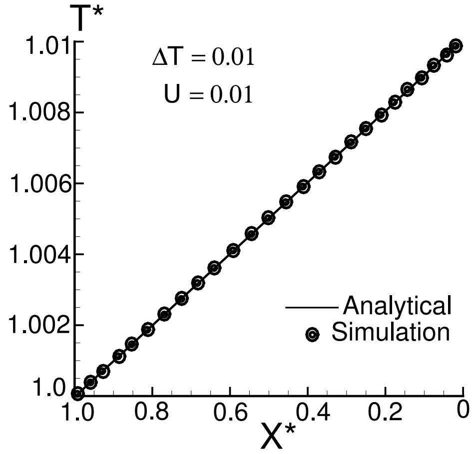

Figure 2.19: Steady state temperature profile along the non dimensional length $X^* = X/L$. 2-D simulation for grid size 250×50 with wall maintained at $\theta_{\mathrm{w}} = 1.01 \times \theta_0$ and constant velocity U for Ma = 0.00775, Re = 7 and Kn = 0.001

We used the same set up to validate the kinetic nature of the present scheme for studying heat conduction at finite Kn number. A small temperature difference of $\theta_{\mathrm{L}} - \theta_{\mathrm{R}}$ was considered (approximately 1% variations of the average temperature). Analytical solution to the stationary continuous linearized BGK model [65] is

$$\theta(X) = \left[\frac{\theta_{\mathrm{L}} - \theta_{\mathrm{R}}}{1 + 3.88234 * \mathrm{Kn}}\right]\mathrm{X} + \frac{\theta_{\mathrm{L}} + \theta_{\mathrm{R}}}{2}, \tag{2.76}$$

where X is the dimensionless distance from the centre of the channel. From Fig. 2.20 a good agreement with the analytical solution [65] is obtained

Furthermore, in order to validate usefulness of the present scheme for micro flows, we analyze temperature profile in an isothermal gravity driven plane-Poiseuille flow. The body force is same as that mentioned in Eq. (2.47). In this set up it is well known that with increase in Kn there is a minima in the temperature profile [76, 77, 78, 79]. In the present simulation a range of values of Kn is varied from 0.001 to 0.25 while the Ma is varied from 0.01 to 0.15. From Fig 2.21 one can see that for a given Ma=0.01 in Fig Fig 2.21(i, f, c), as the Kn is increased the dip in the temperature profile at the centerline becomes more prominent. The effect of increasing Ma is to increase the difference between maximum and minimum in the temperature profile. These results are in qualitative agreement with those in Ref.[80] and the present model is able to capture the temperature minima for this set up similar to the one observed in DSMC simulations [79].

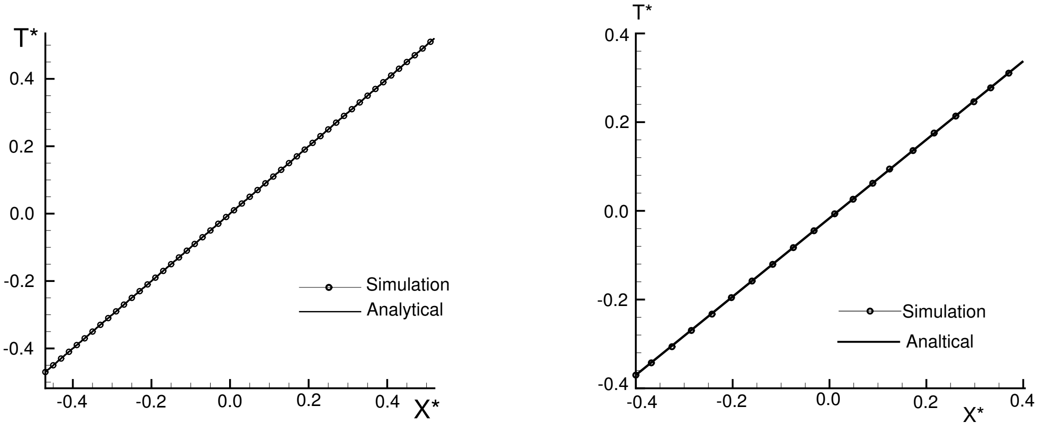

(a) (b)

Figure 2.20: Steady-state temperature variation between parallel walls. Reduced temperature T^* is shown as the function of the non-dimensional distance X* at (a) Kn 0.001 and (b) Kn 0.05. Symbols, simulation; line, analytical solution by Bassanini, Cercignani, and Pagani [66]

2.8.1 Natural Convection

In order to study the effectiveness of the present model to simulate coupled conduction and convection, the problem of natural convection in an enclosure is studied in this section (see Fig. 2.22). Conventionally, Boussinesq approximation has been often used in the study of natural convection in an incompressible fluid with constant viscosity and thermal diffusivity. This approximation takes into account the density change due to local heating only in the body force term. Here, the utility of the present model is tested in an compressible set up with 0.1% of temperature perturbation from reference temperature θ_0 and compared with the result obtained for the problem of a laminar natural convection on a uniform grid with Boussinesq approximation.

The parameter of interest in natural convection problem is the Rayleigh number defined as

$$\mathrm{Ra} = \frac{\mathrm{g}\beta}{\nu\alpha}(\Delta\theta)\mathrm{L}^3. \tag{2.77}$$

where, L is the characteristic length, $\Delta\theta$ is the temperature difference between the wall and the ambient fluid temperature ($= \theta_0$) far from the plate and practically constant, ν is the kinematic viscosity ($\theta_0\,\tau$), α is thermal diffusivity (same as ν for a Prandtl number of unity) and β is the volumetric thermal expansion coefficient defined for an ideal gas at constant pressure as

$$\beta = \frac{1}{V}\left(\frac{\partial V}{\partial \theta}\right)_p = \frac{1}{\theta} \tag{2.78}$$

where we have used β at reference temperature θ_0 so that $\beta = 1/\theta_0$.

The flow characteristics for this set up are well studied and the transition from conductive state to convective state occurs at Rayleigh numbers around $\sim 10^5$, characterized by a rising plume along the hot wall and then the plume losing heat on the cold wall (see Fig. 2.23). The

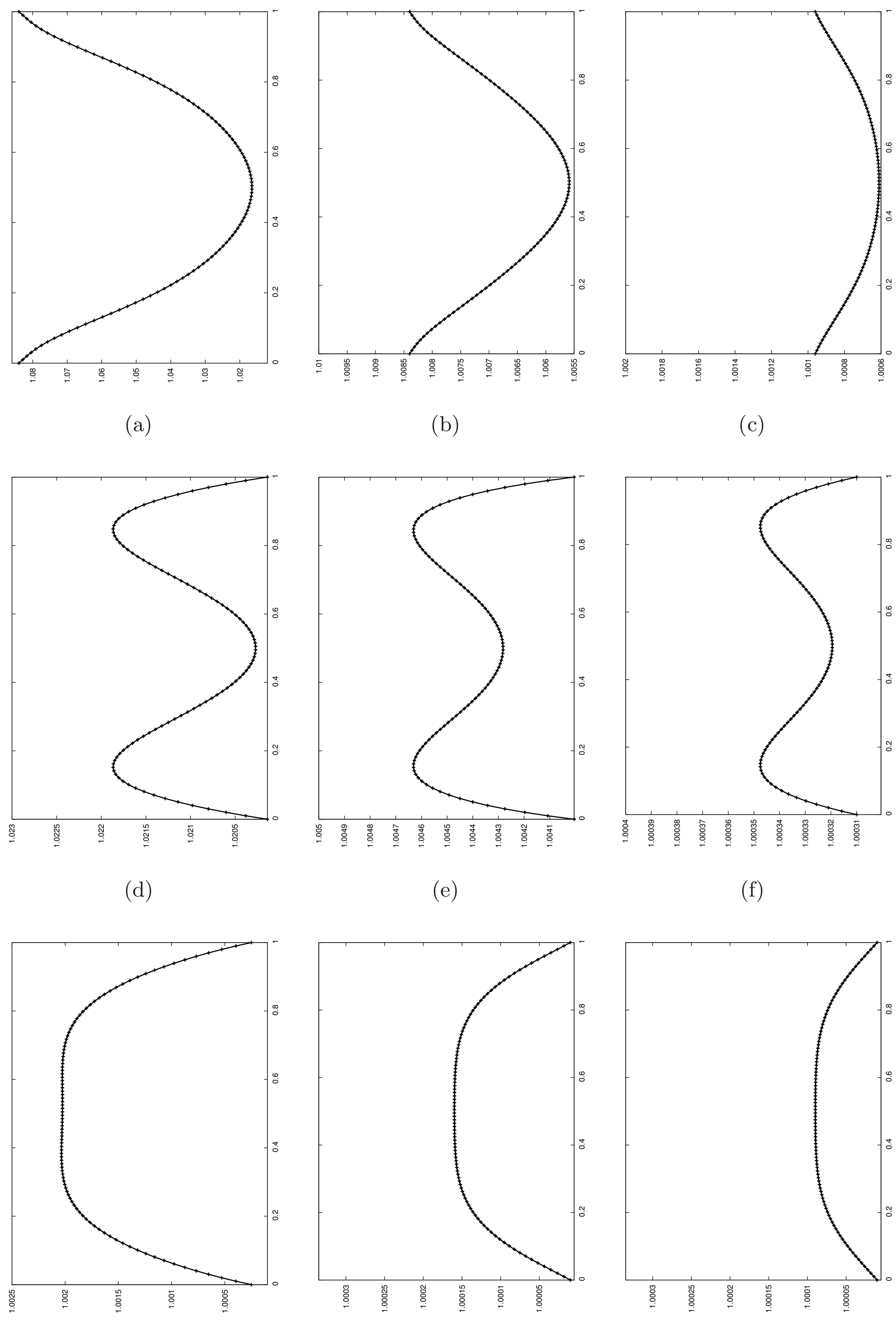

(a) (b) (c)

(d) (e) (f)

(g) (h) (i)

Figure 2.21: Temperature profile across the channel for various Ma and Kn numbers. The two parameters for a given figure is written as (Kn, Ma); (a) (0.25, 0.17) (b) (0.25, 0.04) (c) (0.25, 0.01) (d) (0.20, 0.12) (e) (0.20, 0.05) (f) (0.20, 0.01) (g) (0.001, 0.05) (h) (0.001, 0.02) (i) (0.001, 0.01)

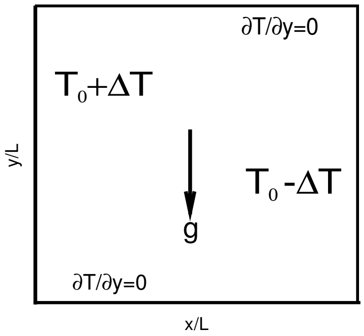

Figure 2.22: Set-up to study natural convection in a square box/cavity, with gravity g directed vertically downward.

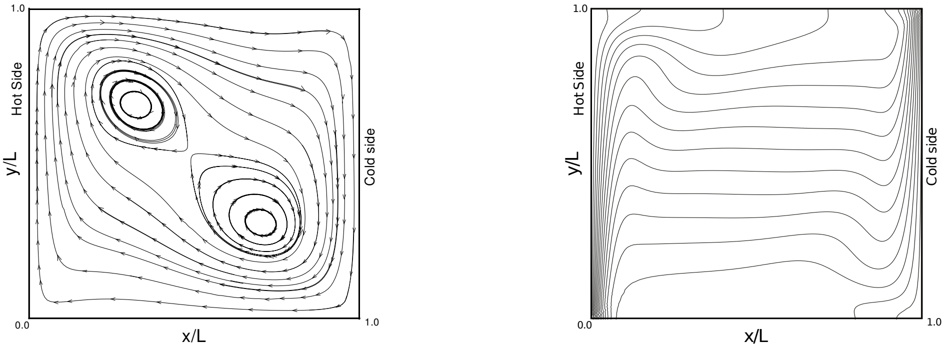

(a)

(b)

Figure 2.23: (a) Streamlines and (b) isotherms for $Ra = 10^5$ for the preset D3Q33 model

streamlines and the isotherms in Fig. 2.23 is in qualitative agreement with Ref. [50, 54, 81, 82].

For quantitative analysis, the present work is contrasted with Ref. [82] for a varying grid size (see the Table 2.6). The benchmark data as reported by Ref. [82] is the average Nusselt number at the constant x-plane for a square cavity of height H defined as

$$\mathrm{Nu} = (-1/\Delta\theta) \int_0^{\mathrm{H}} (\partial_{\mathrm{x}}\theta)\, \mathrm{dy} \tag{2.79}$$

and the temperature gradient as measured at the centre of the cavity defined as

$$\mathrm{S} = (\mathrm{H}/\Delta\theta)(\partial_{\mathrm{y}}\theta)_{\mathrm{x=y=H/2}}. \tag{2.80}$$

Table 2.6: Quantitative analysis for the scaled velocities with the benchmark data of Eggels et al. [82] and Jansen [83].

Grid Size Square	Model	Nu $\mathrm{Ra}^{-1/4}$	$\frac{v_{max}}{(g\beta\Delta TH)}$	$\frac{u_{max}}{(g\beta\Delta TH)}$	S
60	D3Q33	0.2755	0.2697	0.8112	0.9198
	Eggels	0.2732	0.2581	0.8071	0.9087
	Jansen	0.2789	0.2633	0.8145	0.9190
120	D3Q33	0.2786	0.2652	0.8118	0.9157
	Eggels	0.2766	0.2615	0.8133	0.9159
	Jansen	0.2790	0.2621	0.8144	0.9144
240	D3Q33	0.2789	0.2625	0.8124	0.9145
	Eggels	0.2783	0.2621	0.8144	0.9176
	Jansen	0.2791	0.2618	0.8146	0.9132

2.8.2 Rayleigh Bénard Convection

As an another example of coupled conduction convection problem, Rayleigh Bénard Convection (hereafter RBC) is simulated in this section with the help of the present model. As shown in Fig. 2.24, a horizontal fluid layer of height L is confined between two thermally well conducting, parallel plates. The bottom plate is at excess temperature, $\Delta\theta + \theta_0$ and the top plate at θ_0 temperature, where $\Delta\theta$ is the temperature difference. At the top and the bottom walls the

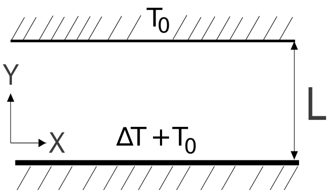

Figure 2.24: Rayleigh Bénard Convection set up

diffusive wall boundary condition [55] is applied, whereas the periodic boundary condition is applied on the vertical walls. The following numerical test is carried out around $Ra \sim 10^4$ and is found in good agreement with that given in [83, 84]. When looked at the rising plume the temperature contours and the streamlines appears as shown in Fig. 2.25.

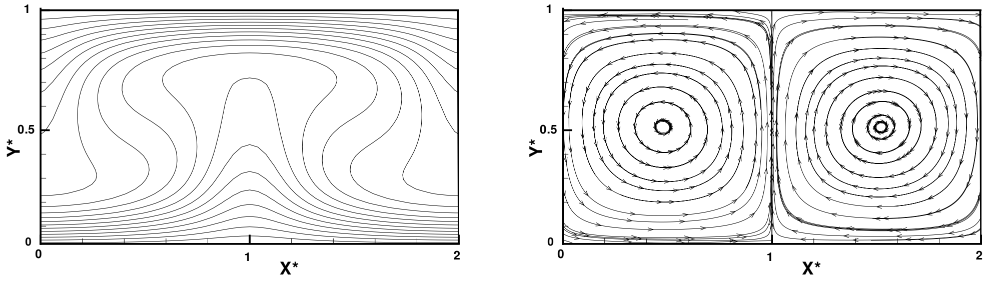

(a) (b)

Figure 2.25: (a) Isotherms (b) Streamlines ; for a steady-state Rayleigh Bénard convection between parallel plates.

The converged values for the the Nusselt number (Nu) is plotted against the Rayleigh number in Fig. 2.26 and compared with the data in Ref. [85].

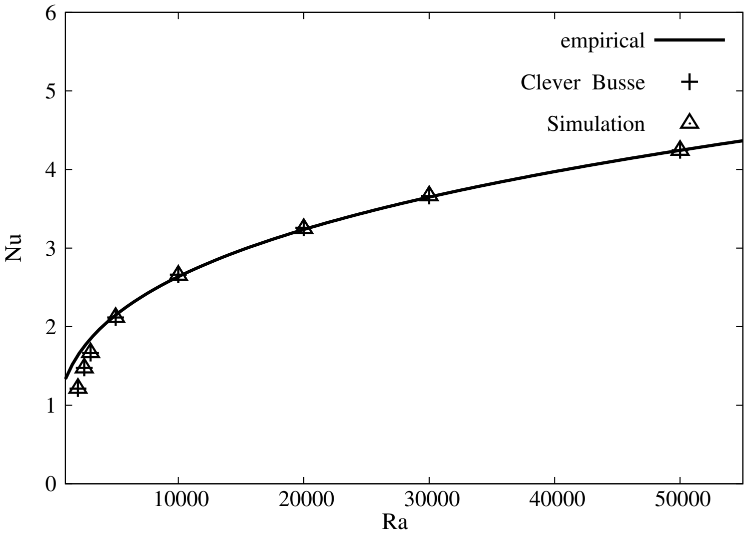

Figure 2.26: Nu vs. Ra for the steady-state Rayleigh Bénard convection between parallel plates. Solid line: Empirical correlation $Nu = 1.56\left(\frac{Ra}{Ra_{\text{critical}}}\right)^{0.296}$; triangle ($\Delta$) for the present simulation and plus ($+$) sign for the Ref. data of Clever & Busse [86].

2.9 Outlook

In the present chapter, we have discussed the construction of an higher order thermal lattice Boltzmann model based on entropic considerations. A minimal thermal LB model with the addition of 6 more velocities to the existing D3Q27 model is proposed. The resulting D3Q33 model is an on-lattice model and hence the streaming part is easy to implement. The D3Q33 model was numerically tested for a variety of test cases and the results obtained were shown to be in good agreement with the expected thermo-hydrodynamic behavior. The model construction procedure highlighted here is general enough to be extended to construct more accurate models.

Chapter 3

Data Structure

3.1 Introduction

The use of lattice based simulations is quite pervasive in computational physics. By now, such methods are important tools for solving partial differential equations in physics. For example, Finite difference time domain (FDTD) for Maxwell equation [86, 87, 88, 89] and lattice Boltzmann (LB) method for hydrodynamics [1, 2, 3, 4]. An algorithmic feature of these methods is that one updates array elements according to some predefined pattern and data is exchanged only between neighboring sites. These features create a highly parallel structure of these algorithms for which they are very popular for massively parallel computing [90, 91, 92]. However, a less discussed aspect for these algorithms is the fact that they are very often "memory bound" rather than CPU bound [93, 94]. In practical terms, it means that just increasing the CPU speed is often not sufficient to get better performance on a single CPU. The increasing gap between CPU speed and memory bandwidth would make such problem even more severe in the foreseeable future. Such a wide difference in CPU and memory bandwidth often means that the choice of data structure is not obvious a priori. Often is the case that the various parts of the same algorithm might have conflicting data structure requirements [93, 95]. The present chapter highlights these issues for LB method and shows that a redesign of the data-structure leads to substantial improvement in performance.

The present chapter is organized as follows. Section 3.2 reviews the existing data structures viz; AOS and SOA for LB implementation, Section 3.3 then defines the performance measures and suggests changes to go beyond the existing data layouts. Section 3.4 shows that for a given data structure the loop transformation can substantially improve computational efficiency. Section 3.5 describes the symmetry and isotropy requirements for a discrete velocity set of a given LB model. Section 3.6 is based on the elementary break up of the discrete velocity set in LB. It introduces a new data-structure which is hybrid of AOS and SOA data structure and is referred as SOAOS. Finally, Section 3.7 discuss implications of this algorithm for grid-based computing in general.

3.2 Existing Data Structures for LB

In this section the algorithmic aspect of LB method are revised. In this method, the central quantity of interest is the discrete distribution function $f_i(\mathbf{x}, t)$, which denotes the probability of finding a molecule at location $\mathbf{x}$ and time t with velocity c_i with $i = 1, 2, ..N_d)$, where N_d being the number of discrete velocities. The evolution equation for the distribution function is typically written as a two step process. First of these steps is the local collision operations,

$$f_i^\star(\mathbf{x},t) = f_i(\mathbf{x},t) + \Omega_i(f(\mathbf{x},t)), \tag{3.1}$$

where f denotes the set of populations and Ω_i is the collision operator which conserves mass, momentum and energy (in isothermal models, energy conservation is ignored) and it depicts a relaxation process of distribution function towards its equilibrium value. Almost all floating point calculation in the LB method are in this step. The second step is advection step, which mimics free propagation of molecules and is given as

$$f_i(\mathbf{x} + \mathbf{c}_i\Delta t, t + \Delta t) = f_i^\star(\mathbf{x},t) \tag{3.2}$$

with Δt as time step. It is to be noted that it is the magnitude and direction of c_i which dictates the connectivity on the grid and hence the amount of cache mismatch during the advection step.

As all the floating point calculations in Eq.(3.1) are local in space i.e. at a given instant of time one uses the update rule for all the i^{th} populations. Using locality principle, it is natural to place all the populations at a given point in neighbouring locations in memory [96] (see Fig. 3.1). Thus, a computer code of LB model concerned with floating point optimization will place all the f_i values for a given point in space in a single structure and build an array of such a structure. Such a data structure is termed as "Array of Structure (AOS)" in computer science and often termed as collision optimized data layout in LB method literature [90, 97].

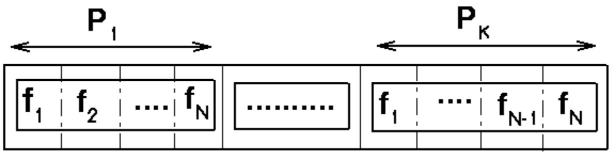

Figure 3.1: Schematic diagram of AOS data-structure. Here, P_K denotes K^{th} spatial point characterized in D-dimension by coordinates x_j with $j = 1 \cdots D$.

However, using locality principle [96] it can be seen from Eq.(3.2) that movement of a given i^{th} population is independent of other. Therefore, all the f_i values for a particular i^{th} direction of movement should be stored sequentially (see Fig. 3.2). In other words, advection code is best written using "Structure of Array (SOA)", also called advection-optimized layout in LB method literature.

Here, it is worth to bring to the notice that in a FORTRAN code, AOS implies keeping populations in fastest running index of a four dimensional array However, all the memory movement involvement in Eq.(3.2), suggest that in such a FORTRAN code, populations should be in slowest running index of a four dimensional array. In other words, advection is best done using Structure of Array (SOA), where all the f_i values for a particular i^{th} direction are stored sequentially making it easier to pick one of the value and place it the neighboring location (see Fig. 3.2).

Thus, one can see that there is an obvious conflict based on the way the populations to

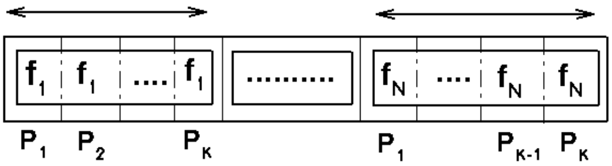

Figure 3.2: Schematic diagram of SOA data-structure. Here, P_K denotes K^{th} spatial point characterized in D-dimension by coordinates x_j with $j = 1 \cdots D$.

be stored and accessed. Such a conflicting data-structure requirements results in a sharp performance drop (as compared to the peak computer performance) for LB methods with larger stencils [93]. Thus, for the LB method it is natural to ask if there is any optimal data-structure which can match the compute efficiency of AOS while achieving the memory bandwidth comparable to SOA ? Here the discussion is restricted to the case of large data sets i.e. where the data cannot fit into the L1 cache and the bandwidth issues are important.

3.3 Performance Measures for LB Implementations

In the present section, ways to quantify efficiency and performance for a LB code is presented. In this work, the single memory implementation of LB code is studied against the double memory implementation where an additional buffer or auxiliary array is used for streamed populations (see Ref. [97] for further details). The concern here is to raise the advection efficiency with AOS data structure as AOS data structure is best choice for getting good efficiency in the compute stage of LB (see for example [93]). Before we do so, we need an efficiency measure for the implementations. Similar to any grid based code, limiting factor affecting LB simulations is often memory bandwidth rather than floating point operations (FLOP) efficiency of the machine, which implies that these codes are memory bound rather than compute bound. This makes peak FLOPS (FLOP per second) as an uninformative performance measure for LB codes, as far as efficiency of the code is concerned. Thus, performance of a given LB simulations is measured often in terms of Mega Lattice-sites Updates Per Second (MLUPS) [90, 97] . It is defined as

$$\text{MLUPS} = \frac{K_x\, K_y\, K_z}{10^6\, T}, \tag{3.3}$$

where K_i denotes the number of grid points in the i^{th} direction and T is the time taken for updating all the grid points. In Fig. 3.3, MLUPS values of advection step is plotted using AOS data structure for various LB models widely used in the literature (D3Q15, D3Q19, D3Q27 see for example Ref. [46], D3Q33 of the present work and D3Q41 from Ref. [48]). The two of the most commonly used algorithm: 8-Loop version called loop based algorithm abbreviated as “LBA-8” and swap based algorithm called “SBA” (see Appendix A and B) has been used to perform advection. In this plot, in order to show the maximum achievable performance, result from SOA data structure for D3Q15 is also plotted as benchmark.

The code performance measured in MLUPS allows one to compare the time taken to update

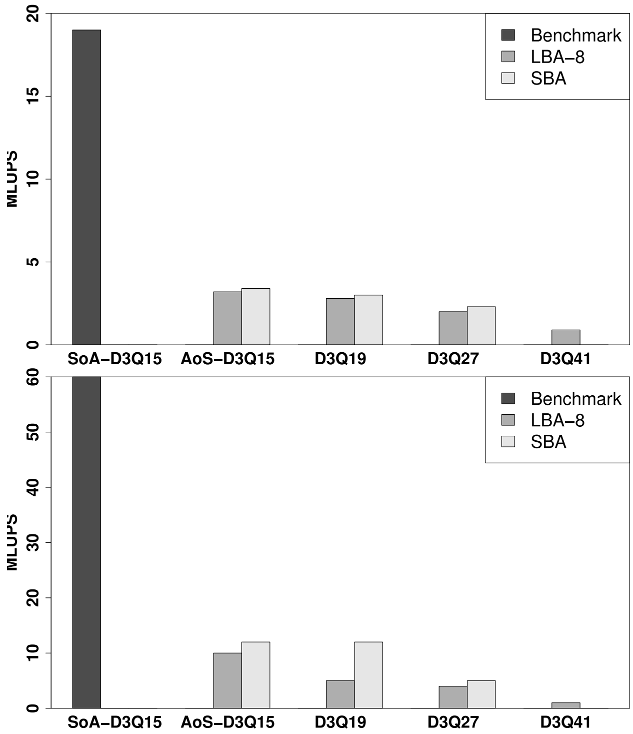

Figure 3.3: MLUPS for SOA and AOS on, Six-Core AMD ® Opteron™Processor 2439 SE (top) and Intel®Xeon™E5-2670 processors (bottom)

a million grid points. Since, MLUPS doesn't take into account the number of discrete velocities N_d, it can't be used to compare different LB models i.e. it is less informative if we are interested in measuring performance as a function of number of discrete velocities. In order to compare efficiency for higher order lattice Boltzmann models, we introduce a new performance measure Mega Elementary Updates Per Second (MEUPS) defined as

$$\text{MEUPS} = \frac{K_x\, K_y\, K_z\, (N_d - 1)}{10^6\, T} = (N_d - 1) \times \text{MLUPS} \tag{3.4}$$

where N_d is 15 for D3Q15, 19 for D3Q19, 27 for D3Q27, 33 for the present D3Q33 model and 41 for D3Q41 model (Ref. [48]). While multiplication of $N_d - 1$ with MLUPS is to normalize the number of memory operations in the advection step (rate limiting step) for different discrete velocity models and the minus 1 in $N_d - 1$ appears because each of the discrete velocity model under consideration has a zero velocity population, which does not require any shift. Thus, MEUPS not only takes into account the effect of grid size but also the number of variables handled at each grid point. The utility of MEUPS can again be reinforced by contrasting it with MLUPS in the following discussion.

MLUPS as a performance measure is not able to distinguish between the two effect: drop due to large number of discrete velocities, drop due to poor memory bandwidth utilizations. As, MEUPS is already accounting for increase in number of discrete velocities, any visible drop there is solely due to poor memory utilizations in higher order LB. To highlight this aspect, we have taken SOA implementation of D3Q15 model as benchmark and scaled the MLUPS and MEUPS

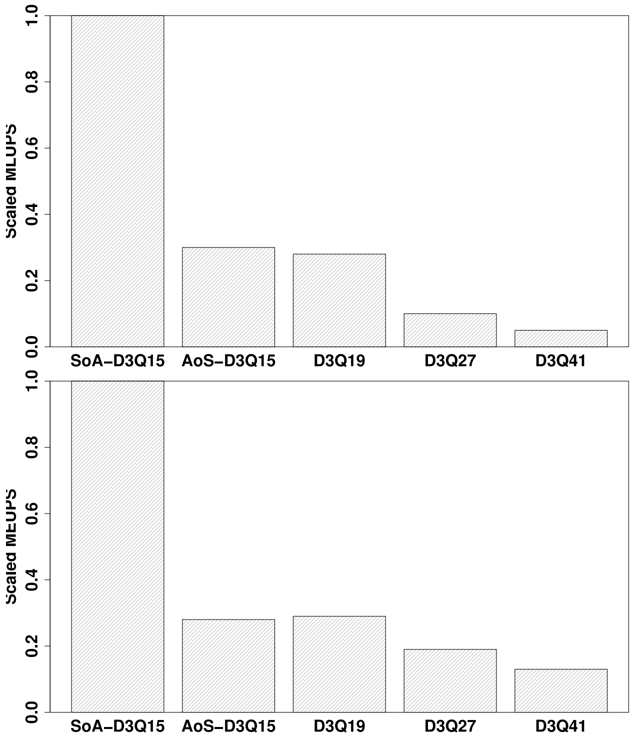

Figure 3.4: Comparison of Ratio of MLUPS and MEUPS among different AOS implementations with respect to SOA-D3Q15 on Intel ®Xeon™E5-2670 processors.

values for different $DmQN$ models with AOS implementation with respect to the corresponding values for SOA-D3Q15 model as shown in Fig. 3.4. It can be observed from Fig. 3.4 that the drop of MLUPS from D3Q15 model to D3Q41 is around 20 times. However the drop in MEUPS from D3Q15 to D3Q41 is around 7.5 times, which suggest that deterioration is a direct function of number of discrete velocities ($(N_d - 1) \times MLUPS$) at least over limited range of discrete velocities explored here. Thus, MEUPS is a better measure for performance than MLUPS and henceforth we have chosen to report advection performance in terms of MEUPS.

As shown in Fig.3.5, all of the AOS implementations are unable to utilize the memory bandwidth. One can see that unlike SOA counterpart none of the AOS implementations manage to use even 20% of the bandwidth. Thus, one can see that memory bandwidth utilization is a major bottleneck for grid based computing. In this work the possible ways to improve bandwidth performance without compromising on compute performance is explored for LB method. Firstly, it is shown that a loop reordering can efficiently reuse the data that is being pre-fetched by compiler. This ultimately leads to substantial boost in performance. Finally, a possible alternate to AOS and SOA via hybridization of data structure is proposed. Subsequently it is shown that a suitably designed data structure, which respect physical features of the underlying computational model, via data flow analysis can allow for full bandwidth utilization by LB method.

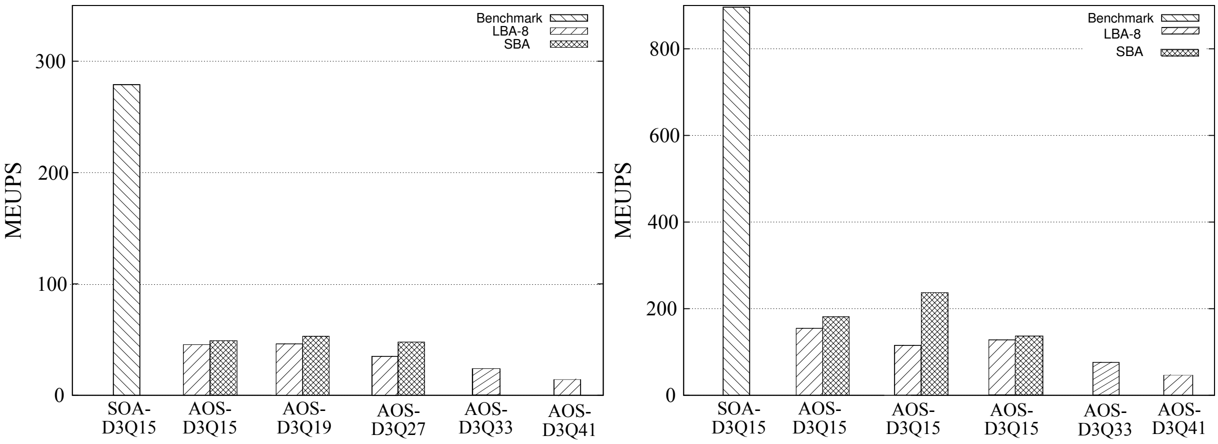

Figure 3.5: MEUPS for SOA and AOS on, Six-Core AMD®Opteron™Processor 2439 SE (left) and Intel ®Xeon™E5-2670 processors (right)

3.4 Loop Reordering

Before doing loop reordering, it is important to note the basis for the data movement in the 8-loop design used in the shift for all direction. It is easy to see that, the 8-loop design is based on purely one dimensional logic. The main idea behind such a loop design is that if data required shift in plus direction then running the loop backwards will ensure that memory location are updated with new values only after older values are shifted to right of their current locations. Assuming that the boundary conditions are taken care one can see that the populations ϕ requiring right shift and the populations ψ requiring left shift can be implemented in 1D as

```
Right Shift
for ( i = K_x+1; i >= 1  ; i = i-1 ){
  ϕ(i) =  ϕ(i-1);
}

Left Shift
for ( i = 1 ; i <= K_x+1 ; i = i+1 ){
  ϕ(i) =  ϕ(i+1);
}
```

Even though the above implementation is easy to understand in 1-D and can be extend easily in 2-D, however, in 3-D imagine writing a set of 3 for loops for each of the 26 velocities in D3Q27 model. Surely, these are too many for loops (3×27. Therefore, what one needs to answer now is that if a larger number of velocities are used or a higher dimension problem (like 4D or 6D LB models) is taken into consideration then is it possible to extend this 1-D logic or does it becomes slow and inefficient because of too many for loops and the high cost associated with the cache mismatch. However, straightforward extension of this logic in 3-D was too conservative. In multi-dimensions, all one needs is that the outer loop is running in opposite to shift direction in the outermost index. For example say the variable ϕ is advecting in $(1, -1)$ direction then

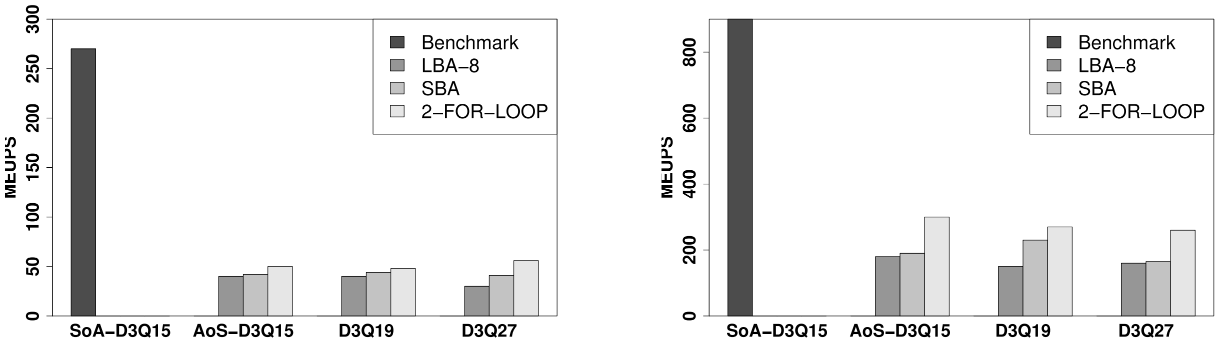

Figure 3.6: MEUPS after loop fusions which allow advection to happen in two *for* loops on, Six-Core AMD®Opteron™Processor 2439 SE (left) and Intel®Xeon™E5-2670 processors (right)

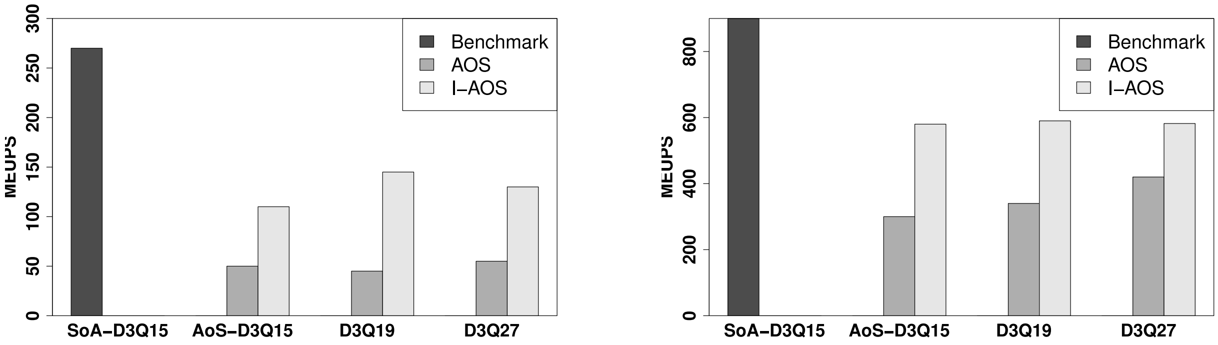

Figure 3.7: MEUPS after breaking the data-structure into building blocks SC, FCC and BCC, with two for loops on, Six-Core AMD®Opteron™Processor 2439 SE (left) and Intel®Xeon™E5-2670 processors(right)

the advection can be written as

```
for ( j = 1                ; j <= $K_y$ ; j = j+1 ){
for ( i = $K_x$ ; i >= 1  ; i = i-1 ){
          $\phi_{(1,-1)}$(i,j) = $\phi_{(1,-1)}$(i-1,j+1);
} }
```

however, the above update can also be written as without changing the outer loop,

```
for ( j = 1 ; j <= $K_y$; j = j+1 ){
for ( i = 1 ; i <= $K_x$; i = i+1 ){
          $\phi_{(1,-1)}$(i,j) = $\phi_{(1,-1)}$(i-1,j+1);
} }
```

if the storage is $\phi_{(1,-1)}(i,j) = \phi_{(1,-1)}[j \times K_x + i]$ then the later update rule is more efficient than the former one. Finally, one would like to highlight the rationale behind redesigning data structure and showcase advantage achieved by it. First, hint for possible performance improvement is there in Fig.3.5, where one can see that D3Q19 model is performing little better than D3Q15 model.

This is remarkable due to the fact that compared to D3Q15 model, D3Q19 is operating with more data per grid point. In order to understand this peculiar feature, first of all one should recall the fact that based on the number of discrete velocities, both D3Q15 model and D3Q19 model are subset of D3Q27 model. While, the D3Q27 model consists of three major building block of simple cubic shell (SC), Face centred cubic shell (FCC) and the body centred cubic shell (BCC). And D3Q15 and D3Q19 models are arrived via pruning of FCC and BCC shell respectively from D3Q27 model. This suggests that the basic building block of a 3-D LB model should play a fundamental role in the data structure design too (see Fig 3.8).

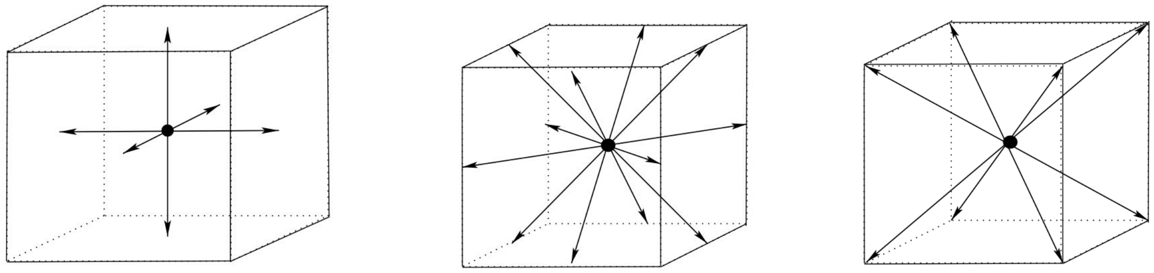
(a) (b) (c)

Figure 3.8: (a) SC (b) FCC and (c) BCC as building blocks of LB

In order to test this hypothesis, an hybrid data structure is constructed where one has an AOS data structure for some subset(s) of velocity as an individual building block rather than trying to fit the whole discrete velocity model in a single or a monolithic data structure. What is done exactly is to lump some of the velocities in a particular data structure and then try to collate all such small data structures to form the working data structure.

As seen in Fig.3.7, this intermediate data structure leads to better performance than the original single AOS data structure for the whole discrete velocity set. However, even after this intermediate data structure, one is able to achieve only close to 50% of the peak performance. The further scope for improvement comes from the basic ansatzes build into the choice of discrete velocities in LB method which are discussed in the next section.

One can easily improve on the intermediate data structure by analysing dependency of data movement in the loop. It is to noted that in a 2-loop formulation of advection, for any given building block say SC,FCC, BCC; only half of the populations get updated in a single for loop. A pseudo code for BCC update via 2 for loop is shown in Appendix. Thus, it seems natural to break the building blocks into two parts. In the next section it is shown that such division of basic building blocks in fact follows a set theoretic algebra.

3.5 Discrete Velocity Set for LB

Following Ref. [43], it can be seen that the choice of discrete velocity set in the LB method is dictated by symmetry and isotropy requirements. The two requirements on the discrete velocity needed to get the correct hydrodynamic description are,

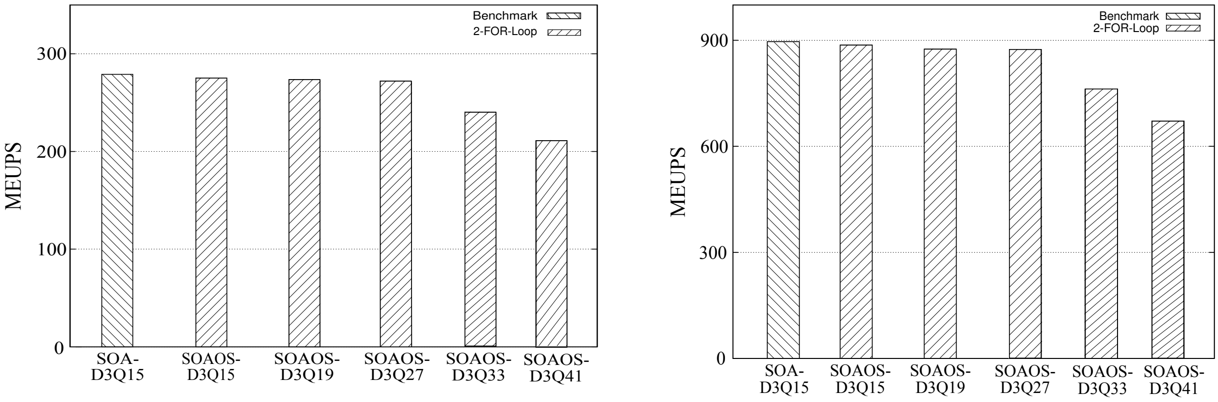

Figure 3.9: MEUPS for SOAOS on, Six-Core AMD®Opteron™Processor 2439 SE (left) and Intel®Xeon™E5-2670 processors (right)

- **Closure under Inversion:** If a discrete velocity $\mathbf{c}_i \equiv (c_{ix}, c_{iy}, c_{iz})$ is an element of the set, so should be its inverse i.e.

$$\mathbf{c}_i \in \mathcal{C} \implies -\mathbf{c}_i \in \mathcal{C}. \tag{3.5}$$

- **Closure under Reflection:** If a discrete velocity $\mathbf{c}_i \equiv (c_{ix}, c_{iy}, c_{iz})$ is an element of the set, then so should be all the possible reflections of it i.e.

$$\mathbf{c}_i \in \mathcal{C} \implies (\bar{c}_{ix}, \bar{c}_{iy}, \bar{c}_{iz}) \in \mathcal{C} \tag{3.6}$$

  where $\bar{c}_{ij}$ with $j = x, y, z$ denotes all possible permutations of $\mathbf{c}_i$ components.

These requirements shows that the essential building blocks that satisfy the closure conditions for the LB method are the SC, FCC and BCC shells (see Fig. 3.8), later these elementary shells are used as the new data-structure itself. The present data flow analysis seems to suggest that data structure must also adhere to such a decomposition. This possibility is explored in the next section.

3.6 Hybrid Data-Structure: SOAOS

Motivated by the construction of the LB method from building blocks [43], a hybrid data-structure termed as “Structure-of-Array-of-Structures (SOAOS)” is built, where AOS is constructed over individual building blocks rather than over entire data set. As seen in Fig.3.7, this intermediate data-structure leads to a better performance, which is about 50% of the peak value.

One then improves upon this intermediate data-structure by breaking the SC, FCC and BCC elementary shells into more atomic building blocks. As said earlier that in the LBA-2 implementation, for any given building block (SC,FCC, BCC) only half of them get updated in a single ’for’ loop. Thus it seems natural to break every block into two parts along the outer loop

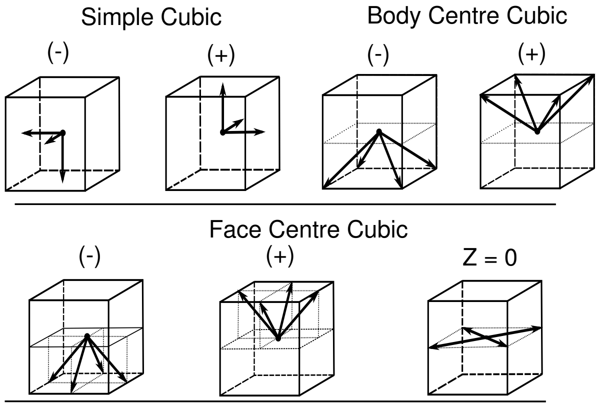

Figure 3.10: SoAoS data-structure construction from AOS for LBM

direction and not to insist on the condition of closure under inversion for individual blocks i.e. to say that if say for SC shell the (1,0,0), (0,1,0) and (0,0,1) are grouped in one shell say SC plus then the velocity (-1,0,0) might be kept in some other group instead of SC plus. Furthermore, instead of the earlier stated condition of reflection in D-dimension, one creates a restrictive reflection condition in $D-1$ dimension. This implies that if a discrete velocity $\mathbf{c}_i \equiv (c_{ix}, c_{iy}, c_{iz})$ is an element of the set, then all possible reflections of it in $D-1$ dimensions with z as outer loop direction are also members of the set, i.e.

$$\mathbf{c}_i \in \mathcal{C} \implies (\bar{c}_{ix}, \bar{c}_{iy}, c_{iz}) \in \mathcal{C} \tag{3.7}$$

where $\bar{c}_{ij} \in \{c_{ix}, c_{iy}\}$ with $j = x, y$. In Fig. 3.10 the SOAOS data-structure based on these considerations is presented. Fig. 3.9 shows that this SOAOS structure is indeed able to almost saturate the memory bandwidth and, hence, is the best alternative to SOA for advection.

Finally, Fig. 3.11 shows that the present model is also able to replicate the performance of AOS for computation too. For non triviality, a multiple relaxation time collision model is implemented where the floating point operations are always higher as compared to single time relaxation BGK collision models [98]. This ensures that the quantitative benefit reported for SOAOS approach remains conservative and provides only the lower bound of gain from the new approach of data structure design. Though, qualitative trends remains similar for different collision models. As a specific example, the reported data is for Quasi-equilibrium type multi-relaxation models proposed in Ref. [99]. For this choice of collision model, the overall application speed-up with the hybrid data-structure (SOAOS) is $1.3X$ over AOS and $1.55X$ over SOA when 256^3 grid points are assigned to each CPU core. Thus the hybrid model of SOAOS, when coupled with the 2-loop advection formulation, provides efficient and optimal LB codes without compromising on the simplicity of the algorithm.

3.7 Outlook

Thus, it can be concluded that the conventional data-structure such as AOS or SOA are alone not optimal for lattice based simulations. In specific case of LB method, it has been shown

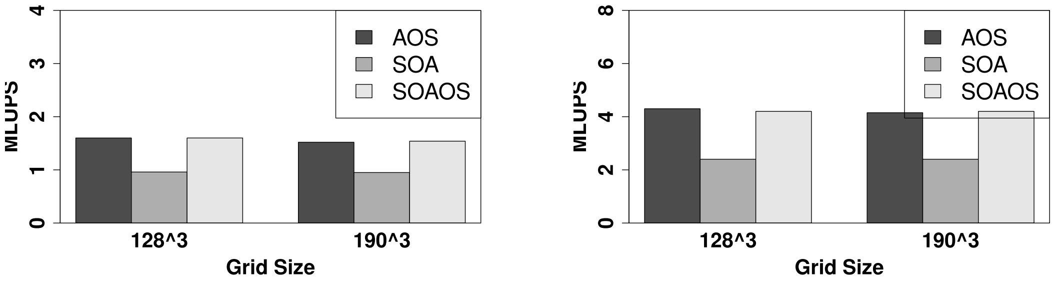

Figure 3.11: Comparison of compute performance in terms of MLUPS for SOAOS with AOS and SOA on, Six-Core AMD®Opteron™Processor 2439 SE (left) and Intel®Xeon™E5-2670 processors (right). The maximum size that could be run on AMD system was limited due to available RAM.

that it is possible to design an optimal data layout, termed as SOAOS, by careful analysis of the algorithm. It is believed that the present approach can be applied to other lattice based simulations too.

Chapter 4

Outlook

The present thesis meets the objective of constructing a higher order lattice Boltzmann model for thermal flows and an efficient implementation of LB models in general. At first, a higher order LB model is constructed by adding just 6 more velocities to the discrete velocity set of D3Q27 model to obtain a "multi-speed on-lattice thermal lattice Boltzmann model" with 33 velocities in 3D with a consistent H-theorem. The utility of the present model is demonstrated with the help of numerical studies performed for a variety of isothermal and thermal flows for e.g. uni-directional flows, lid driven cavity set up, Rayleigh-Bénard instability, velocity and temperature slip in micro flows. The procedure outlined in this thesis for higher order model construction can also be utilized to construct more better and accurate models.

The D3Q33 model was also constructed taking into account that it should be numerically easy to implement with a minimal discrete velocity set. However, the way the discrete velocities are grouped together in a data structure using the AOS or SOA data structure alone is shown to be suboptimal. In this thesis, a hybrid data layout called "Structure-of-Array-of-Structures (SOAOS)" was proposed based on the requirements of physical symmetry and isotropy necessary for recovering hydrodynamics. In SOAOS data structure, the discrete velocities were arranged in a fashion that allowed for full memory bandwidth usage without degrading compute performance. that is both advection and collision friendly.

Finally, the prospective applications of the present work could be

- To extend the theory of general LB model construction to take into account anisotropy of the higher order moments and provide suitable parameters to quantify them.
- More shells could be added to D3Q33 model to obtain more accurate LB model. While the ultimate goal would be obtain an LB model which can simulate a fluid with variable Prandtl number and develop fully compressible NSF solvers via LB method
- The new data structure "SOAOS" could be used as one of the basis for a generic data structure design which could then be in-built in smart compilers that can reshuffle data structure according to the underlying computer architecture so as to obtain an optimal performance with little assistance from the end user.

Appendix A

Discrete Equilibrium Distribution & it's Moments

This appendix outlines the steps involved in obtaining the discrete equilibrium distribution function and it's relevant moments for the case of thermo-hydrodynamics. We first make use of the closure under inversion property of the discrete velocity model to obtain

$$
\begin{aligned}
\sum_{i=1}^{N_d} w_i \, \Gamma^{c_i^2/\theta_0} \left(B_{ix}^{c_{ix}/\sqrt{\theta_0}} \, B_y^{c_{iy}/\sqrt{\theta_0}} \, B_z^{c_{iz}/\sqrt{\theta_0}} \right) &= \frac{\rho}{A}, \\
\sum_{i=1}^{N_d/2} w_i \, \Gamma^{c_i^2/\theta_0} \, |c_{i\kappa}| \left(B_x^{c_{ix}/\sqrt{\theta_0}} \, B_y^{c_{iy}/\sqrt{\theta_0}} \, B_z^{c_{iz}/\sqrt{\theta_0}} - B_x^{-c_{ix}/\sqrt{\theta_0}} \, B_{iy}^{-c_{iy}/\sqrt{\theta_0}} \, B_{iz}^{-c_{iz}/\sqrt{\theta_0}} \right) &= \frac{\rho u_\kappa}{A}, \\
\sum_{i=1}^{N_d/2} w_i \, \Gamma^{c_i^2/\theta_0} \, \frac{c_i^2}{2} \left(B_x^{c_{ix}/\sqrt{\theta_0}} \, B_y^{c_{iy}/\sqrt{\theta_0}} \, B_z^{c_{iz}/\sqrt{\theta_0}} + B_x^{-c_{ix}/\sqrt{\theta_0}} \, B_{iy}^{-c_{iy}/\sqrt{\theta_0}} \, B_{iz}^{-c_{iz}/\sqrt{\theta_0}} \right) &= \frac{E}{A}.
\end{aligned}
\tag{A.1}
$$

This non-linear equation has an explicit solution at reference temperature θ_0, which yields

$$
A_0(\theta_0) = 1 \quad \Gamma_0(\theta_0) = 1. \tag{A.2}
$$

Now, one expands Γ_0 by perturbation expansion around the reference temperature solutions $\Gamma_0(\theta_0)$ with $\Delta\theta$ as smallness parameter

$$
\Gamma_0(\theta) = 1 + \Delta\theta \, \Gamma_0^{(1)} + \Delta^2\theta \, \Gamma_0^{(2)} + \Delta^3\theta \, \Gamma_0^{(3)} + \Delta^4\theta \, \Gamma_0^{(4)} + \cdots . \tag{A.3}
$$

On making use of above equation in $z_i = \Gamma_0^{y_i}$, one can write

$$
\begin{aligned}
z_i =& 1 + y_i \sum_{n_1=1}^{\infty} (\Delta^{n_1}\theta) \Gamma_0^{(n_1)} + \frac{y_i(y_i-1)}{2} \sum_{n_1=1}^{\infty} \sum_{n_2=1}^{\infty} (\Delta^{n_1+n_2}\theta) \Gamma_0^{(n_1)} \Gamma_0^{(n_2)} + \\
& \frac{y_i(y_i-1)(y_i-2)}{6} \sum_{n_1=1}^{\infty} \sum_{n_2=1}^{\infty} \sum_{n_3=1}^{\infty} (\Delta^{n_1+n_2+n_3}\theta) \Gamma_0^{(n_1)} \Gamma_0^{(n_2)} \Gamma_0^{(n_3)} + \cdots .
\end{aligned}
\tag{A.4}
$$

Using Eq. 2.33, we also have

$$
\begin{aligned}
\sum_{i=1}^{N_d} w_i \, z_i \, (y_i - D) =& 2D \sum_{n_1=1}^{\infty} (\Delta^{n_1}\theta) \Gamma_0^{(n_1)} + \left(\frac{g_3}{2} - \frac{D(D+1)(D-2)}{2}\right) \sum_{n_1=1}^{\infty} \sum_{n_2=1}^{\infty} (\Delta^{n_1+n_2}\theta) \Gamma_0^{(n_1)} \Gamma_0^{(n_2)} \\
& + \left(\frac{g_4}{6} - \frac{(D-3)g_3}{6}\right) \sum_{n_1=1}^{\infty} \sum_{n_2=1}^{\infty} \sum_{n_3=1}^{\infty} (\Delta^{n_1+n_2+n_3}\theta) \Gamma_0^{(n_1)} \Gamma_0^{(n_2)} \Gamma_0^{(n_3)} + \cdots ,
\end{aligned}
\tag{A.5}
$$

where we have introduced the following notation for the moments of weights as

$$g_n = \sum_{i=1}^{N_d} w_i \prod_{k=1}^{n} (y_i - k + 1) \tag{A.6}$$

for any positive integer n and corresponding to n^{th} moment the quantity $\sum_{i=1}^{N_d} w_i y_i^n$ is related to g_n as

$$\begin{aligned}\sum_{i=1}^{N_d} w_i y_i^n =& g_n + \frac{n(n-1)}{2} g_{n-1} + \frac{n(n-1)(n-2)(3n-5)}{24} g_{n-2} + \frac{n(n-1)(n-2)^2(n-3)^2}{48} g_{n-3} + \\ & \frac{n(n-1)(n-2)(n-3)(n-4)}{120 * 48} (485\,n - 150\,n^2 + 15\,n^3 - 502)\, g_{n-4} + \cdots .\end{aligned} \tag{A.7}$$

Therefore, ${A_0}^{-1}$ can be calculated as

$$\begin{aligned}{A_0}^{-1} =& 1 + D \sum_{n_1=1}^{\infty} (\Delta^{n_1}\theta)\Gamma_0^{(n_1)} + \frac{D(D+1)}{2} \sum_{n_1=1}^{\infty}\sum_{n_2=1}^{\infty} (\Delta^{n_1+n_2}\theta)\Gamma_0^{(n_1)}\Gamma_0^{(n_2)} + \\ & \frac{g_3}{6} \sum_{n_1=1}^{\infty}\sum_{n_2=1}^{\infty}\sum_{n_3=1}^{\infty} (\Delta^{n_1+n_2+n_3}\theta)\Gamma_0^{(n_1)}\Gamma_0^{(n_2)}\Gamma_0^{(n_3)} + \cdots ,\end{aligned} \tag{A.8}$$

The above expression can be simplified by introducing the following deviations from Maxwell-Boltzmann value for g's as

$$h_n = g_n - g_n^{\text{MB}} \tag{A.9}$$

The $\Gamma_0(\theta_0)$ series is then calculated as

$$\begin{aligned}\Gamma_0 =& 1 + \frac{\Delta\theta}{2} - \frac{\Delta^2\theta}{16\,D}(6D + h_3) + \frac{\Delta^3\theta}{192\,D^2}\Big(52D^2 + 30Dh_3 + 8D^2h_3 + 3h_3^2 - 2Dh_4\Big) + \\ & \frac{\Delta^4\theta}{3072\,D^3}\Big(-568D^3 - 700D^2h_3 - 376D^3h_3 - 40D^4h_3 - 210Dh_3^2 - 80D^2h_3^2 - 15h_3^3\Big) + \\ & \frac{\Delta^4\theta}{3072\,D^3}\Big(104D^2h_4 + 20D^3h_4 + 20Dh_3h_4 - 4D^2h_5\Big)\end{aligned} \tag{A.10}$$

Once the Γ_0 is known then A_0 can be calculated. Then the equilibrium expression can be obtained for D=3 as

$$
\begin{aligned}
\bar{f}_i^{\text{eq}} = w_i\rho\Bigg[&1 + \frac{\Delta\theta}{2}\left(y_i - 3\right) + \frac{\Delta^2\theta}{8}\left(15 - 10y_i + y_i^2 - \underline{\frac{h_3}{6}\left(y_i - 3\right)}\right) + \\
&\frac{\Delta^3\theta}{48}\left(-105 + 105y_i - 21y_i^2 + y_i^3 + \underline{\frac{h_3^2}{12}\left(y_i - 3\right) + \frac{h_3}{2}\left(-35 + 16y_i - y_i^2\right) - \frac{h_4}{6}\left(y_i - 3\right)}\right) + \\
&\frac{\Delta^4\theta}{384}\left(945 - 1260y_i + 378y_i^2 - 36y_i^3 + y_i^4\right) + \frac{\Delta^4\theta}{384}\left(-\underline{\frac{5}{72}h_3^3\left(y_i - 3\right) + \frac{h_3^2}{12}\left(267 - 110y_i + 5y_i^2\right)}\right) + \\
&\frac{\Delta^4\theta}{384}\left(\underline{\frac{h_3}{18}\left(8163 + 5h_4\left(y_i - 3\right) - 4881y_i + 594y_i^2 - 18y_i^3\right)}\right) + \\
&\frac{\Delta^4\theta}{384}\left(\underline{-\frac{h_5}{6}\left(y_i - 3\right) + \frac{h_4}{6}\left(-153 + 69y_i - 4y_i^2\right)}\right) + \ldots\Bigg]
\end{aligned}
\tag{A.11}
$$

where, the underlined part represents the residue or deviation from the expected discrete projection of $\bar{f}_i^{\text{MB}}$. Before proceeding further, it is useful to see that the fourth order moment at zero velocity can be written from the equilibrium expression Eq. (A.11) as

$$
\sum_i \bar{f}_i^{\text{eq}} c_{i\alpha} c_{i\beta} c_i^2 = \rho\theta^2\delta_{\alpha\beta}5 + \bar{h}_4\,\rho\theta_0^2\delta_{\alpha\beta}
\tag{A.12}
$$

where, $\bar{h}_4$ is dependent on h_n's as

$$
\begin{aligned}
\bar{h}_4 = \Bigg[&h_3\frac{\Delta\theta}{6} + \frac{\Delta^2\theta}{144}\left(-84h_3 - h_3^2 + 6h_4\right) + \frac{\Delta^3\theta}{1728}\left(1308h_3 + 120h_3^2 + h_3^3 - 252h_4 - 8h_3h_4 + 12h_5\right) \\
&+ \frac{\Delta^4\theta}{384\times 216}\left(-49104h_3 - 23988h_3^2 - 780h_3^3 - 5h_3^4 + 20016h_4 + 3396h_3h_4\right) + \\
&\frac{\Delta^4\theta}{384\times 216}\left(50h_3^2h_4 - 48h_4^2 - 2232h_5 - 84h_3h_5 + 72h_6\right)\Bigg].
\end{aligned}
\tag{A.13}
$$

First of all, at zero velocity and arbitrary temperature

$$
\tilde{\sigma}_{\alpha\beta} = 0, \quad \tilde{Q}_{\alpha\beta\gamma} = 0, \quad \tilde{q}_{\alpha} = 0, \quad \tilde{R} = \frac{p^2}{\rho}(\bar{h}_4).
\tag{A.14}
$$

It can be seen that at least for linear thermal equilibrium to be correct it is necessary that $\tilde{R} \to 0$ which is possible provided $h_3 \to 0$. This completes the discussion for zero velocity eqilibrium while for non zero velocity equilibrium we need to evaluate appropriate moments of

f_i^{eq}. For convenience, the zero velocity equilibrium expression can be rearranged as

$$\begin{aligned}\bar{f}_i^{\text{eq}} = w_i\rho\Bigg[& 1 - \frac{h_3\Delta^3\theta}{48} + \frac{10\Delta^4\theta\, h_3}{128} + \frac{\Delta^4\theta\, h_3^2}{384} - \frac{h_4\Delta^4\theta}{384} \\ & + \frac{\Delta\theta}{2}\,(y_i - 3)\Bigg(1 - \frac{\Delta\theta\, h_3}{24} + \frac{(36\,h_3 + h_3^2 - 2\,h_4)\,\Delta^2\theta}{288} - \frac{\Delta^3\theta}{13824}\Big(3324h_3 + 360h_3^2 + 5h_3^3 - 348h_4 - 20h_3h_4 + 1 \\ & + \frac{\Delta^2\theta}{8}\Big(15 - 10y_i + y_i^2\Big)\Bigg(1 - \frac{h_3\,\Delta\theta}{12} - \frac{h_4\Delta^2\theta}{72} + \frac{\Delta^2\theta\, h_3}{4} + \frac{5h_3^2\,\Delta^2\theta}{576}\Bigg) + \\ & \frac{\Delta^3\theta}{48}\Big(-105 + 105y_i - 21y_i^2 + y_i^3\Big)\Big(1 - \frac{\Delta\theta\, h_3}{8}\Big) + \frac{\Delta^4\theta}{384}\Big(945 - 1260y_i + 378y_i^2 - 36y_i^3 + y_i^4\Big) + \cdots\Bigg]\end{aligned} \tag{A.15}$$

so that the contracted fourth order moment can be evaluated as

$$\sum_i \bar{f}_i^{\text{eq}} c_{i\alpha}c_{i\beta}c_i^2 = \frac{\rho\,\theta_0^2}{3}\left(3 + 3\,\Delta\theta + \sum_i \frac{\bar{f}_i^{\text{eq}}}{\rho}(y_i^2 - y_i)\right)\delta_{\alpha\beta}. \tag{A.16}$$

This gives

$$\begin{aligned}\sum_i \bar{f}_i^{\text{eq}} c_{i\alpha}c_{i\beta}c_i^2 = 5\rho\,\theta^2\delta_{\alpha\beta} + \frac{\rho\,\theta_0^2\delta_{\alpha\beta}}{3}\Bigg[& \frac{\Delta\theta h_3}{2} + \frac{\Delta^2\theta}{48}\Big(6h_4 - 84h_3 - h_3^2\Big) + 12\Bigg(-\frac{h_3\Delta^3\theta}{48} + \frac{10\Delta^4\theta\, h_3}{128} + \frac{\Delta^4\theta\, h_3^2}{384} - \\ & + \frac{\Delta\theta}{2}\,(h_3 + 54)\Bigg(\frac{(36\,h_3 + h_3^2 - 2\,h_4)\,\Delta^2\theta}{288} - \frac{\Delta^3\theta}{13824}\Big(3324h_3 + 360h_3^2 + 5h_3^3 - 348h_4 - 20h_3h_4 + 12h_5\Big)\Bigg) \\ & + \frac{\Delta^2\theta}{8}\,(120 + h_4 - 5h_3)\Bigg(-\frac{h_3\,\Delta\theta}{12} - \frac{h_4\Delta^2\theta}{72} + \frac{\Delta^2\theta\, h_3}{4} + \frac{5h_3^2\,\Delta^2\theta}{576}\Bigg) \\ & + \frac{\Delta^3\theta}{48}\,(h_5 - 12h_4 + 19h_3)\Big(1 - \frac{\Delta\theta\, h_3}{8}\Big) + \frac{\Delta^4\theta}{384}\,(11h_3 + 109h_4 - 22h_5 + h_6) + \cdots\Bigg].\end{aligned} \tag{A.17}$$

The above expression is written in above fashion to show the leading MB contribution plus the error. And within the error term with temperature perturbation wise distribution

$$\begin{aligned}\sum_i \bar{f}_i^{\text{eq}} c_{i\alpha}c_{i\beta}c_i^2 = 5\rho\,\theta^2\delta_{\alpha\beta} + \rho\,\theta_0^2\delta_{\alpha\beta}\Bigg[& \frac{\Delta\theta h_3}{6} + \frac{\Delta^2\theta}{144}\left(-84h_3 - h_3^2 + 6h_4\right) + \\ & \frac{\Delta^3\theta}{1728}\left(1308h_3 + 120h_3^2 + h_3^3 - 252h_4 - 8h_3h_4 + 12h_5\right) \\ & + \frac{\Delta^4\theta}{384\times 216}\left(-49104h_3 - 23988h_3^2 - 780h_3^3 - 5h_3^4 + 20016h_4 + 3396h_3h_4\right) + \\ & \frac{\Delta^4\theta}{384\times 216}\left(50h_3^2h_4 - 48h_4^2 - 2232h_5 - 84h_3h_5 + 72h_6\right)\Bigg]\end{aligned} \tag{A.18}$$

and extending further,

$$\sum_i \bar{f}_i^{\mathrm{eq}} c_{i\alpha} c_{i\beta} c_i^2 c_i^2 = 35\rho\,\theta^2\delta_{\alpha\beta} + \rho\,\theta_0^2\delta_{\alpha\beta}\Bigg[\frac{\Delta\theta}{6}\left(6h_3 + h_4\right) + \frac{\Delta^2\theta}{144}\Big(-840h_3 - 6h_3^2 - h_3h_4 + 6h_5\Big) + \frac{\Delta^3\theta}{1728}\Big(8640h_3 + 1056h_3^2 + 6h_3^3 - 1740h_4 + 24h_3h_4 + h_3^2h_4 - 2h_4^2 - 72h_5 - 6h_3h_5 + 12h_6\Big) + \cdots\Bigg] \tag{A.19}$$

Now, while looking at the finite velocity moments one needs the expression for $\sum_i \bar{f}_i^{\mathrm{eq}} c_{i\alpha} c_{i\beta} c_{i\gamma} c_{i\kappa}$

$$\begin{aligned} \sum_i \bar{f}_i^{\mathrm{eq}} c_{i\alpha} c_{i\beta} c_{i\gamma} c_{i\kappa} &= A\,\Delta\alpha\beta\gamma\kappa + B\,\delta\alpha\gamma\kappa\beta, \\ \sum_i \bar{f}_i^{\mathrm{eq}} c_{i\alpha} c_{i\beta} c_i^2 &= 5\,A\,\delta\alpha\beta + B\,\delta\alpha\beta, \\ 5\rho\,\theta^2 + \rho\,\theta_0^2\,\bar{h}_4 &= 5\,A\, + B, \\ B &= 5\rho\,\theta^2 + \rho\,\theta_0^2\bar{h}_4 - 5\,A \end{aligned} \tag{A.20}$$

where $A = \sum_i \bar{f}_i^{\mathrm{eq}} c_{ix}^2 c_{iy}^2$. Till quadratic in temperature perturbation one gets,

$$A = \rho\Bigg[\sum_i w_i c_{ix}^2 c_{iy}^2 + \frac{\Delta\theta}{2}\sum_i w_i c_{ix}^2 c_{iy}^2\left(\frac{c_i^2}{\theta_0} - 3\right) + \frac{\Delta^2\theta}{8}\sum_i w_i c_{ix}^2 c_{iy}^2\left(15 - 10\frac{c_i^2}{\theta_0} + \frac{c_i^4}{\theta_0^2}\right) - \frac{\Delta^2\theta}{8}\left(\frac{h_3}{6}\sum_i w_i c_{ix}^2 c_{iy}^2\left(\frac{c_i^2}{\theta_0} - 3\right)\right) + \ldots\Bigg] \tag{A.21}$$

this can be written in a convenient form with the substitution

$$\begin{aligned} \theta_0^2 k_1 &= \sum_i w_i c_{ix}^2 c_{iy}^2 - \theta_0^2, \\ \theta_0^2 k_2 &= \sum_i w_i c_{ix}^2 c_{iy}^2\left(\frac{c_i^2}{\theta_0} - 3\right) - 4\theta_0^2, \\ \theta_0^2 k_3 &= \sum_i w_i c_{ix}^2 c_{iy}^2\left(15 - 10\frac{c_i^2}{\theta_0} + \frac{c_i^4}{\theta_0^2}\right) - 8\theta_0^2 \end{aligned} \tag{A.22}$$

and so on. This gives,

$$\begin{aligned}
A &= \rho\left[k_1\theta_0^2 + \theta_0^2 + \frac{\Delta\theta}{2}\left(k_2\theta_0^2 + 4\theta_0^2\right) + \frac{\Delta^2\theta}{8}\left(k_3\theta_0^2 + 8\theta_0^2 - \frac{h_3}{6}\left(k_2\theta_0^2 + 4\theta_0^2\right)\right) + \dots\right],\\
&= \rho\,\theta_0^2\left(1 + 2\,\Delta\theta + \Delta^2\theta\right) + \rho\,\theta_0^2\left[k_1 + \frac{\Delta\theta}{2}\,(k_2) + \frac{\Delta^2\theta}{8}\left(k_3 - \frac{h_3}{6}\left(k_2 + 4\theta_0^3\right)\right) + \dots\right],\\
&= \rho\theta^2 + \rho\,\theta_0^2\left[k_1 + \frac{\Delta\theta}{2}\,(k_2) + \frac{\Delta^2\theta}{8}\left(k_3 - \frac{h_3}{6}k_2\right) + \dots\right], \qquad \text{(A.23)}\\
B &= 5\rho\,\theta^2 + \rho\,\theta_0^2\bar{h}_4 - 5\,\rho\theta^2 - 5\,\rho\,\theta_0^2\left[k_1 + \frac{\Delta\theta}{2}\,(k_2) + \frac{\Delta^2\theta}{8}\left(k_3 - \frac{h_3}{6}k_2\right) + \dots\right],\\
&= \rho\,\theta_0^2\bar{h}_4 - 5\,\rho\,\theta_0^2\left[k_1 + \frac{\Delta\theta}{2}k_2 + \frac{\Delta^2\theta}{8}\left(k_3 - \frac{h_3}{6}k_2\right) + \dots\right]
\end{aligned}$$

this gives finally,

$$\sum_i \bar{f}_i^{\text{eq}} c_{i\alpha}c_{i\beta}c_{i\gamma}c_{i\kappa} = \rho\theta^2\,\Delta\alpha\beta\gamma\kappa + \rho\,\theta_0^2\left[k_1 + \frac{\Delta\theta}{2}k_2\right]\Delta\alpha\beta\gamma\kappa + \rho\,\theta_0^2\bar{h}_4\,\delta\alpha\gamma\kappa\beta - 5\,\rho\,\theta_0^2\left[k_1 + \frac{\Delta\theta}{2}k_2\right]\delta\alpha\gamma\kappa\beta \qquad \text{(A.24)}$$

Once the desired temperature perturbation expansion in $\bar{f}_i^{\text{eq}}$ is obtained, the velocity perturbation can be built on top of this by introducing the smallness parameter ϵ for velocity perturbation in low Mach no. as

$$\begin{aligned}
f_i^{\text{eq}} =& \bar{f}_i^{\text{eq}}\Bigg[1 + \epsilon(\alpha^{(1)} + \beta_\kappa^{(1)}c_{i\kappa} + \gamma^{(1)}c_i^2) + \epsilon^2\left(\alpha^{(2)} + \beta_\kappa^{(2)}c_{i\kappa} + \gamma^{(2)}c_i^2 + \frac{1}{2}(\alpha^{(1)} + \beta_\kappa^{(1)}c_{i\kappa} + \gamma^{(1)}c_i^2)^2\right)\\
&+ \epsilon^3\left((\alpha^{(1)} + \beta_\kappa^{(1)}c_{i\kappa} + \gamma^{(1)}c_i^2)(\alpha^{(2)} + \beta_\kappa^{(2)}c_{i\kappa} + \gamma^{(2)}c_i^2) + (\alpha^{(3)} + \beta_\kappa^{(3)}c_{i\kappa} + \gamma^{(3)}c_i^2)\right)\\
&+ \epsilon^3\left(\frac{1}{6}(\alpha^{(1)} + \beta_\kappa^{(1)}c_{i\kappa} + \gamma^{(1)}c_i^2)^3\right) + \dots\Bigg].
\end{aligned} \qquad \text{(A.25)}$$

Solving at various orders, at order ϵ,

$$\begin{aligned}
\sum_i \bar{f}_i^{\text{eq}}\left(\alpha^{(1)} + \beta_\kappa^{(1)}c_{i\kappa} + \gamma^{(1)}c_i^2\right) &= 0,\\
\sum_i \bar{f}_i^{\text{eq}}c_{i\alpha}\left(\alpha^{(1)} + \beta_\kappa^{(1)}c_{i\kappa} + \gamma^{(1)}c_i^2\right) &= \rho\,u_\alpha,, \qquad \text{(A.26)}\\
\sum_i \bar{f}_i^{\text{eq}}c_i^2\left(\alpha^{(1)} + \beta_\kappa^{(1)}c_{i\kappa} + \gamma^{(1)}c_i^2\right) &= 0
\end{aligned}$$

for which the following calculations was required,

$$\sum_i \bar{f}_i^{\text{eq}} c_{i\alpha}c_{i\kappa} = \rho\theta\delta\alpha\kappa \qquad \text{(A.27)}$$

this gives,

$$
\begin{aligned}
\beta_\kappa^{(1)} &= \frac{\rho\, u_\alpha}{\sum_i \bar{f}_i^{\mathrm{eq}} c_{i\alpha} c_{i\kappa}}, \\
&= \frac{u_\kappa}{\theta},
\end{aligned}
\tag{A.28}
$$

and $\alpha^{(1)} = 0$, $\gamma^{(1)} = 0$. Next, at order ϵ^2,

$$
\begin{aligned}
\sum_i \bar{f}_i^{\mathrm{eq}} \left(\alpha^{(2)} + \beta_\kappa^{(2)} c_{i\kappa} + \gamma^{(2)} c_i^2 + \frac{u_\kappa u_\alpha}{2\theta^2} c_{i\kappa} c_{i\alpha} \right) &= 0, \\
\sum_i \bar{f}_i^{\mathrm{eq}} c_{i\alpha} \left(\alpha^{(2)} + \beta_\kappa^{(2)} c_{i\kappa} + \gamma^{(2)} c_i^2 + \frac{u_\kappa u_\eta}{2\theta^2} c_{i\kappa} c_{i\eta} \right) &= 0, \\
\sum_i \bar{f}_i^{\mathrm{eq}} c_i^2 \left(\alpha^{(2)} + \beta_\kappa^{(2)} c_{i\kappa} + \gamma^{(2)} c_i^2 + \frac{u_\kappa u_\alpha}{2\theta^2} c_{i\kappa} c_{i\alpha} \right) &= \rho\, u^2
\end{aligned}
\tag{A.29}
$$

this simplifies to,

$$
\begin{aligned}
\alpha^{(2)} + 3\,\theta\,\gamma^{(2)} + \frac{u^2}{2\theta} &= 0, \\
3\,\theta\,\alpha^{(2)} + 3\,\theta^2 \left(5 + \frac{\theta_0^2}{\theta^2}\,\bar{h}_4 \right) \gamma^{(2)} + \frac{u^2}{2} \left(5 + \frac{\theta_0^2}{\theta^2}\,\bar{h}_4 \right) &= u^2
\end{aligned}
\tag{A.30}
$$

For the above calculations the following equation was used,

$$
\sum_i \bar{f}_i^{\mathrm{eq}} c_{i\alpha} c_{i\kappa} c_i^2 = \left(5\,\rho\theta^2 \ + \rho\theta_0^2\,\bar{h}_4 \right) \delta_{\alpha\kappa}
\tag{A.31}
$$

which gives,

$$
\begin{aligned}
\gamma^{(2)} &= -\frac{u^2}{6\theta^2} \underbrace{\left[\frac{\bar{h}_4 \left(\frac{\theta_0}{\theta} \right)^2}{\frac{\bar{h}_4}{3} \left(\frac{\theta_0}{\theta} \right)^2 + 2} \right]}_{\hat{h}_4} = -\frac{u^2}{6\theta^2} \hat{h}_4, \\
\alpha^{(2)} &= -\frac{u^2}{2\theta} (1 - \hat{h}_4),
\end{aligned}
\tag{A.32}
$$

and $\beta_\kappa^{(2)} = 0$. Finally setting $\epsilon = 1$ one obtains,

$$
f_i^{\mathrm{eq}} = \bar{f}_i^{\mathrm{eq}} \left[1 + \frac{u_\kappa c_{i\kappa}}{\theta} - \frac{u^2}{2\theta} \left(1 - \hat{h}_4 \right) - \hat{h}_4 \frac{u^2}{6\theta^2}\, c_i^2 + \frac{1}{2} \left(\frac{u_\kappa c_{i\kappa}}{\theta} \right)^2 + \dots \right]
\tag{A.33}
$$

where,

$$\begin{aligned}\hat{h}_4 =&\frac{\bar{h}_4\left(\frac{\theta_0}{\theta}\right)^2}{\frac{\bar{h}_4}{3}\left(\frac{\theta_0}{\theta}\right)^2+2},\\ =&\frac{3\,\bar{h}_4}{\bar{h}_4+6\,(1+\Delta\theta)^2},\\ =&\frac{\bar{h}_4}{2+\frac{\Delta\theta}{18}\left(h_3+72\right)+\frac{\Delta^2\theta}{432}\left(-84h_3-h_3^2+6h_4+864\right)+\Delta^3\theta\,()+\Delta^4\theta\,()+\dots}\end{aligned} \tag{A.34}$$

which indeed goes to zero as $h_4 \to 0$. Therefore, the finite velocity residual moments are

- Residual stress

$$\begin{aligned}\tilde{\sigma}_{\alpha\beta} &= \langle c_{i\alpha}c_{i\beta}\rangle - \rho u_\alpha u_\beta - p\delta_{\alpha\beta},\\ &= -\frac{\rho\,u^2}{2}\delta_{\alpha\beta}\left(1-\hat{h}_4\right) - \hat{h}_4\frac{\rho\,u^2}{6}\left(5+\frac{\theta_0^2}{\theta^2}\,\bar{h}_4\right)\delta_{\alpha\beta} + \frac{u_\kappa u_\gamma}{2\theta^2}\sum_i^{N_d}\bar{f}_i^{\mathrm{eq}}c_{i\kappa}c_{i\gamma}c_{i\alpha}c_{i\beta} - \rho u_\alpha u_\beta,\\ &= -\hat{\mathbf{h}}_\mathbf{4}\frac{\rho\,u^2}{3}\delta_{\alpha\beta} + \bar{\mathbf{h}}_\mathbf{4}\left(\hat{\mathbf{h}}_\mathbf{4}+1\right)\frac{\rho\,u^2}{(\theta/\theta_0)^2}\delta_{\alpha\beta} + \left(\mathbf{k_1}+\frac{\Delta\theta}{2}\mathbf{k_2}\right)\frac{\rho\,u_\kappa u_\gamma}{2(\theta/\theta_0)^2}\left(\Delta_{\alpha\beta\kappa\gamma}-5\delta_{\alpha\beta\kappa\gamma}\right)\end{aligned} \tag{A.35}$$

- Heat tensor and Residual Heat flux

$$\begin{aligned}\tilde{Q}_{\alpha\beta\gamma} &= \langle c_{i\alpha}c_{i\beta}c_{i\gamma}\rangle - p\left(u_\alpha\delta_{\gamma\beta}+u_\beta\delta_{\alpha\gamma}+u_\gamma\delta_{\alpha\beta}\right) - \rho u_\alpha u_\beta u_\gamma,\\ &= \bar{\mathbf{h}}_\mathbf{4}\frac{\rho\,u_\kappa}{\theta}\delta_{\alpha\beta\gamma\kappa}\,\theta_0^2 + \left(\mathbf{k_1}+\frac{\Delta\theta}{2}\mathbf{k_2}+\frac{\Delta^2\theta}{8}\left(\mathbf{k_3}-\frac{\mathbf{h_3}}{6}\mathbf{k_2}\right)\right)\frac{\rho\,u_\kappa}{\theta}\left(\Delta_{\alpha\beta\kappa\gamma}-5\delta_{\alpha\beta\kappa\gamma}\right)\theta_0^2,\\ \tilde{q}_\alpha &= \frac{1}{2}\left\langle c_{i\alpha}c_i^2\right\rangle - \frac{5}{2}\rho\,u_\alpha\,\theta - \frac{1}{2}\rho\,u_\alpha\,u^2,\\ &= \bar{\mathbf{h}}_\mathbf{4}\left(\frac{\rho\,u_\alpha}{2\theta}\right)\theta_0^2\end{aligned} \tag{A.36}$$

- Residual fourth order moments

$$\begin{aligned}\tilde{R}_{\alpha\beta} &= \left\langle c_{i\alpha}c_{i\beta}c_i^2\right\rangle - 5\,\rho\,\theta^2\,\delta_{\alpha\beta} - 7\rho\,\theta\,u_\alpha u_\beta - u^2\left(\rho u_\alpha u_\beta + p\delta_{\alpha\beta}\right),\\ &= \left[1-\frac{u^2}{2\theta}\left(1-\hat{h}_4\right)\right]\sum_i^{N_d}\bar{f}_i^{\mathrm{eq}}c_{i\alpha}c_{i\beta}c_i^2 - \left(\hat{h}_4\frac{u^2}{6\theta^2}\right)\sum_i^{N_d}\bar{f}_i^{\mathrm{eq}}c_{i\alpha}c_{i\beta}c_i^2c_i^2\\ &+\left(\frac{u_\kappa u_\gamma}{2\theta^2}\right)\sum_i^{N_d}\bar{f}_i^{\mathrm{eq}}c_{i\kappa}c_{i\gamma}c_{i\alpha}c_{i\beta}c_i^2 - 5\,\rho\,\theta^2\,\delta_{\alpha\beta} - 7\rho\,\theta\,u_\alpha u_\beta - u^2\left(\rho u_\alpha u_\beta + p\delta_{\alpha\beta}\right)\end{aligned} \tag{A.37}$$

where,

$$\sum_i \bar{f}_i^{\mathrm{eq}} c_{i\alpha} c_{i\beta} c_i^2 c_i^2 = 35\rho\,\theta^2 \delta_{\alpha\beta} + \rho\,\theta_0^2 \delta_{\alpha\beta} \left[\frac{\Delta\theta}{6}\left(6h_3 + h_4\right) + \frac{\Delta^2\theta}{144}\left(-840h_3 - 6h_3^2 - h_3h_4 + 6h_5\right) + \right.$$
$$\left. \frac{\Delta^3\theta}{1728}\left(8640h_3 + 1056h_3^2 + 6h_3^3 - 1740h_4 + 24h_3h_4 + h_3^2h_4 - 2h_4^2 - 72h_5 - 6h_3h_5 + 12h_6\right) + \cdots \right] \tag{A.38}$$

so, if one considers f_i^{eq} till linear in u i.e. $f_i^{\mathrm{eq}} = \bar{f}_i^{\mathrm{eq}} + \bar{f}_i^{\mathrm{eq}}\left(\frac{u_\kappa c_{i\kappa}}{\theta}\right)$, then

$$\begin{aligned} \tilde{R}^{\mathrm{eq}}_{\alpha\beta} =& \sum_i^{N_d} \bar{f}_i^{\mathrm{eq}} c_{i\alpha} c_{i\beta} c_i^2 - 5\,\rho\,\theta^2\,\delta_{\alpha\beta} - 7\rho\,\theta\,u_\alpha u_\beta - u^2\left(\rho u_\alpha u_\beta + p\delta_{\alpha\beta}\right) \approx \quad \mathbf{\bar{h}_4}\,\rho\,\theta_0^2\,\delta_{\alpha\beta}, \\ \tilde{R}^{\mathrm{eq}} =& \left\langle c_i^2 c_i^2 \right\rangle - 15\,\rho\,\theta^2 - 7\rho\,\theta\,u^2 - u^2\left(\rho u^2 + 3\,p\right) \approx \quad 3\,\mathbf{\bar{h}_4}\,\rho\,\theta_0^2 \end{aligned} \tag{A.39}$$

where each of the boldface terms in above all equations goes to zero for an ideal LB model. While for the present D3Q33 model these residual moments are shown in Eq (2.46) and the details are presented below.

We have mentioned that for the present model $\{k_1, k_2, h_1, h_2, h_3, h_4\} \to 0$ this implies

$$\begin{aligned} \bar{f}_i^{\mathrm{eq}} =& w_i\rho\left[1 + \frac{\Delta\theta}{2}\left(y_i - 3\right) + \frac{\Delta^2\theta}{8}\left(15 - 10y_i + y_i^2\right) + \frac{\Delta^3\theta}{48}\left(-105 + 105y_i - 21y_i^2 + y_i^3\right) + \right. \\ & \left. \frac{\Delta^4\theta}{384}\left(945 - 1260y_i + 378y_i^2 - 36y_i^3 + y_i^4\right) - \underline{\frac{h_5}{6}\left(y_i - 3\right)}\right], \\ \bar{h}_4 =& \left[\frac{\Delta^3\theta}{1728}\left(24h_5\right) + \frac{\Delta^4\theta}{384 \times 216}\left(-2232h_5 + 72h_6\right)\right], \\ f_i^{\mathrm{eq}} =& \bar{f}_i^{\mathrm{eq}}\left[1 + \frac{u_\kappa c_{i\kappa}}{\theta} - \frac{u^2}{2\theta} + \frac{1}{2}\left(\frac{u_\kappa c_{i\kappa}}{\theta}\right)^2\right]. \end{aligned} \tag{A.40}$$

At zero velocity and arbitrary temperature

$$\begin{gathered} \tilde{\sigma}_{\alpha\beta} = 0, \quad \tilde{Q}_{\alpha\beta\gamma} = 0, \quad \tilde{q}_\alpha = 0, \\ \tilde{R} = \frac{p^2}{\rho}\left[\frac{\Delta^3\theta}{48}\left(2h_5\right) + \frac{\Delta^4\theta}{384 \times 216}\left(-2232h_5 + 72h_6\right)\right] \end{gathered} \tag{A.41}$$

and at non zero velocity and temperature

- Residual Stress, $\quad \tilde{\sigma}_{\alpha\beta} = 0$

- Heat tensor and Residual Heat flux

$$\begin{aligned}\tilde{Q}_{\alpha\beta\gamma} =& \left[\frac{\Delta^3\theta}{48}\left(2h_5\right) + \frac{\Delta^4\theta}{384\times 216}\left(-2232h_5 + 72h_6\right)\right]\frac{\rho\, u_\kappa}{\theta}\delta_{\alpha\beta\gamma\kappa}\,\theta_0^2 \\ &+ \left(\frac{\Delta^2\theta}{8}\mathbf{k_3}\right)\frac{\rho\, u_\kappa}{\theta}\left(\Delta_{\alpha\beta\kappa\gamma} - 5\delta_{\alpha\beta\kappa\gamma}\right)\theta_0^2, \\ \tilde{q}_\alpha =& \left[\frac{\Delta^3\theta}{48}\left(2h_5\right) + \frac{\Delta^4\theta}{384\times 216}\left(-2232h_5 + 72h_6\right)\right]\left(\frac{\rho\, u_\alpha}{2\theta}\right)\theta_0^2\end{aligned} \tag{A.42}$$

- Residual fourth order moments

$$\begin{aligned}\tilde{R}_{\alpha\beta} =& \left[\frac{\Delta^3\theta}{48}\left(2h_5\right) + \frac{\Delta^4\theta}{384\times 216}\left(-2232h_5 + 72h_6\right)\right]\rho\,\theta_0^2\,\delta_{\alpha\beta}, \\ \tilde{R} =& 3\left[\frac{\Delta^3\theta}{48}\left(2h_5\right) + \frac{\Delta^4\theta}{384\times 216}\left(-2232h_5 + 72h_6\right)\right]\rho\,\theta_0^2.\end{aligned} \tag{A.43}$$

Appendix B

Pseudo Codes for Advection Implementation

The basic algorithm for LB can be understood in terms of advection of two scalar variables $\phi(x)$ and $\psi(x)$ in one dimension as

$$\begin{aligned} \phi(x) &= \phi(x+\Delta x) \\ \psi(x) &= \psi(x-\Delta x), \end{aligned} \tag{B.1}$$

where x denotes the spatial location and Δx is the grid spacing. This set of equations can be implemented without wasting memory in two possible ways, which are typically called "loop based algorithm" (LBA) and "swap based algorithm" (SBA). In the LBA version of advection the data dependence in the 'update' step is broken by a proper choice of the loop direction. In particular, the following combination,

```
for (i = 1 to K)      {$\phi$(i) = $\phi$(i+1)},
for (i = K to 1)      {$\psi$(i) = $\psi$(i-1)}
```

of forward and backward looping can be used to implement Eq.(B.1).

The same equation (Eq.B.1) can also be implemented using the duality between 'swap' and 'shift' as

```
for (i = 0 to K)     {SWAP($\phi$(i), $\psi$(i+1))}.
```

After the end of this step of the swap-based implementation of Eq.(B.1), the relative memory location for the two populations gets interchanged, which needs to be taken care [97].

All higher dimensional algorithms which do not waste memory are derivatives of the 1-D alternatives of LBA and SBA. In higher dimensions, while the 'swap' algorithm remains conceptually same. In this section, it is shown that the extension of the 'shift' version to higher dimensions is non-trivial. One recalls that, in the 'shift' version, the loop direction is chosen as opposite to the shift direction. This implies that one has 8 possible loop orderings corresponding to the 'plus' or 'minus' shift in any direction. For example, for two scalar variables $\phi(x, y, z)$ and $\psi(x, y, z)$,

$$\begin{aligned} \phi(x,y,z) &= \phi(x+\Delta, y+\Delta, z+\Delta) \\ \psi(x,y,z) &= \psi(x-\Delta, y-\Delta, z+\Delta) \end{aligned} \tag{B.2}$$

where Δ is the grid spacing, Eq.(B.2) can be implemented as

```
for(k= 1 to $K_z$){
   for(j= 1 to $K_y$){
      for(i= 1 to $K_x$){
            $\phi$ (i,j,k) = $\phi$(i+1,j+1,k+1); }}
   for(j= $K_y$ to 1){
      for(i= $K_x$ to 1){
            $\psi$ (i,j,k) = $\psi$(i-1,j-1,k+1); }}
   }}
```

This version, which is typically implemented in many available source codes, which is termed here as 8-loop versions of LBA or LBA-8. However, this straightforward extension of one-dimensional logic in 3-D is too conservative. Data flow analysis in the pseudo code presented above shows that the values of ϕ and ψ in xy plane at $z = k$ are taken from the xy plane at $z = k + 1$. Thus, the data dependence is purely one-dimensional and only the direction of the outer loop matters. The pseudo code for such an implementation will be,

```
for(k= 1 to $K_z$){
    for(j= 1 to  $K_y$){
        for(i= 1 to $K_x$){
            $\phi$ (i,j,k) = $\phi$(i+1,j+1,k+1);
              $\psi$ (i,j,k) = $\psi$(i-1,j-1,k+1);          }}}
```

and is referred in this thesis as the 2-loop version of LBA or LBA-2. This algorithm when applied to say BCC shell, appears like

```
for(  k = 1; k <= $K_z$; k++){
for(  j = 1; j <= $K_y$; j++){
for(  i = 1; i <= $K_x$; i++){
     $f_{(-1,-1,-1)}$ (i, j, k) = $f_{(-1,-1,-1)}$ ( i+1, j+1, k+1);
     $f_{(+1,-1,-1)}$ (i, j, k) = $f_{(+1,-1,-1)}$ ( i-1, j+1, k+1);
     $f_{(+1,+1,-1)}$ (i, j, k) = $f_{(+1,+1,-1)}$ ( i-1, j-1, k+1);
     $f_{(-1,+1,-1)}$ (i, j, k) = $f_{(-1,+1,-1)}$ ( i+1, j-1, k+1);
}}}

for(  k = $K_z$    ; k  >= 1       ;  k--){
for(  j = 1      ; j  <= $K_y$     ;  j++){
for(  i = 1      ; i  <= $K_x$     ;  i++){
     $f_{(+1,+1,+1)}$ (i, j, k) = $f_{(+1,+1,+1)}$ ( i-1, j-1, k-1);
     $f_{(-1,+1,+1)}$ (i, j, k) = $f_{(-1,+1,+1)}$ ( i+1, j-1, k-1);
     $f_{(-1,-1,+1)}$ (i, j, k) = $f_{(-1,-1,+1)}$ ( i+1, j+1, k-1);
     $f_{(+1,-1,+1)}$ (i, j, k) = $f_{(+1,-1,+1)}$ ( i-1, j+1, k-1);
}}}
```

References

[1] C.K. Aidun and J.R. Clausen. Lattice-Boltzmann method for complex flows. *Annu. Rev. Fluid Mech.*, 42:439–472, 2010.

[2] R. Benzi, S. Succi, and M. Vergassola. The lattice Boltzmann equation: theory and applications. *Phys. Rep.*, 222(3):145–197, 1992.

[3] S. Chen and G.D. Doolen. Lattice Boltzmann method for fluid flows. *Annu. Rev. Fluid Mech.*, 30(1):329–364, 1998.

[4] S. Succi. *The Lattice Boltzmann Equation for Fluid Dynamics and Beyond.* Oxford University Press, USA, 2001.

[5] I. V. Karlin, A Ferrante, and H. C. Öttinger. Perfect Entropy Functions of the Lattice Boltzmann Method. *Europhys. Lett.*, 47:182–188, 1999.

[6] S. Ansumali, I. V. Karlin, and H. C. Öttinger. Minimal Entropic Kinetic Models for Simulating Hydrodynamics. *Europhys. Lett.*, 63:798–804, 2003.

[7] S. Succi, I. V. Karlin, and H. Chen. Colloquium: Role of the H theorem in lattice Boltzmann hydrodynamic simulations. *Rev. Mod. Phys.*, 74(4):1203, 2002.

[8] D. S. Clague, B. D. Kandhai, R. Zhang, and P. M. A. Sloot. Hydraulic permeability of (un)bounded fibrous media using the lattice Boltzmann method. *Phys. Rev. E*, 61:616–625, 2000.

[9] Zhaoli Guo and T. S. Zhao. Lattice Boltzmann model for incompressible flows through porous media. *Phys. Rev. E*, 66:036304, Sep 2002.

[10] Anthony JC Ladd. Numerical simulations of particulate suspensions via a discretized Boltzmann equation. Part 1. Theoretical foundation. *J. Fluid Mech.*, 271(1):285, 1994.

[11] Anthony JC Ladd. Numerical simulations of particulate suspensions via a discretized Boltzmann equation. Part 2. Numerical results. *J. Fluid Mech.*, 271(1):311–339, 1994.

[12] J. Zhang, P. C. Johnson, and A. S. Popel. Red blood cell aggregation and dissociation in shear flows simulated by lattice Boltzmann method. *J. Biomech.*, 41:47–55, 2008.

[13] S.S. Chikatamarla, C. E. Frouzakis, I. V. Karlin, A. G. Tomboulides, and K. B. Boulouchos. Lattice Boltzmann method for direct numerical simulation of turbulent flows. *J. Fluid Mech.*, 656:298–308, 2010.

[14] G.R. McNamara, A.L. Garcia, and B.J. Alder. Stabilization of thermal lattice Boltzmann models. *J. Stat. Phys.*, 81(1):395–408, 1995.

[15] George Vahala, Pavol Pavlo, Linda Vahala, and Nicos S. Martys. Thermal lattice-Boltzmann models (tlbm) for compressible flows. *Int. J. Mod. Phys. C*, 09(08):1247–1261, 1998.

[16] Paulo C. Philippi, Luiz A. Hegele, Luís O. E. dos Santos, and Rodrigo Surmas. From the continuous to the lattice Boltzmann equation: The discretization problem and thermal models. *Phys. Rev. E*, 73:056702, May 2006.

[17] S. Williams, J. Carter, L. Oliker, J. Shalf, and K. Yelick. Lattice Boltzmann simulation optimization on leading multicore platforms. In *Int. Symp. on Par. and Dist. Proc.,*, pages 1–14. IEEE, 2008.

[18] M. Bernaschi, M. Bisson, T. Endo, S. Matsuoka, and M. Fatica. Petaflop biofluidics simulations on a two million-core system. In *Int. Conf. for HPC, Netw., Stor. and Ana.*, pages 1–12. IEEE, 2011.

[19] M. Bernaschi, M. Bisson, M. Fatica, S. Melchionna, and S. Succi. Petaflop hydrokinetic simulations of complex flows on massive GPU clusters. *Comp. Phy. Comm.*, 2012.

[20] G. Wellein, T. Zeiser, G. Hager, and S. Donath. On the single processor performance of simple lattice Boltzmann kernels. *Computers & Fluids*, 35(8):910–919, 2006.

[21] T. Ciamulski and M. Sypniewski. Linear and superlinear speedup in parallel FDTD processing. In *Int. Symp. on Anten. and Prop. Soc.,*, pages 4897–4900. IEEE, 2007.

[22] V. Heuveline, M.J. Krause, and J. Latt. Towards a hybrid parallelization of lattice Boltzmann methods. *Computers & Mathematics with Applications*, 58(5):1071–1080, 2009.

[23] P. L. Bhatnagar, E. P. Gross, and M. Krook. A Model for Collision Processes in Gases. I. Small Amplitude Processes in Charged and Neutral One-Component Systems. *Phys. Rev.*, 94:511–525, 1954.

[24] H. Chen, S. Chen, and W. H. Matthaeus. Recovery of the navier-stokes equations using a lattice-gas boltzmann method. *Phys. Rev. A*, 45(8):5339–5342, 1992.

[25] Y. H. Qian, D. d'Humières, and P. Lallemand. Lattice BGK Models for Navier-Stokes Equation. *Europhys. Lett.*, 17:479–484, 1992.

[26] J. E. Broadwell. Study of Rarefied Shear Flow by the Discrte Velocity Method. *J. Fluid Mech.*, 19:401–414, 1964.

[27] J.E. Broadwell. Shock structure in a simple discrete velocity gas. *Physics of Fluids*, 7(8):1243–1247, 1964.

[28] J. Hardy, Y. Pomeau, and O. De Pazzis. Time evolution of a two-dimensional model system. i. invariant states and time correlation functions. *Journal of Mathematical Physics*, 14:1746, 1973.

[29] J. Hardy, Y. Pomeau, and O. De Pazzis. Time evolution of a two-dimensional classical lattice system. *Physical Review Letters*, 31(5):276–279, 1973.

[30] J. Hardy, O. De Pazzis, and Y. Pomeau. Molecular dynamics of a classical lattice gas: Transport properties and time correlation functions. *Physical Review A*, 13(5):1949, 1976.

[31] S. Wolfram. Statistical mechanics of cellular automata. *Reviews of modern physics*, 55(3):601, 1983.

[32] U. Frisch, B. Hasslacher, and Y. Pomeau. Lattice-gas automata for the navier-stokes equation. *Physical review letters*, 56(14):1505–1508, 1986.

[33] G.R. McNamara and G. Zanetti. Use of the boltzmann equation to simulate lattice-gas automata. *Physical Review Letters*, 61(20):2332–2335, 1988.

[34] FJ Higuera, S. Succi, and R. Benzi. Lattice gas dynamics with enhanced collisions. *EPL (Europhysics Letters)*, 9(4):345, 1989.

[35] F.J. Alexander, S. Chen, and J.D. Sterling. Lattice Boltzmann Thermohydrodynamics. *Phys. Rev. E*, 47:R2249–R2252, 1993.

[36] Seung Hyun Kim, Heinz Pitsch, and Iain D. Boyd. Accuracy of higher-order lattice boltzmann methods for microscale flows with finite knudsen numbers. *J. Comput. Phys.*, 227(19):8655–8671, 2008.

[37] S. Ansumali and I. V. Karlin. Consistent lattice boltzmann method. *Phys. Rev. Lett.*, 95(26):260605, 2005.

[38] S. Ansumali, I. V. Karlin, S. Arcidiacono, A. Abbas, and N. I. Prasianakis. Hydrodynamics beyond navier-stokes: Exact solution to the lattice boltzmann hierarchy. *Phys. Rev. Lett.*, 98(12):124502, 2007.

[39] X. Shan and X. He. Discretization of the Velocity Space in the Solution of the Boltzmann Equation. *Phys. Rev. Lett.*, 80(1):65–68, 1998.

[40] T. Abe. Derivation of the lattice Boltzmann method by means of the discrete ordinate method for the Boltzmann equation. *J. Comput. Phys.*, 131(1):241–246, 1997.

[41] Shyam S. Chikatamarla and Iliya V. Karlin. Entropy and Galilean Invariance of Lattice Boltzmann theories. *Phys. Rev. Lett.*, 97:190601, Nov 2006.

[42] X. Shan, X. Yuan, and H. Chen. Kinetic Theory Representation of Hydrodynamics: a way beyond the Navier-Stokes equation. *J. Fluid Mech.*, 550:413–441, 2006.

[43] W.P. Yudistiawan, S.K. Kwak, DV Patil, and S. Ansumali. Higher-order Galilean-invariant lattice Boltzmann model for microflows: single-component gas. *Phy. Rev. E*, 82(4):046701, 2010.

[44] C.K. Aidun and J.R. Clausen. Lattice-Boltzmann method for complex flows. *Annu. Rev. Fluid Mech.*, 42:439–472, 2010.

[45] H Grad. Principles of the Kinetic Theory of Gases. *Handbuch der Physik*, XII, 1958.

[46] S. Succi. *The Lattice Boltzmann Equation for Fluid Dynamics and Beyond.* Oxford University Press, Oxford, 2001.

[47] Takeshi Kataoka and Michihisa Tsutahara. Lattice boltzmann model for the compressible navier. *Phys. Rev. E*, 69(3):035701, 2004.

[48] S. S. Chikatamarla and I. V. Karlin. Lattices for the lattice Boltzmann method. *Phys. Rev. E*, 79:046701, 2009.

[49] Solomon Kullback. *Information theory and statistics.* Courier Dover Publications, 1968.

[50] Z. Guo, B. Shi, and C. Zheng. A coupled lattice BGK model for the boussinesq equations. *Int. J. Num. Meth. Fluids*, 39(4):325–342, 2002.

[51] Li-Shi Luo. A unified theory of non-ideal gas lattice Boltzmann models. *Phys. Rev. Lett*, 81(8):1618–1621, 1998.

[52] JM Buick and CA Greated. Gravity in a lattice Boltzmann model. *Phy. Rev. E*, 61(5):5307, 2000.

[53] C. Zheng Z. Guo and B. Shi. Discrete lattice effects on the forcing term in the lattice Boltzmann method. *Phy. Rev. E*, 65:046308, 2002.

[54] HN Dixit and V. Babu. Simulation of high Rayleigh number natural convection in a square cavity using the lattice Boltzmann method. *Int. J Heat Mass Transfer*, 49(3):727–739, 2006.

[55] S. Ansumali and I.V. Karlin. Kinetic boundary conditions in the lattice Boltzmann method. *Phy. Rev. E*, 66(2):026311, 2002.

[56] Shiwani Singh, Siddharth Krithivasan, Iliya V Karlin, Sauro Succi, and Santosh Ansumali. Energy conserving lattice Boltzmann models for incompressible flow simulations. *Int. J. Mod. Phys. C*, 2013.

[57] Tasos Papanastasiou, Georgios Georgiou, and Andreas N Alexandrou. *Viscous fluid flow.* CRC, 1999.

[58] S. Kakac and Y. Yener. *Heat conduction.* Hemisphere Publications, 2007.

[59] R Byron Bird, Warren E Stewart, and Edwin N Lightfoot. *Transport phenomena.* Wiley, 2006.

[60] S Ubertini, P Asinari, and S Succi. Three ways to lattice boltzmann: a unified time-marching picture. *Phys. Rev. E*, 81(1):016311, 2010.

[61] Philip G Drazin and Norman Riley. *The Navier-Stokes equations: a classification of flows and exact solutions*, volume 334. Cambridge University Press, 2006.

[62] William Graebel. *Advanced fluid mechanics.* Academic Press, 2007.

[63] W.P. Yudistiawan, S. Ansumali, and I.V. Karlin. Hydrodynamics beyond Navier-Stokes: The slip flow model. *Phy. Rev. E*, 78(1):016705, 2008.

[64] C. Cercignani. *Theory and Application of the Boltzmann Equation.* Scottish Academic Press, Edinburgh, 1975.

[65] P. Bassanini, C. Cercignani, and C. D. Pagani. Comparision of kinetic theory analysis of linearized heat transfer between parallel plates. *Int. J. Heat Mass Transfer*, 10:447–460, 1967.

[66] S. Hou. Simulation of the Cavity Flow by the Lattice Boltzmann Method. *J. Comp. Phys.*, 118:329–347, 1995.

[67] Zhaoli Guo, Baochang Shi, and Nengchao Wang. Lattice BGK model for incompressible navier–stokes equation. *J. Comput. Phys.*, 165(1):288–306, 2000.

[68] RA Brownlee, Alexander N Gorban, and Jeremy Levesley. Nonequilibrium entropy limiters in lattice Boltzmann methods. *Phys. A*, 387(2):385–406, 2008.

[69] F Tosi, S Ubertini, S Succi, H Chen, and IV Karlin. Numerical stability of entropic versus positivity-enforcing lattice Boltzmann schemes. *Mathematics and Computers in Simulation*, 72(2):227–231, 2006.

[70] S Borok, S Ansumali, and IV Karlin. Kinetically reduced local Navier-Stokes equations for simulation of incompressible viscous flows. *Phy. Rev. E*, 76(6):066704, 2007.

[71] Pietro Asinari, Taku Ohwada, Eliodoro Chiavazzo, and Antonio F Di Rienzo. Link-wise artificial compressibility method. *J. Comput. Phys.*, 2012.

[72] U. Ghia, K. N. Ghia, and C. Y. Shin. High-Re solutions for incompressible flow using the Navier-Stokes equations and a multigrid method. *J. Comp. Phys.*, 48:387–411, 1982.

[73] SP Vanka. Block-implicit multigrid solution of Navier-Stokes equations in primitive variables. *J. Comput. Phys.*, 65(1):138–158, 1986.

[74] Charles-Henri Bruneau and Mazen Saad. The 2d lid-driven cavity problem revisited. *Comp. & Fluids*, 35(3):326–348, 2006.

[75] O Botella and R Peyret. Benchmark spectral results on the lid-driven cavity flow. *Comp. & Fluids*, 27(4):421–433, 1998.

[76] M. Tij and A. Santos. Perturbation Analysis of a Stationary Nonequilibrium Flow Generated by an External Force. *J. Stat. Phys.*, 76:1399–1414, 1994.

[77] M. Tij, M. Sabbane, and A. Santos. Nonlinear Poiseuille Flow in a Gas. *J. Stat. Phys.*, 10:1021–1027, 1998.

[78] M. Sabbane, M. Tij, and A. Santos. Maxwellian Gas Undergoing a Stationary Poiseuille Flow in a Pipe. *Phys. A*, 327:264–290, 2003.

[79] Y. Zheng, A. L. Garcia, and B. J. Alder. Comparision of Kinetic Theory and Hydrodynamics for Poiseuille Flow. *J. Stat. Phys.*, 109:495–505, 2002.

[80] S Ansumali. *Minimal kinetic modeling of hydrodynamics.* PhD thesis, ETH Zurich, Ref. No. 15534, 2004.

[81] JGM Eggels and JA Somers. Numerical simulation of free convective flow using the lattice-Boltzmann scheme. *Int. J.Heat Fluid Flow*, 16(5):357–364, 1995.

[82] Roger Joseph Anna Janssen. *Instabilities in natural-convection flows in cavities.* PhD thesis, Delft Uni. of Tech., The Netherlands, 1994.

[83] N. I. Prasianakis. *Lattice Boltzmann Method for Thermal Compressible Flows.* PhD thesis, ETH Zurich, Ref. No. 17739, 2008.

[84] X. He, S. Chen, and G.D. Doolen. A novel thermal model for the lattice Boltzmann method in incompressible limit. *J. Comput. Phys.*, 146(1):282–300, 1998.

[85] RM Clever and FH Busse. Transition to time-dependent convection. *J. Fluid Mech*, 65(4):625–645, 1974.

[86] K. Yee. Numerical solution of initial boundary value problems involving Maxwell's equations in isotropic media. *IEEE Trans. on Ante. and Prop.*, 14(3):302–307, 1966.

[87] G. Mur. Absorbing boundary conditions for the finite-difference approximation of the time-domain electromagnetic-field equations. *IEEE Trans. on Elect. Comp.*, 14(4):377–382, 1981.

[88] J.P. Berenger. A perfectly matched layer for the absorption of electromagnetic waves. *J. Comput. Phys.*, 114(2):185–200, 1994.

[89] A. Taflove and S.C. Hagness. *Computational electrodynamics*, volume 160. Artech house, Boston and London, 2000.

[90] S. Williams, J. Carter, L. Oliker, J. Shalf, and K. Yelick. Lattice Boltzmann simulation optimization on leading multicore platforms. In *Parallel and Distributed Processing, 2008. IPDPS 2008. IEEE International Symposium on*, pages 1–14. IEEE, 2008.

[91] M. Bernaschi, M. Bisson, T. Endo, S. Matsuoka, and M. Fatica. Petaflop biofluidics simulations on a two million-core system. In *Int. Conf. for HPC, Netw., Stor. and Ana.*, pages 1–12. IEEE, 2011.

[92] M. Bernaschi, M. Bisson, M. Fatica, S. Melchionna, and S. Succi. Petaflop hydrokinetic simulations of complex flows on massive GPU clusters. *Comp. Phy. Comm.*, 2012.

[93] G. Wellein, T. Zeiser, G. Hager, and S. Donath. On the single processor performance of simple lattice Boltzmann kernels. *Computers & Fluids*, 35(8):910–919, 2006.

[94] T. Ciamulski and M. Sypniewski. Linear and superlinear speedup in parallel fdtd processing. In *Int. Symp. on Anten. and Prop. Soc.,*, pages 4897–4900. IEEE, 2007.

[95] V. Heuveline, M.J. Krause, and J. Latt. Towards a hybrid parallelization of lattice Boltzmann methods. *Computers & Mathematics with Applications*, 58(5):1071–1080, 2009.

[96] P.J. Denning. The locality principle. *Communications of the ACM*, 48(7):19–24, 2005.

[97] K. Mattila, J. Hyväluoma, T. Rossi, M. Aspnäs, and J. Westerholm. An efficient swap algorithm for the lattice Boltzmann method. *Comp. Phys. Comm.*, 176(3):200–210, 2007.

[98] J. Latt and B. Chopard. Lattice Boltzmann method with regularized pre-collision distribution functions. *Math and Comp. in Simulation*, 72(2):165–168, 2006.

[99] S. Ansumali, S. Arcidiacono, SS Chikatamarla, NI Prasianakis, AN Gorban, and IV Karlin. Quasi-equilibrium lattice Boltzmann method. *EuroPhys. J. B*, 56(2):135–139, 2007.